FRACTURE MECHANICS STUDY OF TUBULAR JOINT WELD TOE DEFECTS WITH THREE-DIMENSIONAL FINITE ELEMENTS

By

SHIZHONG HAN

Bachelor of Science in Mechanical Engineering
Northeast University of Technology
Shenyang, China
1982

Master of Science in Mechanical Engineering
Northeast University of Technology
Shenyang, China
1986

Submitted to the Faculty of the Graduate College
of the Oklahoma State University
in partial fulfillment of the requirements
for the Degree of
DOCTOR OF PHILOSOPHY
December, 1992

FRACTURE MECHANICS STUDY OF TUBULAR JOINT

WELD TOE DEFECTS WITH THREE-

DIMENSIONAL FINITE ELEMENTS

Thesis Approved:

G. Steven Gipson

Thesis Adviser

D. K. Good

Fred Zuercher

C K Rhee

Thomas C. Collins

Dean of the Graduate College

ACKNOWLEDGEMENTS

I wish to thank my major professor, G. Steven Gipson, for his invaluable assistance and support in my graduate program at Oklahoma State University. Special gratitude goes to Dr. H. Chong Rhee for giving me the initial motive and continuous guidance in my research; to Dr. F. J. Zwerneman and Dr. J. K. Good for serving on my degree committee.

Funding for my research is provided by Amoco Production Research, Arco Oil and Gas, British Gas, Chevron Oil Field Research, Conoco, Exxon Production Research, Mobil Research and Development, Phillips Petroleum Company, Shell Oil Company, and Texaco. I deeply appreciate the support from these companies. Special thanks to Conoco PRD managers Dr. R. M. Vennett, Dr. W. H. Thomason, and Dr. M. M. Salama, and the computer system engineers, Kent Blancett and Bruce Sachetti, for providing me with all the pleasant and efficient working environment at Conoco Inc. for more than three years. Thanks to Dr. R. K. Hughes and the School of Civil Engineering for partial support with a teaching assistantship.

This work is dedicated to my grandparents, my wife, Xiaolu, my daughter, Susan, and to my parents for their love and trust over the years; and to Professor Walter D. Pilkey and Mrs. Barbara Pilkey for their unforgettable help and understanding when I first came and worked with them as a visiting scholar at the University of Virginia.

TABLE OF CONTENTS

Chapter Page

LIST OF TABLES

LIST OF FIGURES

Figure Page

CHAPTER I

INTRODUCTION

In many areas of engineering, steel tubular joints are used widely as standard structural components. The most fatigue-sensitive location in a conventional fixed jacket platform is the weld toe area of a tubular joint [1]. Continuous long-term random wave and wind action causes unavoidable weld toe fabrication defects to become starters for crack initiation and propagation. For most welded components and joints, the propagation phase often dominates [2,3]. Therefore, fracture mechanics can be used to describe the fatigue life and the critical condition of failure of joints with detected cracks.

Fracture mechanics has been applied extensively in aerospace and nuclear power engineering. It is a reliable technique for assessing the influence of defects on structural behavior [4,5]. The stress intensity factor (SIF), indicating the magnitude of the crack tip stress field, is the essential parameter for linear elastic fracture mechanics. Realistic fracture fatigue life calculation demands reliable stress intensity factor solutions. However, there is no closed-form analytical solution available for semi-elliptical cracks in tubular joints. Laboratory tests often show that a typical tubular joint weld toe crack grows along the weld toe contour on the joint surface and curves in the tube-wall direction. Therefore, such a fatigue crack is a doubly warped crack surface with a curved crack front in space, as shown in Figure 1 for a Y-tubular joint.

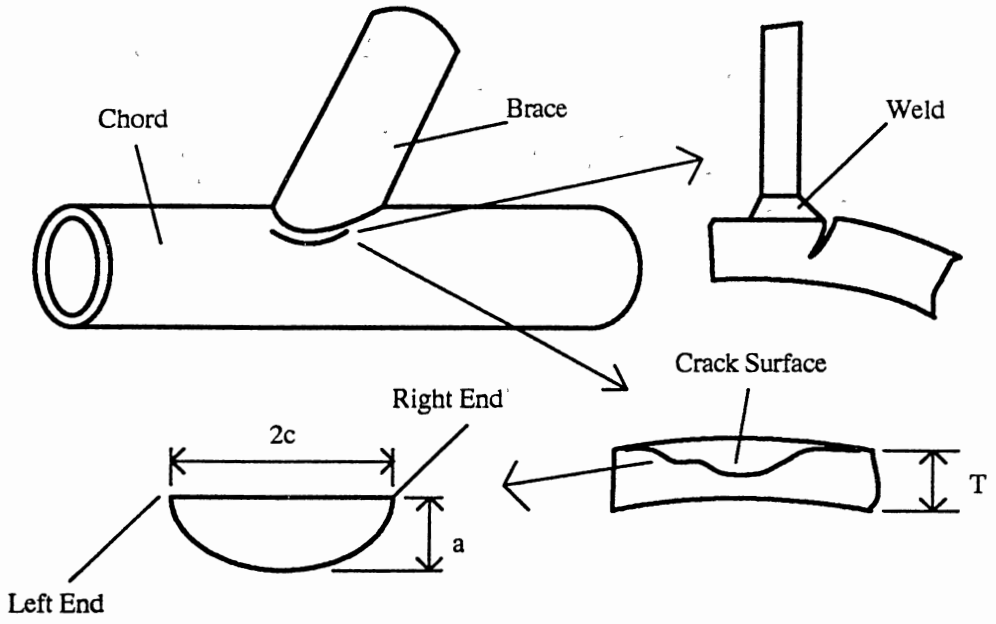

Figure 1. Geometry of Weld Toe Defect

It is extremely difficult to calculate the stress intensity factor solutions, because of the complicated joint/crack geometry and loading conditions. In addition to mode I deformation, modes II and III appear to exist as well [6]. Complete descriptions of fracture modes are presented in the beginning of Chapter III. Most of the theoretical and experimental work on mixed mode fracture are for two-dimensional flat plates with an inclined crack subjected to in-plane tension on brittle materials. Tests in a simple specimen [7,8] indicate that a mixed mode crack tends to transform into a mode I crack under fatigue loading. However, the same type of rapid mode transformation has not

been clearly observed in tubular joints. It is not known for certain how to use stress intensity factors for cracks that are initially in a mixed mode.

For fracture and fatigue analysis of tubular joints in the offshore industry, many simplified methods for SIF solutions were proposed on the basis of many uncertain assumptions for joint/crack geometry and stress distributions. In most cases, the validity of the assumptions have not or cannot be verified. Most of these methods are suitable for tensile stress only. Destructive shear stresses which are common at the crack location of a tubular joint are ignored.

To develop rational and efficient fracture mechanics analysis procedures for tubular joints, it is necessary to understand the weld toe fracture behavior through accurate SIF solutions. Various general approaches in the open literature and their limitations to obtain stress intensity factors were reviewed recently by Shields et al. [9]. One approach for calculating the SIF solutions for tubular weld toe cracks is the finite element method with the three-dimensional solid elements. The procedure developed by Rhee [10] is the most general for engineering problems with crack-like defects. This procedure has been validated by other researchers as mentioned in the end of Chapter II. With advanced development in finite element pre-/post-processing computer software such as PRETUBE [11] and KAARL [12], and rapid development in computer hardware technology [13], reliable 3-D FEM is a pragmatic approach for solving engineering fracture and fatigue problems. This is because experimental determination of SIF's is extremely difficult and expensive. On the basis of efficiency and practicality, the stress intensity factor solutions for cracks at tubular joint weld toe are much easily obtainable by numerical rather than experimental methods.

There is considerable interest in the application of fracture mechanics methods to predict fatigue crack growth in offshore tubular joints [1-3]. The need and motivation for reliable SIF solutions and for better understanding of the fracture mechanics behavior of tubular joints, using the 3-D finite element method, has been demonstrated through a Joint Industry Project (JIP) sponsored by nine American oil companies and British Gas in England.

Some of the important issues in the fracture mechanics application in tubular joints are how to calculate the SIF solutions for the weld toe defects, and what the solutions imply about the physical behavior of the defects. The motivation for this work is to resolve these issues using the most rigorous procedure available. The objectives of this dissertation are to generate a significant number of stress intensity factor solutions under various practical conditions, and to investigate the physical behavior and some implications of these solutions to fatigue crack growth in tubular joints from the viewpoint of fracture mechanics. Various models have been analyzed to study the sensitivity of the stress intensity factor solutions to the 3-D finite element models for tubular joint weld toe defects. A set of empirical formulas for the SIF solutions will be developed to demonstrate the potential of some practical application for tubular T-joint saddle cracks.

All of the 3-D finite element analyses were performed on a VAX 3600 computer, using the TUJAP system [11,14]. Rhee's procedure [10] for SIF calculation was applied through the computer program, KAARL. Figure 2 shows the T, Y, and K tubular joints used in this work.

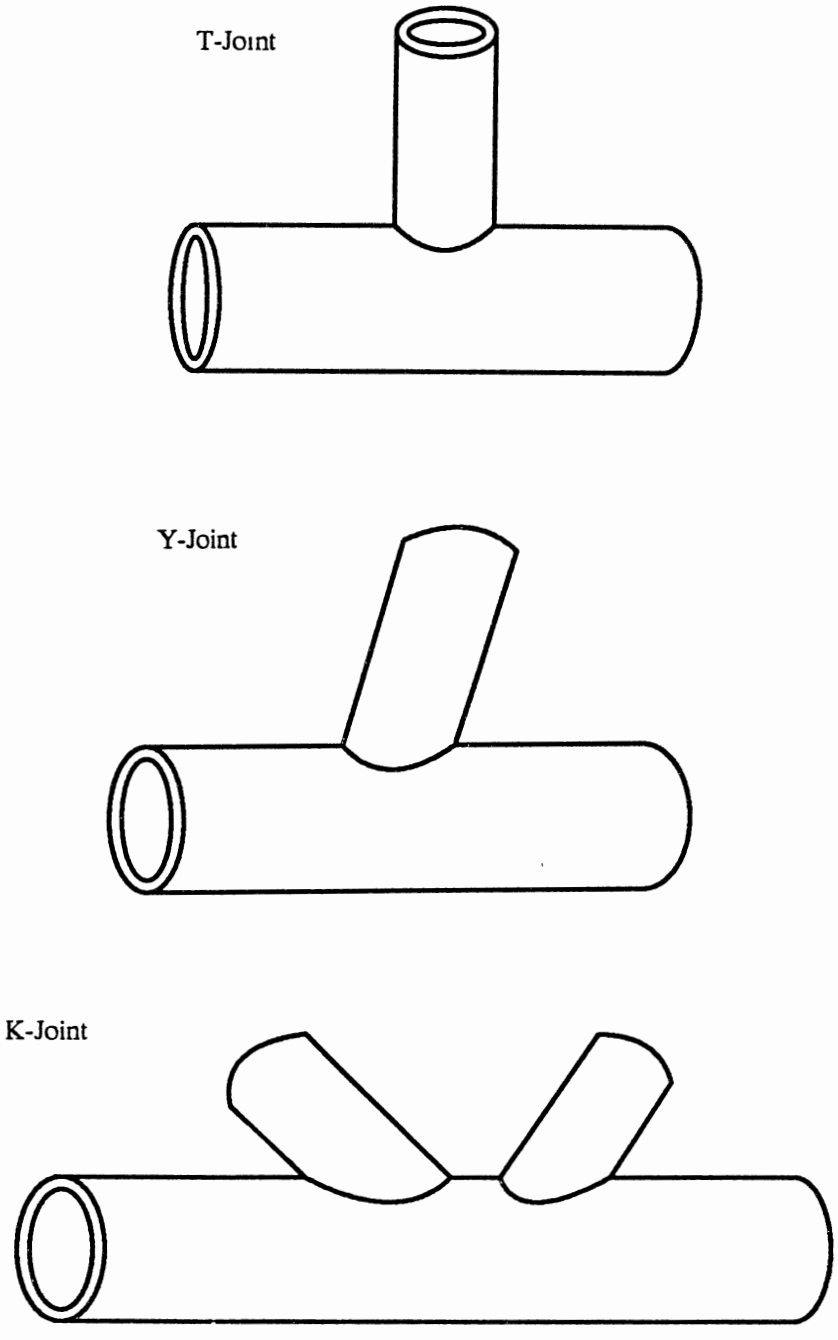

Figure 2. T-, Y-, and K-Tubular Joints

Some important future research problems have been identified in Chapter VII. The proposed recommendations should prove useful to the structural integrity assessment of offshore tubular joints through fracture mechanics method.

CHAPTER II

LITERATURE REVIEW

Fatigue Assessment of Tubular Joints

Tubular joints are the primary members in steel offshore structures. Ocean waves and winds cause fluctuations of the stress levels at the joints, leading to fatigue crack growth and eventual failure. Therefore, in addition to static strength, tubular joints require fatigue strength. Fatigue life is defined as the number of stress cycles taken to reach a pre-defined failure criterion. Fatigue design rules for welded tubular structures are published by many agencies such as the American Welding Society (AWS) [15], the American Petroleum Institute (API) [16], the British Standard Institute [17], the Department of Energy in UK [18], Lloyds Register of Shipping [19], Norwegian Petroleum Directorate Design Rules [20], and Det Norske Veritas (DnV) in Norway [21].

Two basic approaches, the S-N curve method, and the fracture mechanics method, are available for fatigue strength assessment of tubular joints [3]. The conventional S-N curves (stress versus number of cycles to failure) are based on test data and rely on empirical relationships between applied stress ranges and fatigue life. Applied stress has been taken as the punching shear stress, which is shear stress in the wall of the chord equivalent to the load distribution component normal to the chord surface along the brace/chord intersection. However, hot spot stress [22], which is defined as a local

maximum stress in a tubular joint, yields more consistent results [2,3, 23]. The current practice for fatigue strength design is to use the hot spot stress in conjunction with S-N curves [3, 24].

Although the conventional S-N curve method has been used successfully in fatigue design, the success has been due primarily to engineering judgements. One of the serious problems associated with S-N curves is that the effect of a crack-like defect in the joint weld toe cannot be considered. The assessment of defect propagation behavior and of the remaining life of an existing structure with detected fatigue cracks requires the fracture mechanics approach. The fracture mechanics approach is also used to investigate critical joints in a structure at the design stage. For offshore structures, subcritical fatigue crack growth is the primary fracture mechanics concern. The brittle fracture is considered in the design stage only in association with fatigue crack propagation [1]. In the tubular joints of offshore structures, the environmental temperature of the sea and the external wave load are low enough to justify the assumption of linear elastic fracture mechanics behavior.

Paris and Erdogan [25] developed a well known equation, often referred to as the Paris law, for crack growth rate in linear elastic fracture mechanics. The crack growth rate is expressed as a function of the crack-tip stress intensity factor range ΔK. The Paris law is in the form:

$$\frac{da}{dN} = C(\Delta K_I)^m \tag{1}$$

where C and m are material constants, obtained from simple pre-cracked specimen test,

da/dN is the crack growth rate, and ΔK_I is the mode I stress intensity factor range between the maximum SIF and minimum SIF in a fatigue cycle ($\Delta K_I = K_{Imax} - K_{Imin}$). The relationship between crack growth rate (da/dN) and ΔK_I observed for many structural metals, when tested in a non-corrosive environment and under constant amplitude cyclic loading is shown in Figure 3. The Paris law in its simplest form provides an adequate description of crack growth at an intermediate range of growth rates under mode I loading. Various modified forms of the Paris law, to consider the environment, mean stress (R ratio), and threshold effects, was reviewed in Reference 26. Based on different hypotheses, mixed mode crack propagation problems were converted to an equivalent mode I case, and several modified Paris laws were used for tubular joint fatigue strength assessment. Rhee [27] used an effective SIF defined by the crack energy release rate [4,5] of a self-similar crack growth to calculate the fatigue life of a K-tubular joint, while Kim and Tsai [28] applied the concept of energy density factor [29,30] in a T-tubular joint. In most simplified methods, only a mode I SIF is calculated as to be discussed in the following, and used in conjunction with the Paris law.

Simplified Methods for Stress Intensity Factors

Obtaining the stress intensity factor (SIF) solutions is extremely difficult because of the complicated geometry and stress distribution of tubular joints. There is no closed form analytical solution available for semi-elliptical cracks in tubular joints. Therefore, many simplified methods were proposed and applied to approximate the SIF solutions for fracture and fatigue analyses in the offshore industry. These methods can be classified as modified handbook solution method, weight function method, line spring element

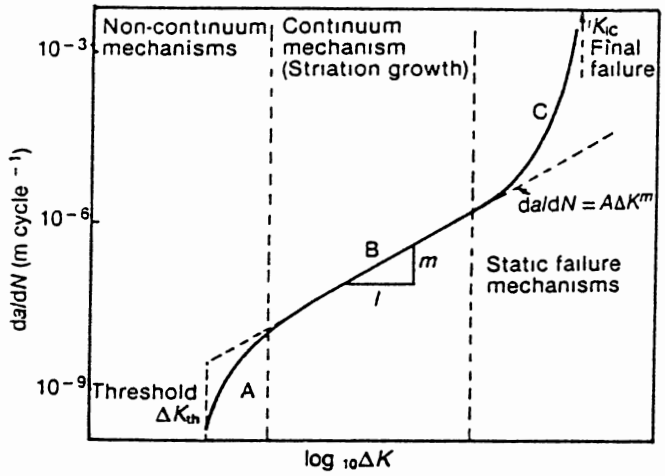

Figure 3. Schematic Illustration of Fatigue-Crack Growth in Steel (from Design of Tubular Joints for Offshore Structures, Volume 2, UEG Publication UR33, 1985)

method, and others including the experimental method, the Aptech method, compliance method, virtual crack extension method, and alternating method.

Various simplified assumptions have been made for the stress distributions along the tubular joint weld toe and in the wall-thickness direction. The curvature of the crack surface is normally ignored. It is difficult to assess the uncertainties resulting from these oversimplifications [1]. Agreement between different solution methods is often poor for tubular joints [31]. Little information is available regarding the assessment and validation

of these simplified methods. To clarify the problems caused by theses assumptions, the essential approach and the limitations of these simplified methods will be reviewed in the following sections.

Modified Handbook Solutions

The SIF solutions for a simple and regular crack and geometry are readily available in handbooks [32-34]. Two popular formulas are developed by Newman and Raju [35], and Scott and Thorpe [36]. Using the results of three-dimensional finite element analyses, Newman and Raju derived an empirical stress intensity factor formula for semi-elliptical surface cracks. The formula applies for cracks of arbitrary aspect factor in finite sized plate under bending or uniform tension.

$$K=(\sigma_t+H\sigma_b)\sqrt{\pi a/Q}F \qquad (2)$$

where σ_t and σ_b are tensile stress and bending stress, respectively, Q, H, and F are functions of a, c, b and T as shown in Figure 4.

Scott and Thorpe [36] reviewed several crack tip stress intensity factor solutions for semi-elliptical surface cracks in plates. They proposed a set of SIF formulas for surface cracks in plate strips. The solution for a pure membrane stress σ_m, and a pure bending stress σ_b, may be written respectively, as

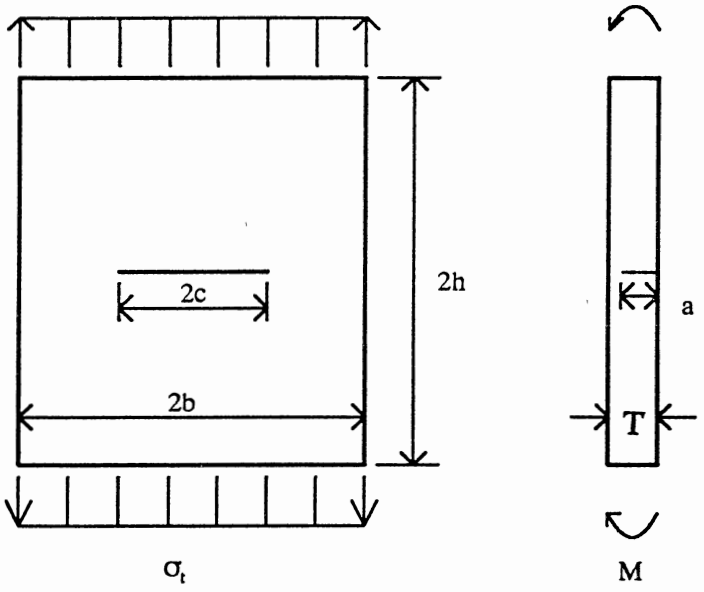

Figure 4. Surface Crack in a Finite Plate

$$K_m(\theta) = \sigma_m \sqrt{\pi a}\, Y_m(\theta)$$
$$K_b(\theta) = \sigma_b \sqrt{\pi a}\, Y_b(\theta) \qquad (3)$$

where Y_m and Y_b are the total correction factors for a surface crack in an infinite plate under a pure membrane load and under a pure bending load, respectively, and θ is the angle in parametric equations describing the position along the crack front starting from the free surface. The total SIF is the sum of the SIF due to bending and membrane load components. Note that membrane stress here also implies uniform tensile stress.

To apply these formulas, the stress along brace and chord intersection of a tubular joint is assumed to be split into membrane and bending components:

$$\sigma = \sigma_m + \sigma_b \quad (4)$$

However, the actual stress distribution is nonlinear due to severe stress concentration along the weld toe on the outer surface.

In Reference 37, Equation 2 was modified by introducing several factors to consider the influence of weld geometry (M_k), non-uniform stress field over a through-thickness crack in a plate, and non-straight crack, etc. All these factors were based on 2-D analytical solutions.

Aaghaakouchak et el. [31] mentioned that it seemed reasonable to apply flat plate solutions for analysis of relatively deep (i.e. a/T > 0.2) cracks in tubular joints. Equation 2 was used to calculate the SIF for cracks in tubular T and Y joints. The tensile σ_m and bending σ_b stresses for several configurations were calculated by decomposing the hot-spot stress using the ratio of bending to membrane stress. A correction factor was introduced for moment redistribution as a crack grows in an indeterminant structure. Some comparative study [31] indicated that the SIF for a semi-elliptical crack at the weld toe subjected to a normal tension or bending are significantly different from a similar crack in a flat plate under the same nominal loading when the relative crack depth (a/T) is < 0.2.

Hsu [38] modified Scott and Thorpe's solution by applying two correction factors, M_k and M_c. The M_k factor, similar to the existing notch correction factor, accounts for the influence of local weld toe geometry. The M_c factor accounts for stress variation around the tubular weld connection. The finite element method (2-D constant strain

elements) was used for the calculation of M_k, and 3-D finite element stress analysis for the M_c calculation.

Scott and Thorpe's formula was also used in Reference 39. The influence of the weld geometry was taken into account by a magnification factor $M_k > 1.0$. A fictive crack length was added to the actual crack length for the stress intensity factor calculation, since small cracks at a notch tend to grow faster than the rates predicted by the Paris equation. However, the values of M_k were from those determined for a constant depth surface crack (a/c = 0) instead of a semi-elliptical crack. The actual structure is a shell intercepted by another shell. The M_k values were for a tensile loaded plate type structure. For plate bending, the M_k values may be different. Furthermore, the influence of the plate width was not taken into account.

Recently, Stacey [40] applied the Newman and Raju solutions of the SIF, in conjunction with 2-D finite element stress analysis, to fatigue assessment of a tubular joint. He indicated that realistic predictions could be obtained using SIF solutions for tubular joints, and a considerable amount of further work in this area is required.

Weight Function Methods

Rice [41] described a weight function method to calculate the stress intensity factor K_I for a through-thickness crack in a plate under symmetrical loading. The weight function method was further studied in References 42 and 43 for some particular cracks in infinite solid and for crack in plates. In order to apply this weight function method, a reference analytical solution must be known for the stress intensity factor K_r and the

crack opening displacement field $u_r(x,y)$ in the plate for a reference load. The difficulty is that only a few solutions for the crack opening displacement field are available, though there are many K_I solutions.

Based on the general weight function concept [42], Oore and Burns [44] studied the weight functions for embedded planar cracks in infinite 3-D solids with known solutions, and proposed that these weight functions could be written in the following general form:

$$W_{QQ'} = \frac{\sqrt{2}}{\pi l_{QQ'}^2 \left(\int_s \frac{ds}{\rho_Q^2}\right)^{1/2}} \tag{5}$$

where, as shown in Figure 5, Q′ is the location where K_I is desired, and Q is the application point of load P, a pair of symmetric opening forces. The length $l_{QQ'}$ and ρ_Q are the distance between Q and Q′, and the distance from Q to the centroid of an elemental length ds along the crack boundary, respectively. Therefore, using the weight function $W_{QQ'}$ at each point on the surface of a crack, and the stresses at the crack location in the fictitiously uncracked material, one can calculate the stress intensity factor K_I from the area integral:

$$K_I(Q') = \int_A \sigma_Q W_{QQ'} dA \tag{6}$$

where dA denotes an infinitesimal element of crack surface area centered at Q.

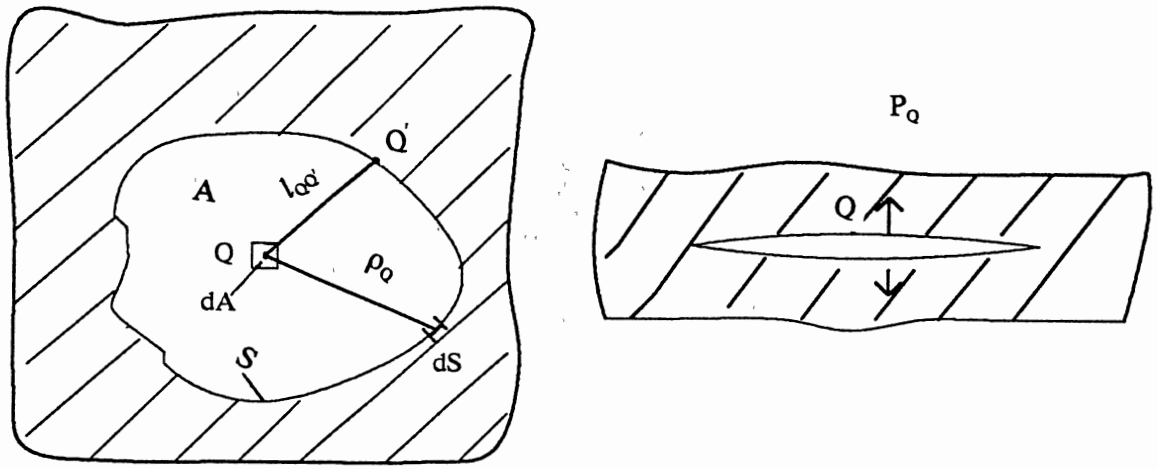

Figure 5. Crack Embedded in an Infinite Solid

The resulting stress intensity factor K_I at Q′ due to a concentrated load P at point Q is given by

$$K_{Q'} = P_Q W_{QQ'} \tag{7}$$

It has been shown [44] that the integral in Equation 6 could be used to obtain K_I for a variety of embedded cracks under normal loading compared with published K_I solutions available. Equation 6 is also referred to as the O-Integral. Except for the embedded circular crack, and embedded infinitely long straight fronted crack, numerical quadrature techniques must be used to solve Equation 6.

The weight function method has been used to obtain the stress intensity factors for surface cracks in tubular joints in several references [45-47]. In order to apply Equation 5 to surface cracks, the following assumption was made:

$$\frac{K_{surface}}{K_{embedded}} = constant = M_f \tag{8}$$

where it is postulated that M_f is independent of the applied stress field. Formulas by Newman and Raju [35] and others [48] can be used to obtain $K_{surface}$ for a semi-elliptical surface crack in a plate under uniform tension. $K_{embedded}$ is the SIF for the corresponding elliptical crack in an infinite, uniformly stressed solid [49].

Several alternatives have been proposed on the basis of surface correction and simplification of stress distribution along the tubular weld toe. With the stresses measured on the inner and outer tube surfaces, stress through the thickness is divided into bending and membrane stresses as in Equation 4. Using this information and a hot-spot stress range (σ_h) assumed constant around the intersection (weld toe), one can model the through-thickness stress distribution. However, this assumption makes no account for decreasing stress field along the intersection away from the hot-spot stress site. An average stress distribution was derived [50] by

$$S_{Av} = \frac{1}{\pi}\int_0^{\pi} S(\varphi)\,d\varphi \tag{9}$$

for axial and Out-of-Plane Bending (OPB), and

$$S_{Av} = \frac{1}{\pi}\int_{-\pi/2}^{\pi/2} S(\varphi)\,d\varphi \tag{10}$$

for In-Plane Bending (IPB). $S(\varphi)$ is the stress concentration factor as a function of the

angular position around the intersection (Figure 6). It is said that this average stress distribution places too much emphasis on the stress distribution away from the hot-spot stress site. Dover and Connolly [47] used an exponential function to provide an average stress weighted for the distance from the hot spot stress site.

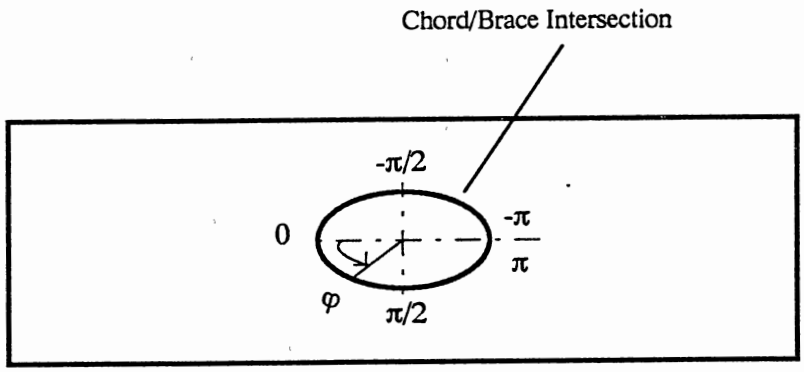

Figure 6. Angular Position around Chord/Brace Intersection

Forbes et al. [51] critically reviewed several weight function methods. Stress intensity factors for semi-elliptical surface cracks in butt-welded T-joints have been obtained using these weight functions. They mentioned that Equation 8 significantly underpredicted K_I when bending contribute more than 25% of the stress at the crack's originating surface. To take into account this effect, an improved surface correction scheme was proposed for the application of Equation 6.

Line Spring Element Methods

Rice and Levy [52] proposed the concept of line springs for a plate containing a part-through surface crack under bending and tensile loading. The line spring element method is a relatively easy approximation technique for assessing a surface crack in a plate or shell structure. As Rice and Levy stated, the approximation relies heavily on the known solution for an edge cracked strip in plane strain (Figure 7), subjected to an axial force N and moment M per unit length in the direction of plane-strain constraint.

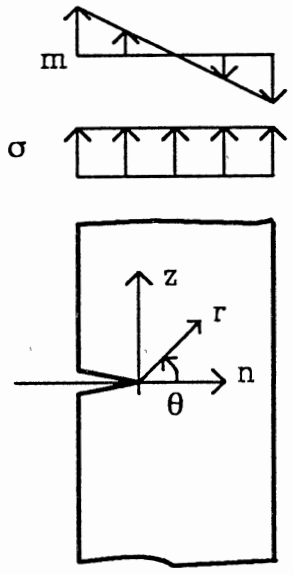

Figure 7. Edge Cracked Strip of Plain Strain

To determine the SIF (K_I only) at points along the crack front, the force and moment transmitted across the cracked section are needed. These forces and moments are obtained through the simple approximate theories of generalized plane stress and Kirchhoff-Poisson plate bending, applied in conjunction with a representation of the surface crack as a continuously distributed line spring with compliance coefficients chosen to match the compliance of an edge cracked strip in plane strain. For a given net force and moment on the strip (Figure 7), the presence of the crack will cause the displacement and rotation of one end relative to the other to increase over the values which would result in an uncracked strip. The increased compliance due to the crack is lumped into the continuously distributed spring. Line spring elements have been incorporated into the ABAQUS [53] finite element program.

Brown [54] mentioned that calibration of the line spring method for a surface-flawed plate in tension was done against the results of Raju and Newman [55]. The resulting distribution of K_I along the crack was overestimated with reference to the results of Raju and Newman. A calibration factor must be applied. However, Brown did not present any data relevant to the line spring element method.

The adaptation of line spring elements to a tubular joint was made for simple joint types by Kim et al. [56] and Huang et al. [57]. Recently, Rice's line spring element method was modified by Kim et al. [28] to calculate the mixed mode stress intensity factors, K_I, K_{II} and K_{III}. Following Rice's assumption, additional displacements are extended for rotations and shear deformations to other axes for an inclined surface crack as shown in Figure 8. Twisting effect on displacement components in t and z directions ($\delta 1$ and $\delta 2$), and in-plane bending moment, are not considered. A circumferential cracked

tube was analyzed using the line spring element method, and compared with Raju and Newman solution [58]. The agreement is good at the deepest crack point when the radius becomes large. However, no SIF value was given at the crack surface point. The SIFs of a surface crack at the crown of a T tubular joint were also given.

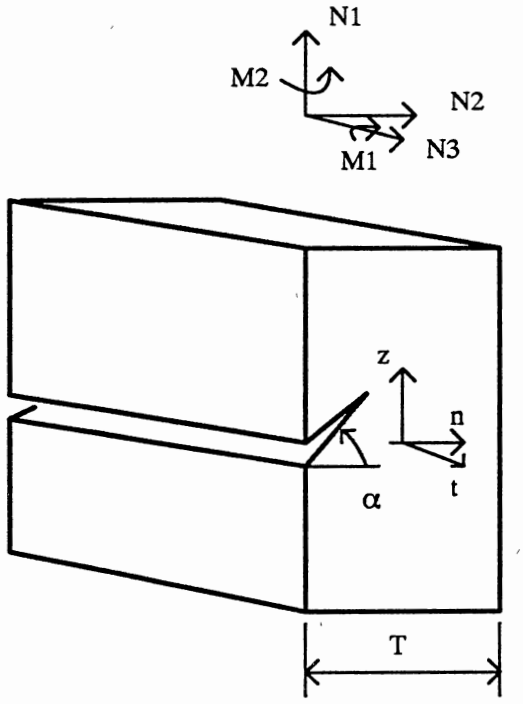

Figure 8. Edge Strip with an Inclined Surface Crack

Other Simplified Methods

In the experimental method [59-61], the mode I stress intensity factor K_I for a crack in a tubular joint is written as

$$K_I = Y\sigma\sqrt{\pi a} \tag{11}$$

where a is the crack depth or half length, σ is the applied stress, and Y is a correction factor.

A typical material crack growth curve can be generated by fatigue-testing small pre-cracked specimens. The Paris law is applied to relate the stress intensity factor range ΔK_I to the fatigue crack growth rate, as in Equation 1. In Reference 60, 'a' in Equation 11 represents crack depth at the deepest point along the crack front, and values C = 4.5×10^{-12} (with K_I in MPa$\sqrt{m}$), and m = 3.3. Therefore, ΔK_{exp} can then be found from the experimental da/dN data at various crack depths, and

$$Y_{exp} = \frac{\Delta K_{exp}}{\Delta\sigma\sqrt{\pi a}} = \left(\frac{1}{C}\frac{da}{dN}\right)^{1/m} / (\Delta\sigma\sqrt{\pi a}) \tag{12}$$

for any crack depth.

The experimental method is very expensive. Furthermore, the K_{exp} may not be the solution to the mode I stress intensity factor, since mixed mode fatigue crack behavior may exist along the tubular joint weld toe.

The Aptech method was used in a joint industry project [62]. This method applies a two-dimensional slice of the complex 3-D geometry present in a tubular joint to calculate the SIF K_I. These two-dimensional slices correspond with the AWS tubular joint weld details (ANSI/AWS D1.1.82). Finite element method was used in the 2-D slice with load and boundary conditions being selected such that the resulting stress distribution matched as closely as possible to empirical data and results from 3-D finite element

analyses of similar joints. Therefore, the flaw models assume that the cracks are infinitely long. No details of this method have been published because of its proprietary nature. A computer program (TJLIFE) using this method has been developed to assess the fatigue crack propagation life of typical tubular joints in offshore structures. The program was verified by data observed in tubular joint tests. At each location, the stress state is defined in terms of the uncracked hot-spot stress,membrane stress, and punching shear. This computer program cannot solve the through-thickness crack problem.

Kam and Vinas-Pich [63] mentioned a slice-displacement compatibility method, on the assumption that the global stiffness of tubular joints does not change until the deepest crack has penetrated the wall thickness. The slice compatibility method involves only a cross section containing the deepest point of the loading crack. All three modes of SIF can be obtained by using a thin three dimensional slice (Figure 9). The displacement field around the section is prescribed and obtained from the initial stress analysis of the joint. The slice compatibility method is still under development. The effect of section size and crack shape correction are not available.

Another 2-D finite element method to approximate K_I was proposed in Reference 64 on the assumption that an isolated part of a T-joint in the cracked area is in plane strain. Brown [54] applied a compliance approach to calculate K_I for through-wall cracks of different lengths. The final results for brace axial tension were

$$\left(\frac{K_I}{P}\right)^2 = \frac{\partial}{\partial a}\left(\frac{EC_{ax}}{2t}\right) \tag{13}$$

and for in-plane bending were

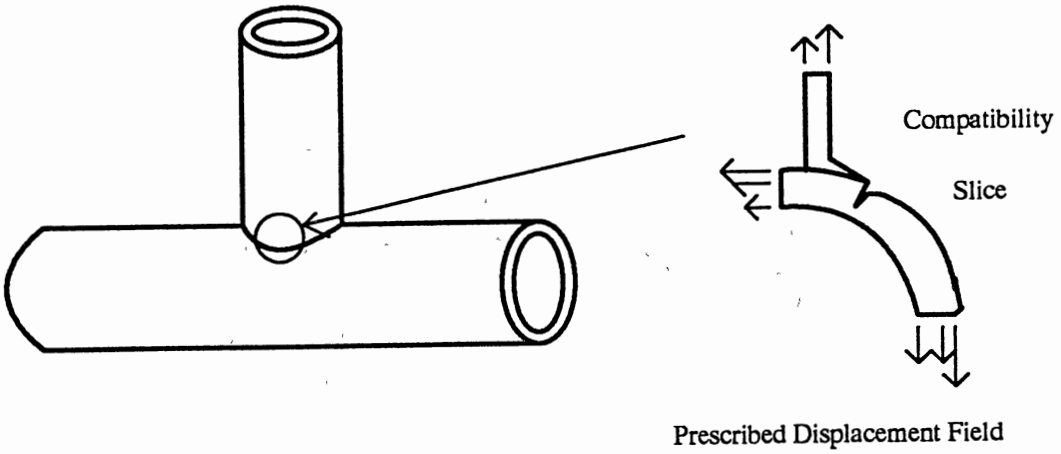

Figure 9. Schematic Diagram of Slice Compatibility Method

$$\left(\frac{K_I}{M}\right)^2 = \frac{\partial}{\partial a}\left(\frac{EC_\theta}{2t}\right) \tag{14}$$

where $C_{ax} = \delta/P$, with P = brace axial tension force, δ = average axial displacement of brace end; $C_\theta = \theta/M$, with M = brace in-plane bending moment, θ = average rotation of brace end; and E = Young's Modulus, t = tube wall thickness.

The exponent 2 was missing in Reference 54. It is important to note that the strain energy release rate for a mode I crack in a plane stress plate, $G = \partial U/\partial a$, was used in the derivation. It was also assumed that all the increased work input was used to drive the through-wall crack in pure mode I only. However, this is inappropriate when mixed mode crack growth is possible.

Rhee [1] also mentioned the virtual crack extension method [65,66], and the finite element alternating method [67-69] used for only plate T joints and cruciform weld plate

joints.

Concluding Remarks

As it can be seen from the previous sections, most simplified methods are developed by assuming that stress is linear across the tube wall-thickness containing the crack and by incorporating the influence of local weld-toe geometry into the SIF solutions for a surface crack in a plate. It is usual to ignore any crack curvature in the wall-thickness or along the weld toe direction.

There are several problems inherent in the application of a simplified method. The first major one is in the handling of shear stresses. Since most of these methods are suitable for tensile stress only, destructive shear stresses which are common at the crack location of a tubular joint are ignored. The second problem is that no known SIF solutions are available to cracks with warped crack surfaces. Thirdly, there exists a difficulty that results from the arbitrariness of the stress distribution and the three dimensionality of the local stress common at the joint weld toe crack. Consequently, the SIF solutions based on simplified methods can contain significant uncertainty.

The most rigorous among these simplified methods is the modified line spring element method [28] used for a T-joint fatigue analysis. Although this method employs mixed mode line spring elements to calculate the mixed mode SIF of the joint weld toe crack, the line spring element is based on the assumption that only plate and shell types of stress states exist along the crack growth path. The line spring element may not be suitable for the determination of the stress state in the weld toe area.

Three-Dimensional Finite Element Method

Due to its current development as an engineering analysis technique, the finite element method (FEM) is the most practical and reliable approach to obtain the SIFs for tubular joint weld toe cracks. Although 3-D finite element analysis was perceived in the past as prohibitively expensive in the industry, it has been indicated to be practical for many classes of tubular joint integrity problems. A fatigue crack growth study was performed for an X-shaped tubular joint under tension loading in Reference 70. Fracture mechanics fatigue life estimation procedures have been developed for offshore structural tubular joints through analyzing a K-joint under the North Sea environment in Reference 27.

Among the various finite element procedures [8,9,71,72] for the SIF solutions, two different approaches can be identified. One is the direct method in which the stress intensity factor solution follows from the stress field or from the displacement field near a crack [5]. The second is an indirect method in which the SIF solution is obtained through its relation with other quantities such as compliance, the elastic energy, or the J-integral as commonly discussed in many text books [4,5,73-75]. However, for problems of mixed mode fracture, the indirect method usually does not allow a distinct separation of the stress intensity factors K_I, K_{II} and K_{III}.

In the early works of FEM, an element with an embedded singularity was developed for elastic problems by Wilson [76] and for elastic-plastic crack problems by Hilton and Sih [77]. This method directly incorporates both the finite element method and the analytical crack tip displacement expansions, and requires special analysis computer

programs. On the other hand, a number of hybrid finite elements with embedded singularities [78,79] have also provided well documented FEM approaches to calculate the SIFs for a crack in three-dimensional structures. Since no commercial computer program with hybrid elements is readily available on the current market, the hybrid finite element techniques are not practical for engineering applications.

The displacement-based FEM programs available on the market provide a very versatile and reliable numerical tool when the quarter-point crack tip element [80-82] is utilized. In this element, the appropriate crack tip square root singularity can be achieved by locating the mid-side nodes near the crack tip of a collapsed isoparametric element at the quarter point position. Ingraffea and Manu [83] developed a consistent method for computing stress intensity factors from three-dimensional quarter-point element nodal displacement. This method permits functional evaluation of the SIFs along the crack front. Embedded, surface, and corner cracks with flat crack surfaces were analyzed successfully using the method.

Only recently the quarter-point finite element method has been used to calculate the mixed mode SIFs for tubular joint weld toe crack with a curved crack front [6] or with a warped crack surface and curved crack front [10]. The method in Reference 6 is a special case of that in Reference 10 which is the most versatile among the direct three-dimensional finite element methods.

Limited SIF solutions using this method through the TUJAP system was compared with those inferred from experimental fatigue crack growth behavior in a large scale offshore tubular T-joint specimen under brace tension loading [84]. The experimental data was from stage of primarily mode I crack growth. The agreement between the

calculated and inferred stress intensity factors is generally very consistent and gives considerable confidence in the finite element fracture mechanics method to predict fatigue crack growth accurately in tubular joints.

CHAPTER III

FRACTURE MECHANICS BEHAVIOR OF WELD TOE DEFECTS OF TUBULAR JOINTS

Concept and Procedure

The fundamental principle of linear elastic fracture mechanics is that the stress field or displacement field ahead of a sharp crack in a structural member can be characterized in terms of a single set of parameters, K_I, K_{II}, and K_{III}, the stress intensity factors. They are functions of sizes and shapes of the crack and structural member, and the nominal stress. Each of these three SIFs corresponds to a type of relative movements of two crack surfaces as shown in Figure 10. These displacement modes represent the local deformation in an infinitesimal element containing a crack front. Each of these modes of deformation corresponds to a basic type of stress field in the vicinity of crack front. In any problems the deformations at the crack front can be treated as one or a combination of these local displacement modes. The concept of small-scale yielding and the existence of a "K dominant" region forms the modern view of linear elastic fracture mechanics [4]. For a given material, the susceptibility of a structural member with crack-like defects to fracture and fatigue is determined by the SIFs.

The displacement field in the vicinity of a point along the crack front under mixed modes are given by [5, 85],

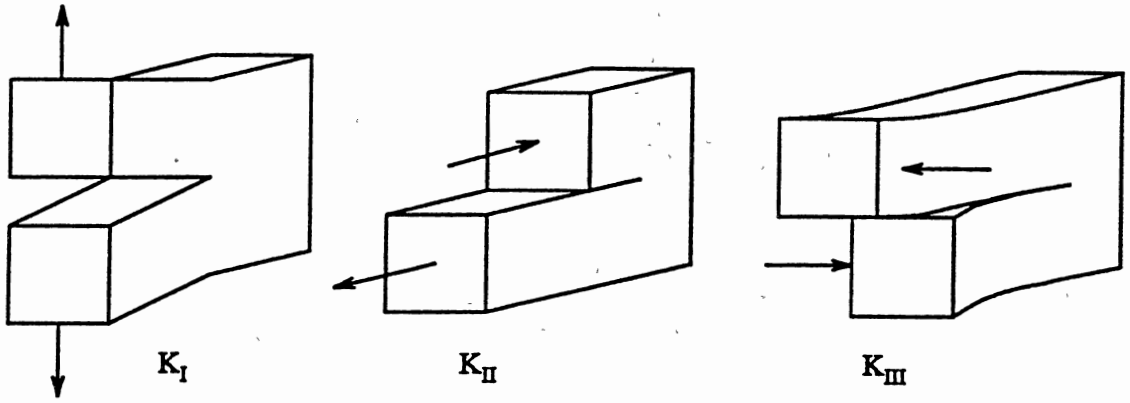

Figure 10. The Three Basic Modes of Crack Surface Displacements

$$\begin{bmatrix} u' \\ v' \\ w' \end{bmatrix} = \frac{(1+\nu)\sqrt{2r}}{E\sqrt{\pi}} \begin{bmatrix} c[(1-2\nu)+s^2] & s[2(1-\nu)+c^2] & 0 \\ s[2(1-\nu)-c^2] & -c[(1-2\nu)-s^2] & 0 \\ 0 & 0 & 2s \end{bmatrix} \begin{bmatrix} K_I \\ K_{II} \\ K_{III} \end{bmatrix} + O(r) \tag{15}$$

where E and ν are Young's modulus and Poisson's ratio, respectively, $c = \cos(\theta/2)$, and $s = \sin(\theta/2)$; u', v', and w' are the displacement components in the crack front local coordinate system. This equation can also be written in short form as,

$$\underline{u}' = \sqrt{r}\underline{B}\underline{K} + O(r) \tag{16}$$

The components σ_{ij} of the crack tip stress field are representable in the form [85-87],

$$\sigma_{ij} = \frac{1}{\sqrt{r}}[K_I f_{ij}^{I}(\theta) + K_{II} f_{ij}^{II}(\theta) + K_{III} f_{ij}^{III}(\theta)] + O(r) \tag{17}$$

where $f_{ij}^{I}(\theta)$, $f_{ij}^{II}(\theta)$, and $f_{ij}^{III}(\theta)$ are dimensionless functions that correspond to modes I, II and III, and depend on the orientation angle θ only. These field equations show that the distributions of the elastic-stress fields and of the deformation fields in the vicinity of the crack tip are invariant in all components subjected to a given mode of deformation and that the magnitudes of these fields can be described uniquely by the stress intensity factors.

The crack local displacement vector $\underline{u} = [u, v, w]^T$ in global coordinate directions along a crack tip radial line (A-B-C, as shown in Figure 11) direction in a collapsed 3-D quarter point element has been shown [6,10] to be,

$$\underline{u} = \sqrt{r/l}\,\bar{\underline{u}} + O(r) \tag{18}$$

where

$$\bar{\underline{u}} = \begin{bmatrix} 4u_B - 3u_A - u_C \\ 4v_b - 3v_A - v_C \\ 4w_B - 3w_A - w_C \end{bmatrix}$$

with l being the arc length of AC, u_i, v_i, and w_i (i = A, B, C) being the ith nodal displacements in the global X, Y, and Z coordinate directions, respectively. The stress field of Equation 17 is realized only when the collapsed nodes at each location of the quarter point element are constrained to have the same displacements. The displacements $\underline{u}$ can be transformed into those in crack-tip local coordinate system (n, z, t) displacement $\underline{u}'$ as

$$\underline{u}' = \sqrt{r/l}\,\underline{R}\bar{\underline{u}} + O(r) \tag{19}$$

where $\underline{R}$ is the coordinate transformation matrix between the global X, Y, Z and the crack-tip n, z, t systems.

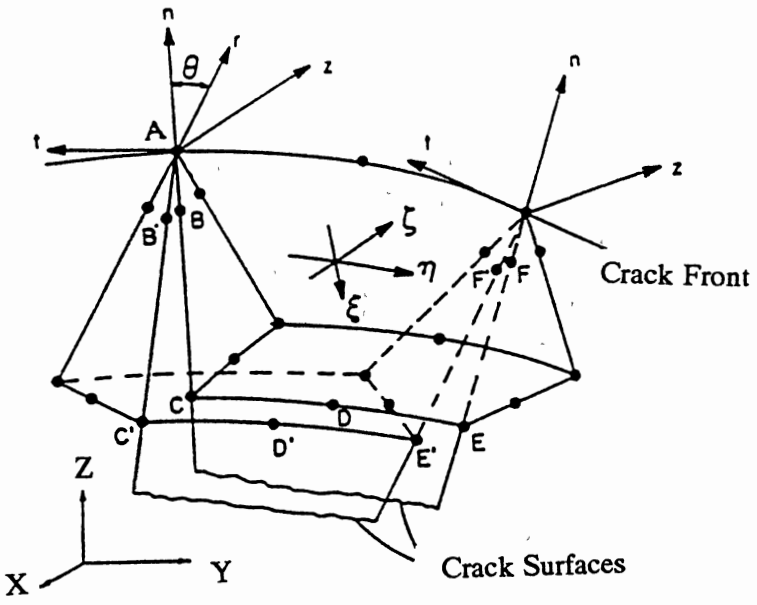

Figure 11. Crack-Tip Radial Line in Quarter Point Element

Comparison of Equations (16) and (19) leads to [6, 10],

$$\underline{B}\underline{K} = \frac{1}{\sqrt{l}}\underline{R}\bar{\underline{u}}$$

or

$$\underline{K} = \underline{D}\underline{R}\bar{\underline{u}} \tag{20}$$

where

$$\underline{D} = \frac{E}{d(1+\nu)}\sqrt{\frac{\pi}{2l}}\begin{bmatrix} c[(1-2\nu)-s^2] & s[2(1-\nu)+c^2] & 0 \\ s[2(1-\nu)-c^2] & -c[(1-2\nu)+s^2] & 0 \\ 0 & 0 & d/2s \end{bmatrix}$$

with $d = c^2[(1-2\nu)^2 - s^4] + s^2[4(1-\nu)^2 - c^4]$. Along an element boundary line with = 0°, K_{III} cannot be calculated from Equation 20, because of $s = 0$ with $\theta = 0°$. The SIF can be calculated from any crack tip radial directions. In this work, θ = -180°, -135°, -90°,

-45°, 0°, 45°, 90°, 135°, and 180° have been used. Young's modulus E is 210,000 MPa, and the Poission's ratio ν is 0.3 for the steel tubular joints.

A user-friendly computer program, KAARL [12], has been developed based on this procedure to convert the common finite element displacement solutions to the SIF solutions for complex crack and joint geometries. KAARL calculates the fully mixed mode SIFs along arbitrarily selected crack-tip radial lines. It can also generate plots of the SIF solutions using the DISSPLAY [88] graphics package. Various debugging features are built into KAARL program so that the SIF solution and its intermediate results can be checked.

Stress Distribution in Tubular Y-Joints

In order to obtain stress distribution information along the chord/brace intersection without defects under brace axial tension and in-plane bending, two Y-joints with different brace diameters (Table 1) were analyzed. In Table 1, the chord diameter is D = 1000.0, θ = 60°, and the chord and brace lengths are 6000 and 3000. The length unit is mm.

One of the Y-joint finite element models is shown in Figure 12. Both of the chord ends were fixed. The weld zone was modeled using 20-noded solid elements. The weld profiles were constructed according to the AWS specification for full penetration from one side (ANSI/AWS D1.1.82). The weld is somewhat larger than the AWS minimum requirement, primarily to maintain the continuity around the chord/brace intersection curve. The default profile was used, and the minimum gap between the two steel parts was set to 4 mm. Other parts of the tubular joint mesh were modeled with 8-noded

thick-shell elements. Transition elements between the 20-node and 8-node elements were also utilized.

TABLE 1

Y-JOINTS WITH DIFFERENT BRACE DIAMETER

β	d	t	T
0.6	600.0	21.7	33.3
0.8	800.0	21.7	33.3

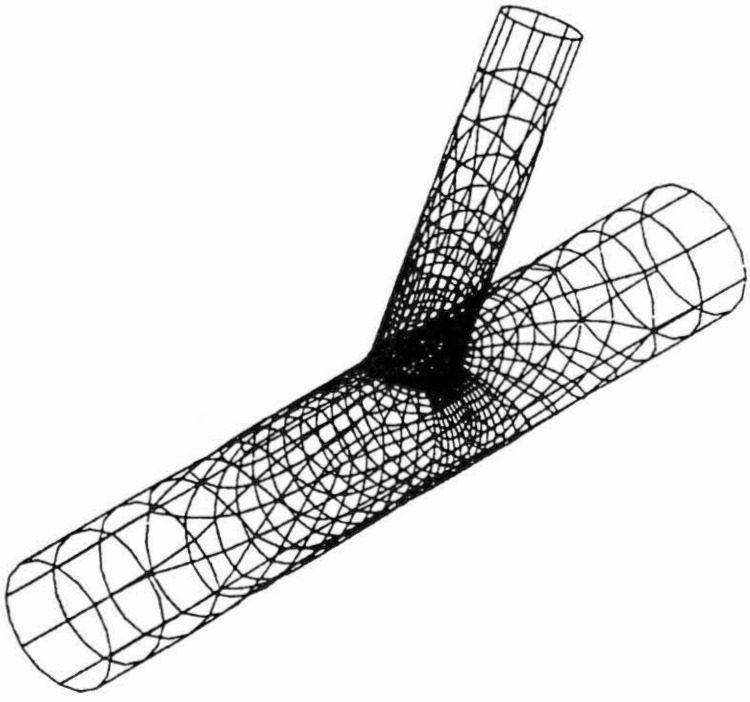

Figure 12. Typical Finite Element Model of Y-Joint

A general purpose FEM post-processor, POSTFEM [89], was used to obtain the stress distributions. The stress concentration factor (SCF) at a point is defined as the point maximum principal stress (in magnitude) divided by the nominal stress at the brace end, as given in Table 2.

TABLE 2

DEFINITION OF NOMINAL STRESSES

Loading Mode	Nominal Stress
Axial Tension (AT)	$\sigma_N = \frac{P}{A}$
Out-of-Plane Bending (OPB)	$\sigma_N = \frac{dM_o}{2I}$
In-Plane Bending (IPB)	$\sigma_N = \frac{dM_i}{2I}$
In-Plane Shear (IPS)	$\sigma_N = \frac{P_i}{A}$
Out-of-Plane Shear (OPS)	$\sigma_N = \frac{P_o}{A}$
Torsion (TOR)	$\sigma_N = \frac{dM_T}{2J}$

where $A = \frac{\pi}{4}(d^2 - (d - 2t)^2)$, $I = \frac{\pi}{64}[d^4 - (d - 2t)^4]$, $J = 2I$,

and P = AT force, M_o = OPB moment,
M_i = IPB moment, P_i = IPS force,
P_o = OPS force, M_T = TOR moment,
d = brace outer diameter, t = brace wall-thickness.

Unit of force: N
Unit of moment: N•mm
Unit of length: mm

Figure 13 shows the SCF distributions on the outer surface of the chord/brace intersection of two Y joints (β = 0.6 and 0.8) under brace axial tension. The two curves in this figure confirm the well known fact that the hot spot under brace axial tension is near the weld toe saddle.

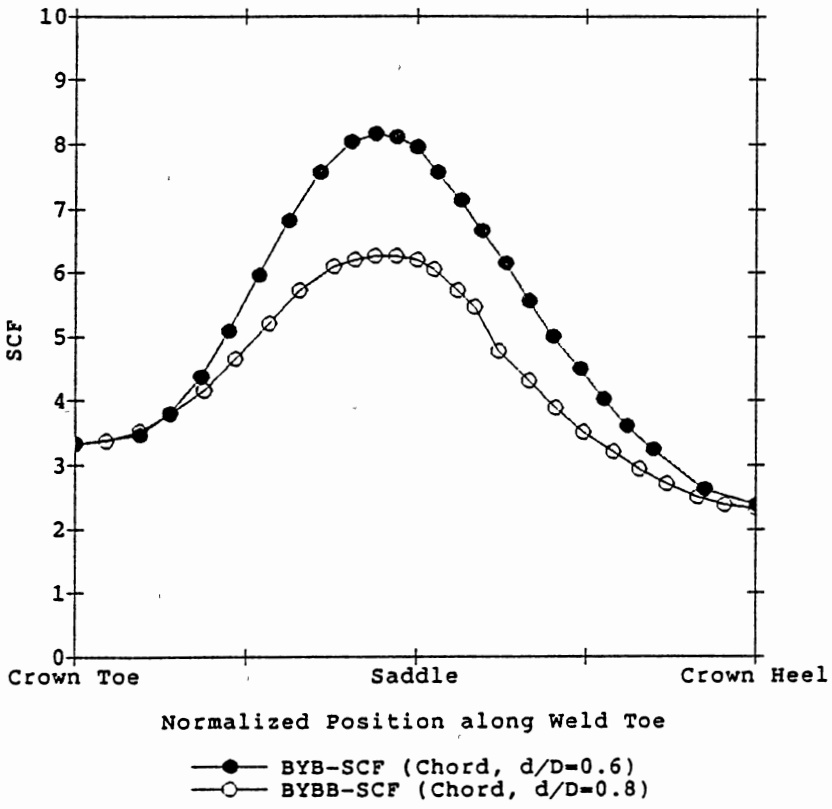

Figure 13. SCF Distributions under Brace Axial Tension

Figures 14 and 15 are the SCF distributions on the outside and inside surfaces of the intersection under brace in-plane bending (IPB), respectively. The hot spot is near the crown toe and the crown heel. The SCF at the toe is slightly greater than that at the heel. The effect of brace diameter is not significant, though the SCF for $\beta = 0.8$ is a little less than that for $\beta = 0.6$. However, the hot spot on the inner surface of the chord/brace intersection is near the mid-point between the crown toe and the saddle, since the state of the stress in the intersection is three dimensional.

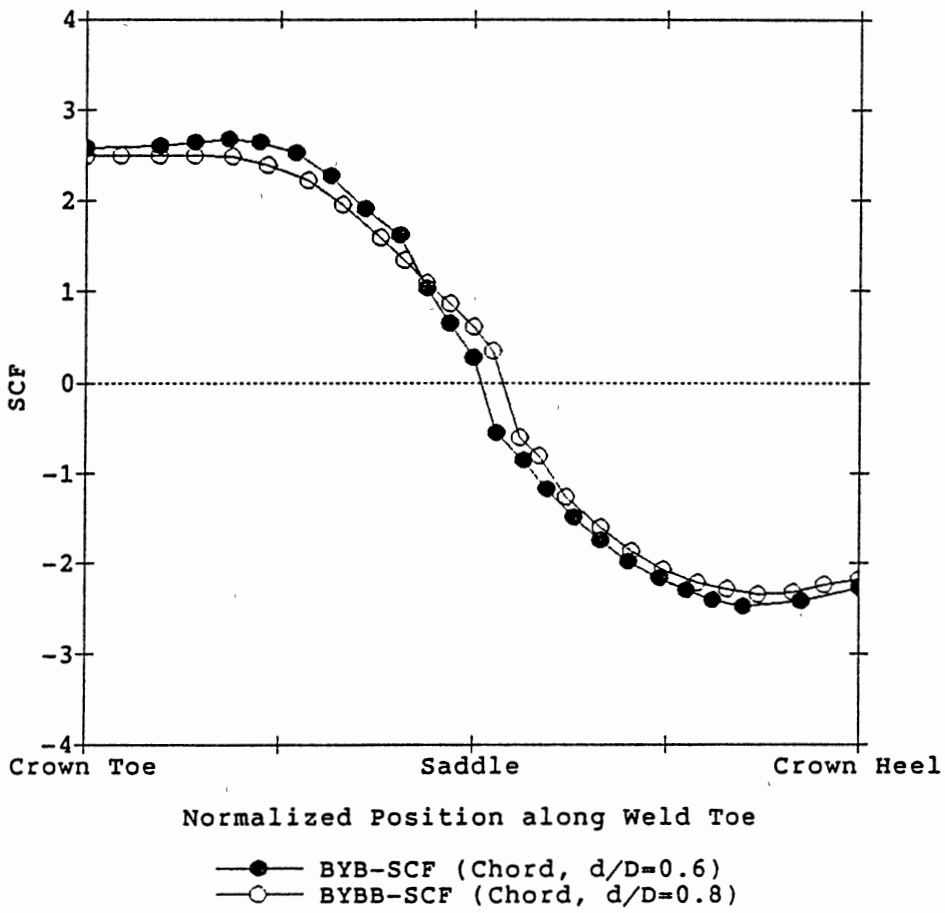

Figure 14. SCF Distributions of Two Y-Joints under In-Plane Bending

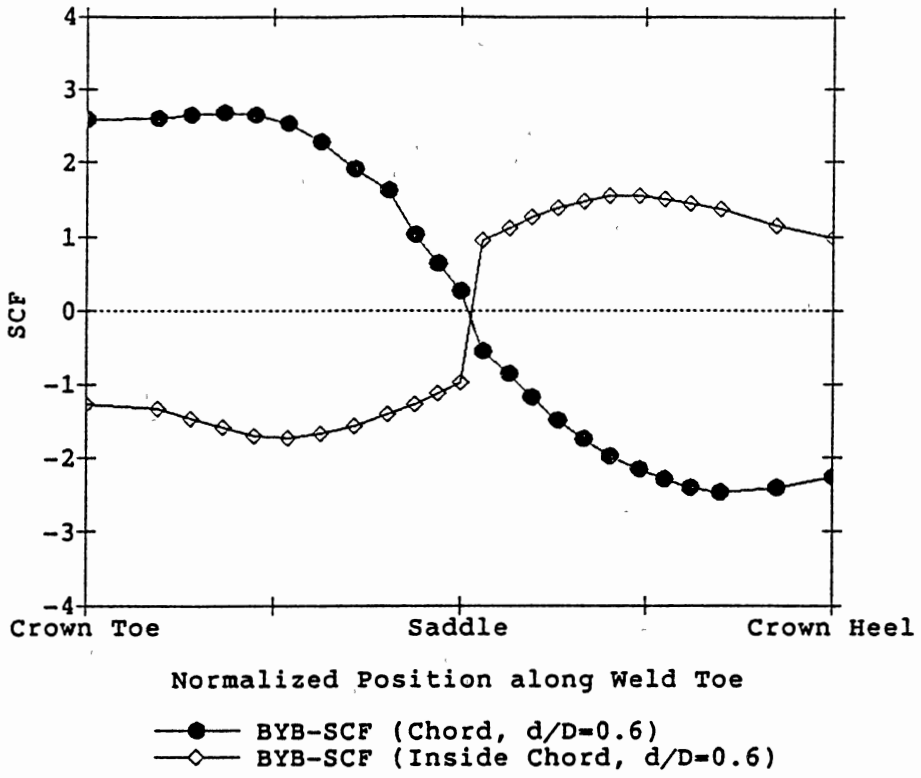

Figure 15. Inner and Outer Surface SCF Distributions

Figure 16 shows the SCF distribution in the chord wall-thickness direction, at the crown toe, saddle point and the crown heel locations, respectively, under brace axial tension (AT). The SCF distribution in the chord wall is not linear due to the high stress concentration on the outer chord surface.

Figure 17 shows the SCF on the outside surface of the brace and chord weld toes for the Y joint with $\beta = 0.6$ under brace axial tension. A similar trend is found for the SCF on the outside surface of the chord and brace weld toes of the Y joint with $\beta = 0.8$. The SCF on the chord side surface is higher than that on the brace side surface.

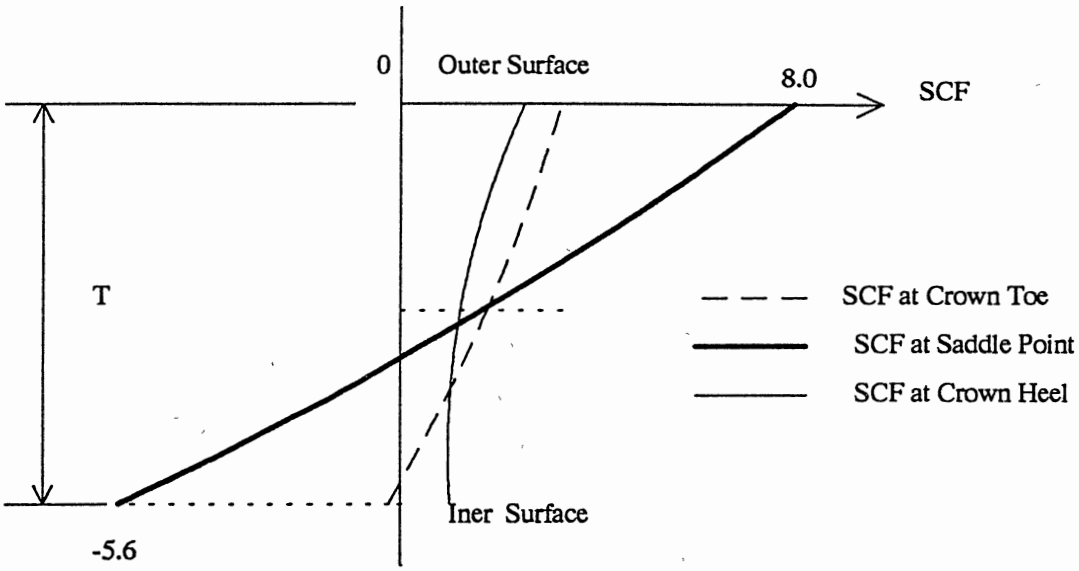

Figure 16. SCF Distributions in Chord Wall-Thickness

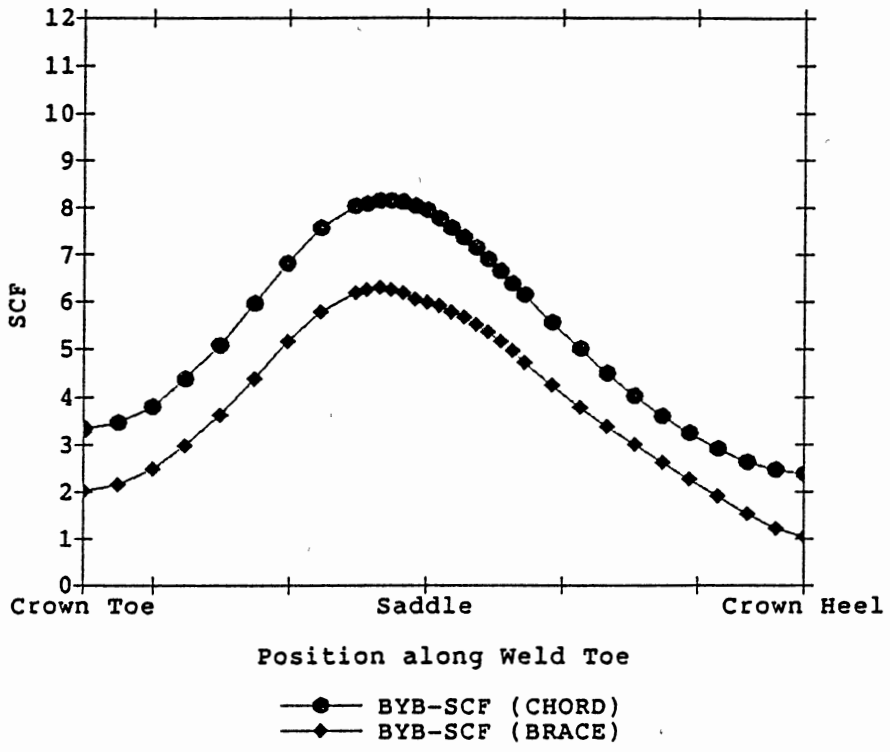

Figure 17. SCF Distribution on Brace and Chord Outer Surface

The comparison of the SCF on the brace side weld toe between the two Y joints (β = 0.6 and 0.8) under brace axial tension is shown in Figure 18. At most locations along the weld toe, the SCF of the smaller brace diameter (β = 0.6) is greater than that for the large brace diameter (β = 0.8).

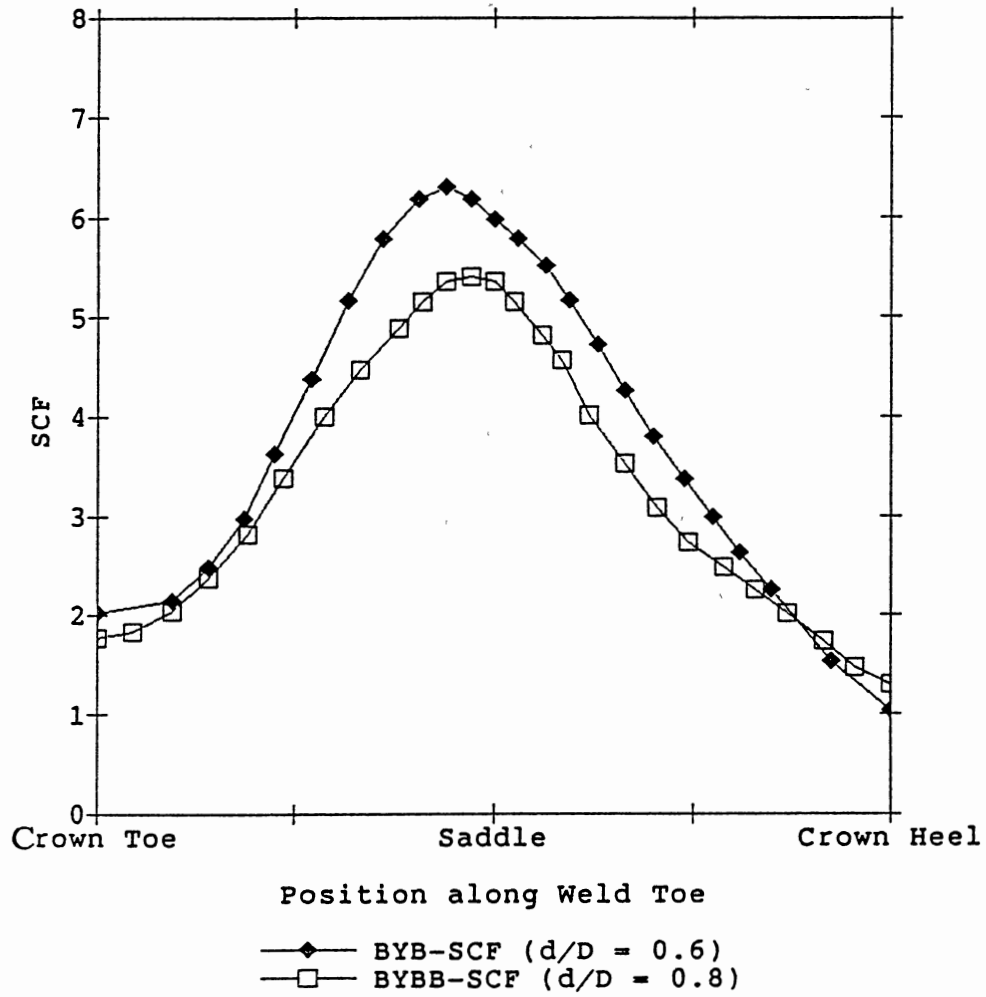

Figure 18. Brace Side SCF of Two Joints

Surface Crack-like Defects Along the Weld Toe

A significant amount of SIF solutions for various surface weld toe cracks of Y- and K-joints have been developed in this work. These solutions provide insights for the understanding of the weld toe defect behavior of tubular joints and can also clarify confusion of the tubular joint fracture behavior in the offshore industry. This chapter summarizes the obtained data and discusses their implication in the tubular joint fracture mechanics problem. As parameters indicating the status of the complex stress distributions along the crack front of a surface crack, these SIF solutions are intended to be guiding parameters to understand the physical behavior of cracked tubular joints with similar configurations to those analyzed.

The following six different problems of the tubular joint fracture mechanics were investigated. Tubular Y joints (Figure 2) were chosen for this investigation.

- Surface cracks at the Y-joint saddle to understand the behavior of shallow and deep weld toe cracks in common tubular joints.
- Comparison of the stress intensity factor solutions of cracks on the chord and brace to understand the differences of the fatigue behavior of the chord and brace of a joint.
- Study of the stress intensity factor solutions between joints with a single crack and double cracks to assess the joint stiffness effects on the stress intensity factor solutions.
- SIFs of surface cracks at crown toe, saddle point, and the middle point between the crown heel and the saddle to study the crack location effect.

- An identical surface crack on the saddle of various Y-joints to investigate the joint dimension and geometry effect.
- Mixed mode stress intensity factor solutions to understand the mixed mode behavior of tubular joint weld toe cracks under complex loading and geometric conditions.

For all models, the crack region was modeled with solid 20-node elements. Crack tip singular quarter-point elements [81] were used around and along the crack front to simulate the crack tip singular stress behavior accurately. More than 450 solid elements were generally used to model the crack region. Other parts of the tubular joint were modeled as those in the stress analysis mentioned in the previous session. The number of the 8-node shell elements in the joint model is generally more than 900. The boundary conditions used depend on the analyzed models. The chord and brace lengths in the previous section were used. Different brace loading cases, i.e., axial tension (AT), in- and out-of-plane bending (IPB and OPB, respectively), in- and out-of-plane shear forces (IS and OS, respectively), and torsion (TOR) were applied in each finite element analysis. Owing to the voluminous data generated from these analyses, only typical results (those of AT and IPB) are discussed. Discussion of the results corresponding to each of the above six issues is given in the following section.

Small and Large Cracks

To study the stress intensity factor behavior for various surface cracks, a single Y-joint was used in the analyses with cracks of different sizes at the joint saddle. The dimension of the Y-joint and a typical finite element mesh pattern in the crack region are shown in Figure 19. The chord was fixed at its both ends.

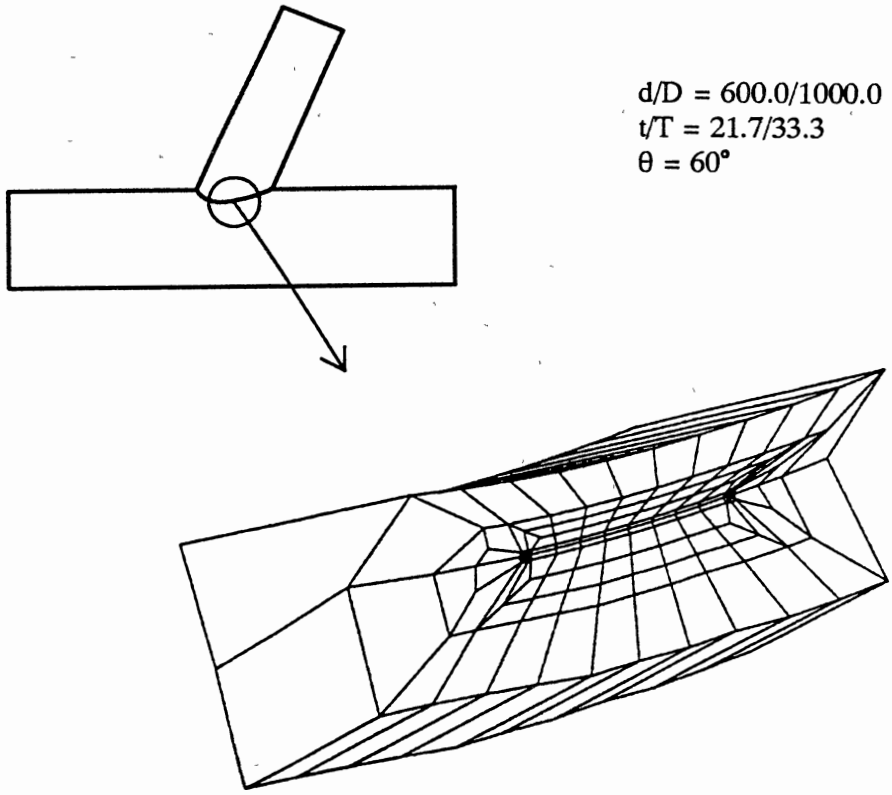

Figure 19. Y-Joint Sizes and Finite Element Mesh of a Weld Toe Crack

Twelve different sizes of cracks were analyzed, one at a time. The parametric values of these cracks are given in Table 3, while Table 4 lists the real dimensions of crack depth (a) and half crack length (c). The symbols S1, S2, ..., S6, and L1, L2, ..., L6 are the names of analysis models, respectively, for small and large cracks. Large and small cracks are modeled similarly with PRETUBE. When the crack is very deep, e.g., a/T =

0.80, one extra layer of elements over the crack front was used to obtain a refined and balanced mesh in the top part of the crack region. For the convenience of data presentation, a normalized SIF is used. Let K_1, K_2, and K_3 (or simply K1, K2 and K3 for convenience in some of the figures) denote the normalized SIF, which is dimensionless and defined as $K_i/(\sigma_N\sqrt{\pi a})$, where K_i is the SIF value (in $MPa\sqrt{mm}$) of Mode I, Mode II, and Mode III, respectively. The nominal brace stress σ_N is defined in Table 2 and a is the crack maximum depth.

TABLE 3

SURFACE CRACKS IN PARAMETRIC VALUES

$\left(\frac{a}{T}, \frac{a}{c}\right)$

a/T \ a/c	0.40	0.30	0.20	0.10
0.05		S1		S4
0.12		S2		S5
0.20	L1	S3	L4	S6
0.50	L2		L5	
0.80	L3		L6	

In this dissertation, symbols K_{1a}, K_{2a}, and K_{3a} (or K1a, K2a and K3a) denote, respectively, the normalized SIF of modes I, II and III at the crack deepest point, while K_{1cL}, K_{2cL} and K_{3cL} (or K1cL, K2cL and K3cL) represent those at the left crack end as shown in Figure 1, respectively.

TABLE 4

CRACK DEPTH AND HALF CRACK LENGTH (mm)

c / a	5.50	13.20	16.67	22.00	33.35	40.00	41.67	66.65	66.70	83.35	133.33
1.67	S1		S4								
4.00		S2				S5					
6.67			L1	S3	L4				S6		
16.67							L2			L5	
26.67								L3			L6

Under Axial Tension (AT). For a constant crack depth an increase in the half crack length (c) leads the crack surface ends away from the hot spot, the saddle region. Consequently, the normalized SIF at the crack end decreases with an increase in c, as shown in Figure 20 for a = 6.67 mm (Models L1, S3, L4 and S6 in Table 4). Note that in this figure, K_{2cL} and K_{3cL} are very low relative to K_{1cL}. Ratio c/d is used as the horizontal axis, where d is the brace diameter. For the SIF at the crack front center (the deepest point), Figure 21 shows that K_1 is dominant, and increases with c, because of the crack size effect on the SIF. The general trends of K_2 and K_3 are similar, but the rate of change is very low comparing to that of K_1.

Define $R_k = K_{1a}/K_{1c}$, the ratio of value of K_1 at the crack front center to that at the crack left end. Figure 22 shows the trend of R_k with crack half length (c), from $R_k < 1.0$, $R_k = 1.0$, to $R_k > 1.0$. When $R_k > 1.0$, the crack tends to grow faster in the wall-thickness direction than that along the weld toe. Figure 22 implies that for relatively long (c/d >

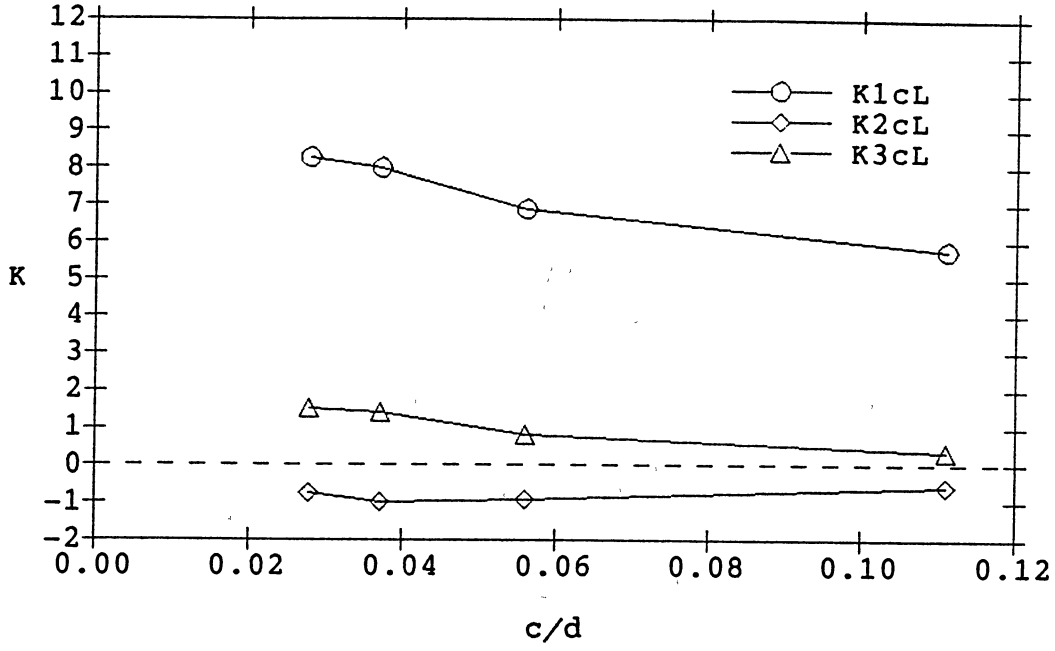

Figure 20. K_{ic} (i = 1, 2, 3) for Cracks of Constant Depth under AT

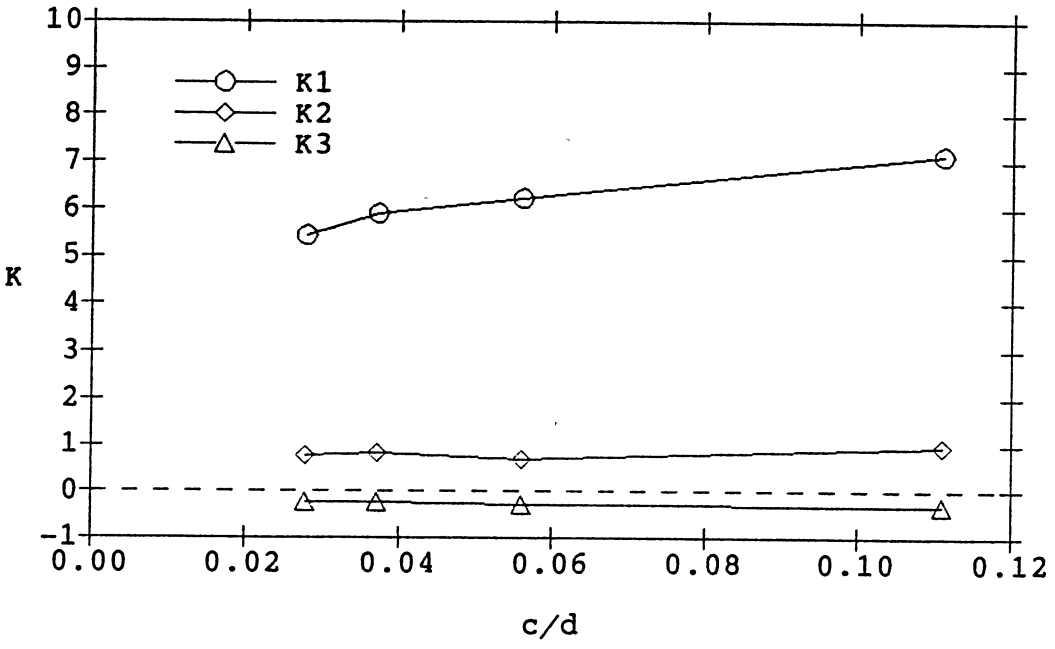

Figure 21. K_{ia} (i = 1, 2, 3) for Cracks of Constant Depth under AT

0.08) and shallow (a/T = 0.20) cracks, the growth in the wall-thickness direction tends to be faster than that along the weld toe, while for relatively short cracks (c/d < 0.08), the crack grows faster along the weld toe than that in the wall-thickness.

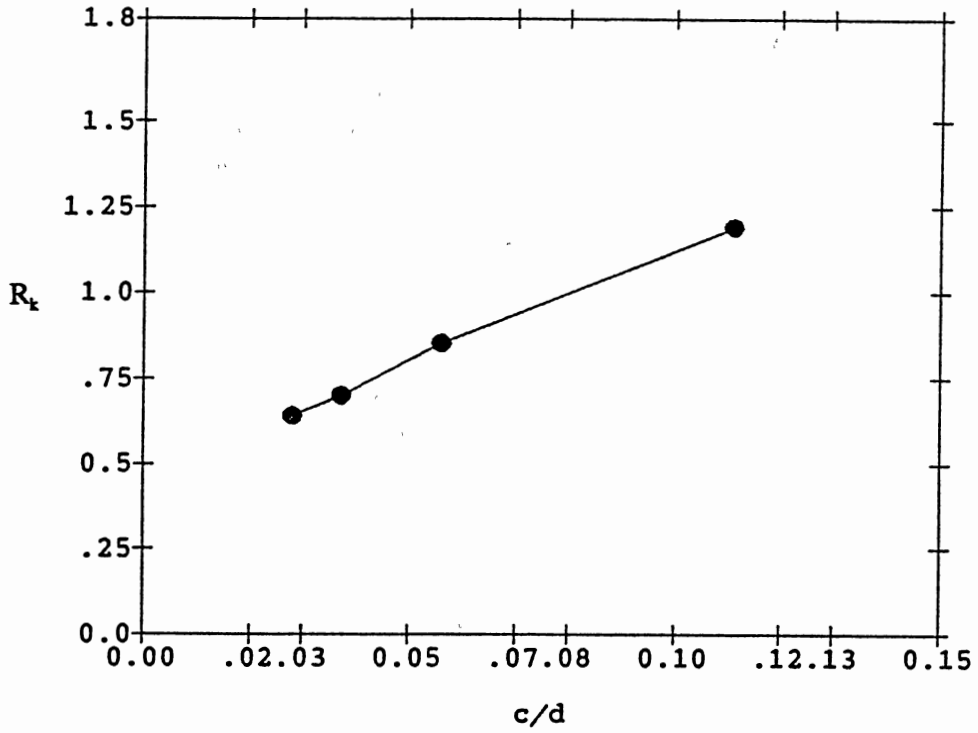

Figure 22. Trend of R_K versus Relative Crack Half Length (c/d)

The behavior of the stress intensity factor for cracks with different aspect ratio a/c, under brace axial tension, are shown in Figures 23 to 27. Note that the SIF in these figures are normalized using a common crack depth, a = 6.67 mm. Figure 23 shows the values of K_1 at the crack front center versus relative crack depth a/T. Each curve corresponds to a specific a/c ratio. This figure indicates that for relative shallow (a/T <

0.20) cracks, the value of K_I at the crack front center (K_{Ia}) increases with a/T. For relatively deep cracks (a/T > 0.5), the value of K_{Ia} may increase or decrease. The rate of change depends on the shape ratio a/c. This is because of the combined effects of crack sizes (a and c) and the stress applied to the cracked region. While increases in crack sizes will make the K_{Ia} greater, these increases will lead the deepest crack front point into a less stressed area (i.e., away from the hot spot on the chord surface), as shown in Figure 16.

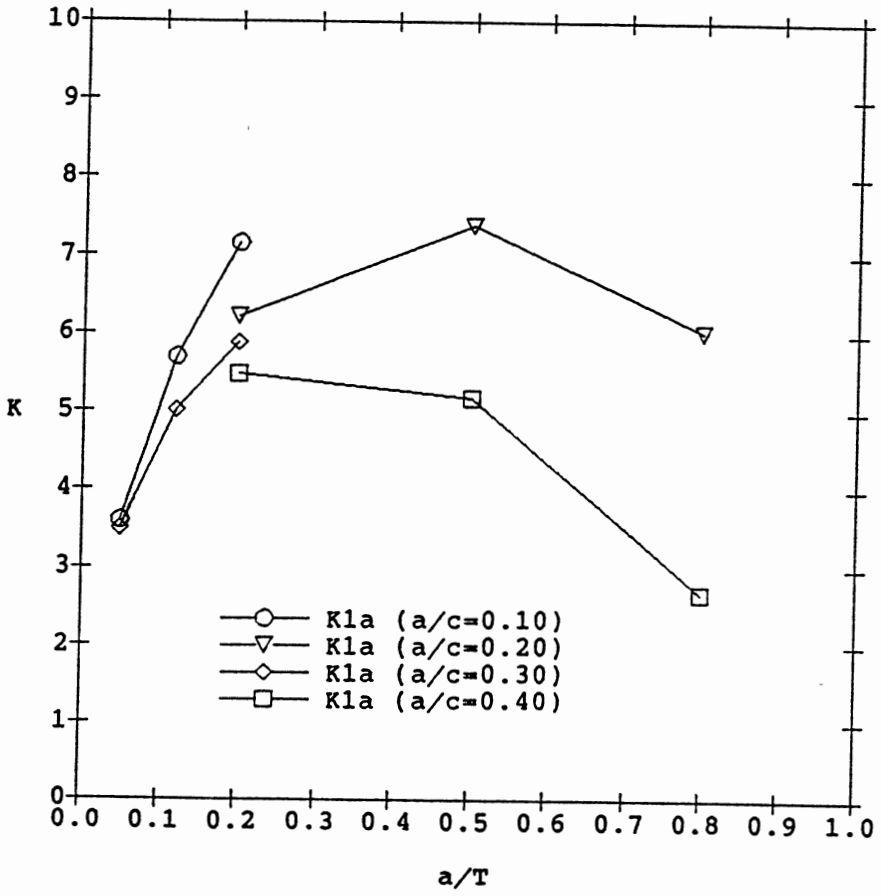

Figure 23. K_{Ia} versus a/T

The trends of K_{2a} and K_{3a} with a/T are shown in Figures 24 and 25, respectively. These values and their changes are not significant comparing to those for K_{1a} (dash lines). Negative signs of K_2 and K_3 means that the directions of the Mode II and Mode III movement of the two crack surfaces are opposite to the chosen local coordinate system along the crack front (Figure 11).

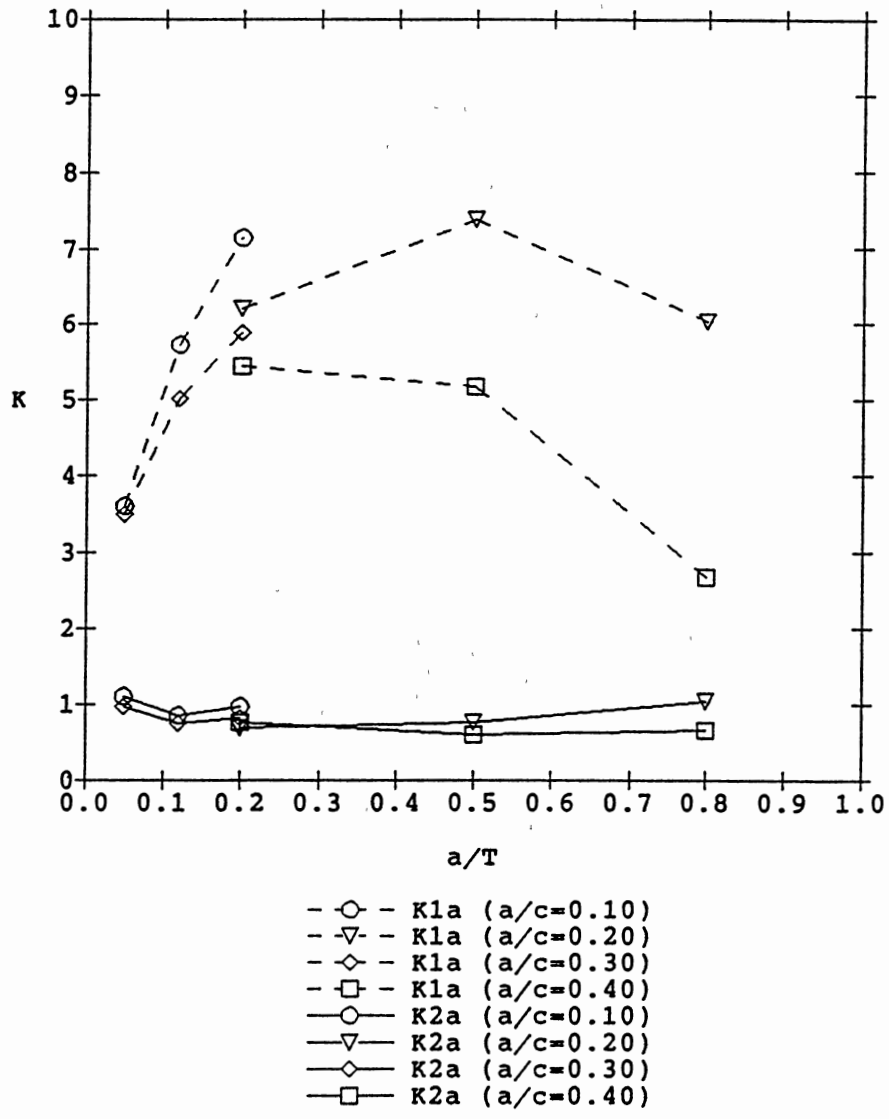

Figure 24. K_{2a} versus a/T

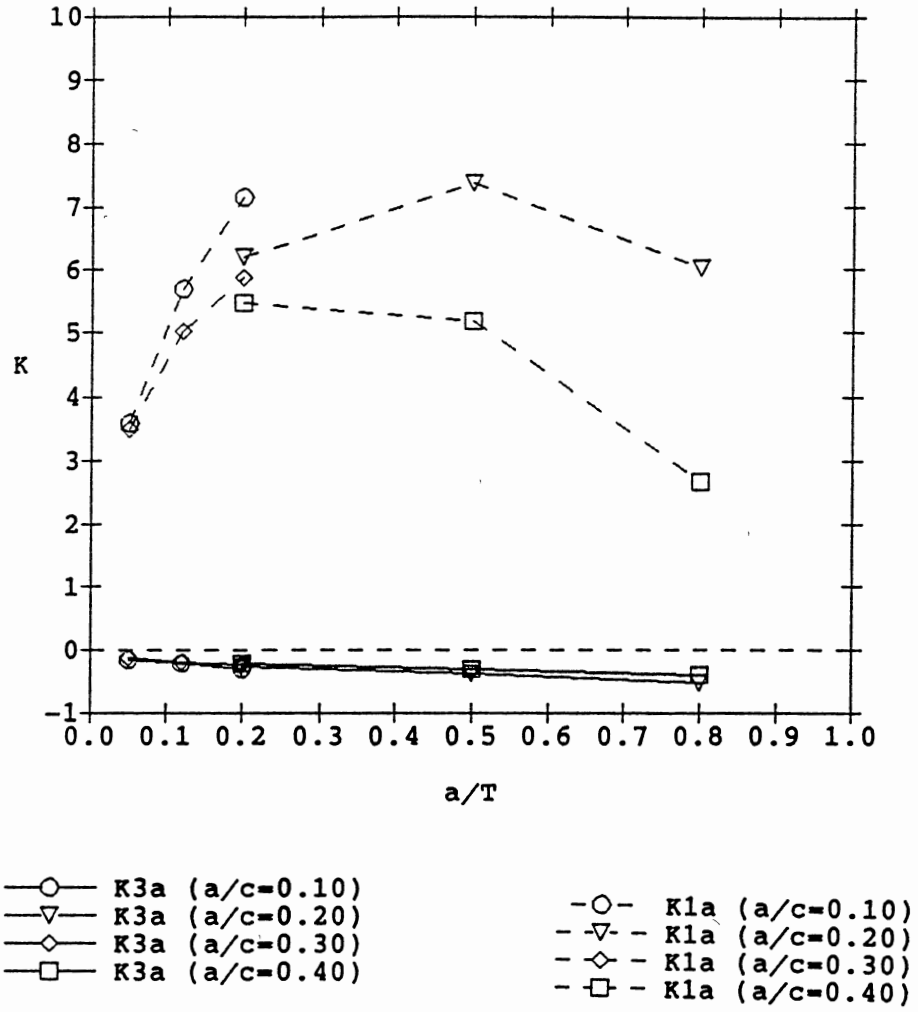

Figure 25. K_{3a} versus a/T

On the left end of the crack surface, the changing trends of the values of K_1 for various ratios of a/c are shown in Figure 26. These curves indicate increasing trends with a/T, though the crack surface end moves away from the hot-spot region. This implies that the crack size effect of a and c on K_1 at the crack surface end (i.e., K_{1cL}) is dominant relative to the stress effect. The absolute values of K_{2cL} and K_{3cL} are much less than K_{1cL}, and generally increase with a/T. The effect of shape ratio a/c on K_{2cL} is also much less compared to that on K_{1cL}, and K_{2cL} is within 15 percent of K_{1cL}.

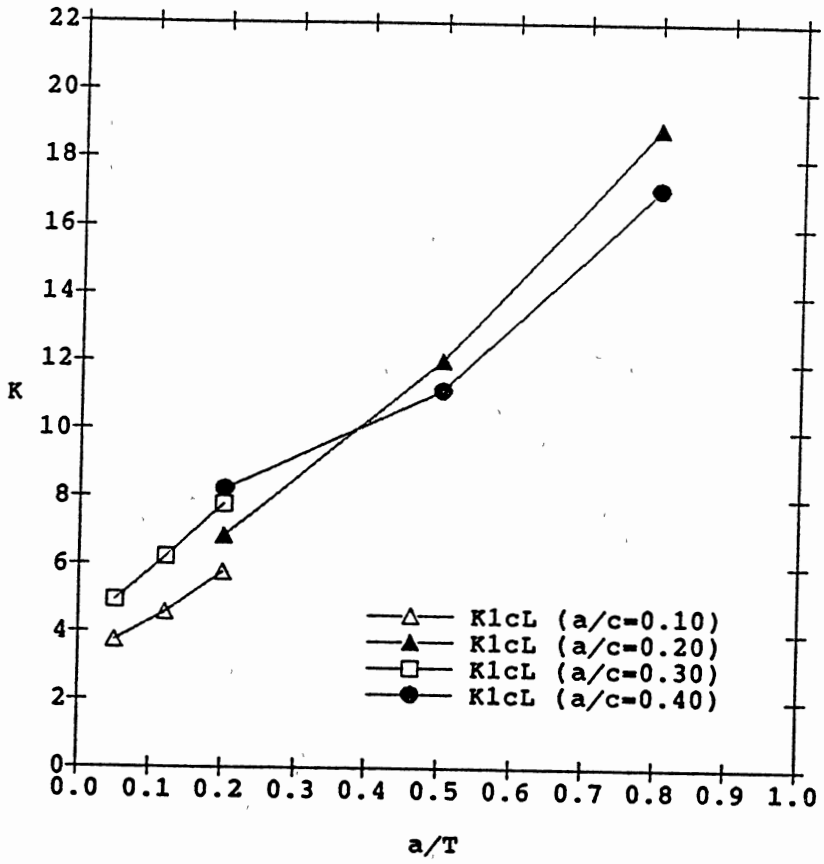

Figure 26. K_{1c} versus a/T

The above analyses indicate that for not very small saddle cracks under brace axial tension, stress intensity factor K_1 is always dominant, while K_2 and K_3 are relatively small. Consider the ratio $R_k = K_{1a}/K_{1cL}$ for these cracks. The results of R_k versus crack depth a/T are shown in Figure 27. This figure implies that very shallow ($a/T < 0.20$) and relatively long cracks ($a/c = 0.10$) tend to grow faster in the wall-thickness direction than along the weld toe since $R_k > 1.0$. For all the other cases analyzed, $R_k < 1.0$, a saddle crack tends to grow faster along the weld toe, though the ratio a/c may also decrease.

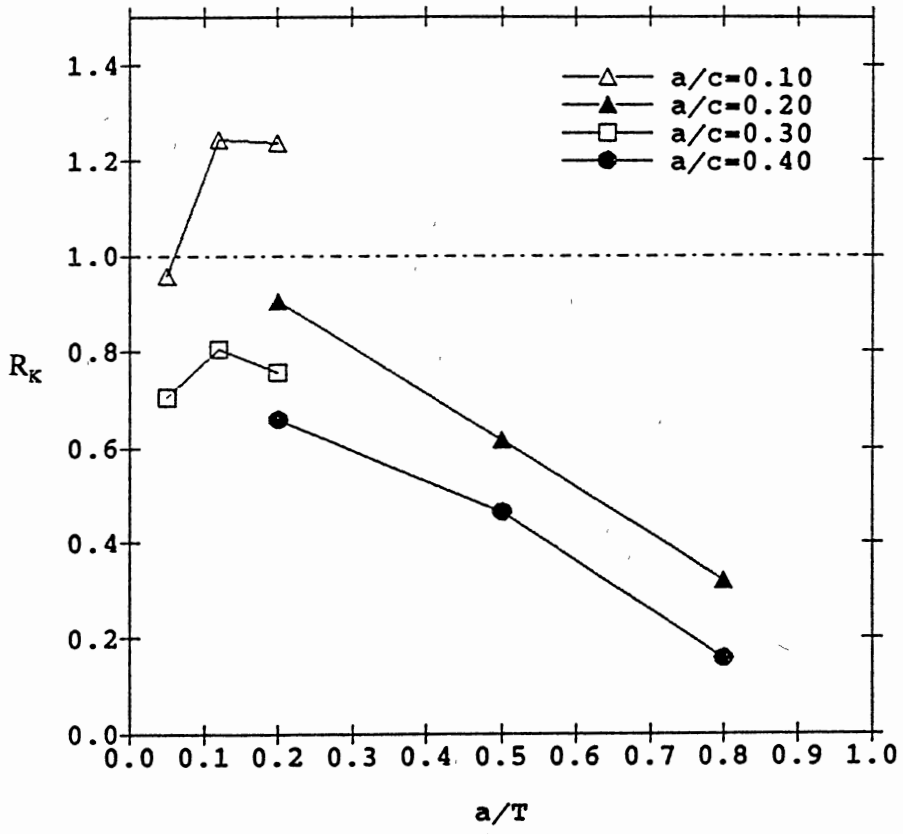

Figure 27. R_K versus a/T

Under In-Plane Bending (IPB). The high stress concentration region of the Y-joint before a crack is introduced is located near the crown and heel (Figure 14). For cracks with constant depth (a = 6.67 mm), the trends of the SIFs versus c/d are shown in Figures 28 to 29. The trends indicate that the effects of K_{2cL} and K_{3cL} decrease for longer cracks, and K_{1cL} increases with crack length (Figure 28). The values of K_{1a} and K_{3a} are of the same order, while K_{2a} is very low. The stress intensity factors at the crack front center increase with crack length, as shown in Figure 29.

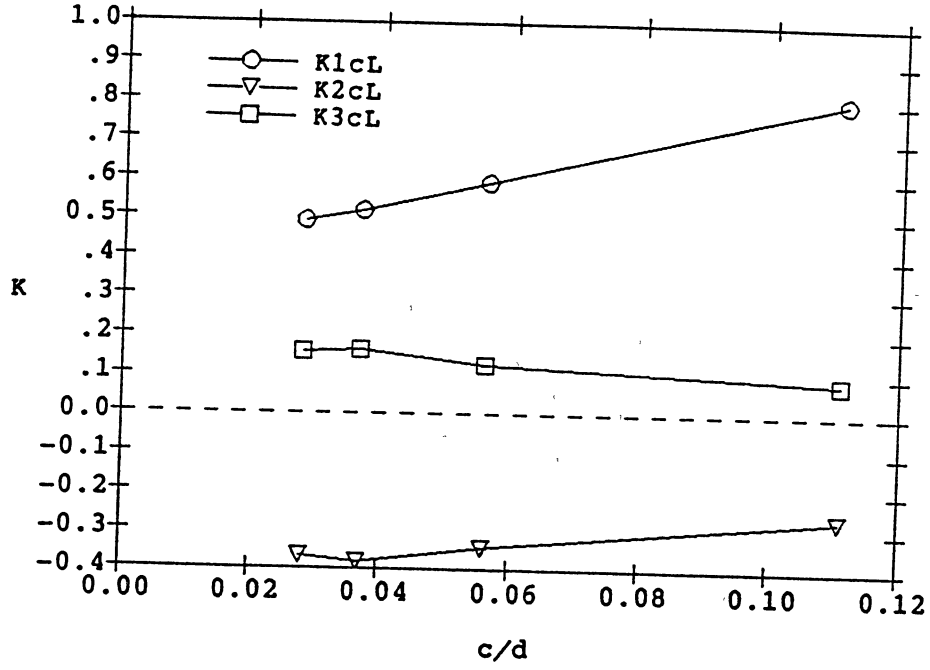

Figure 28. K_{ic} (i = 1, 2, 3) for Cracks of Constant Depth under IPB

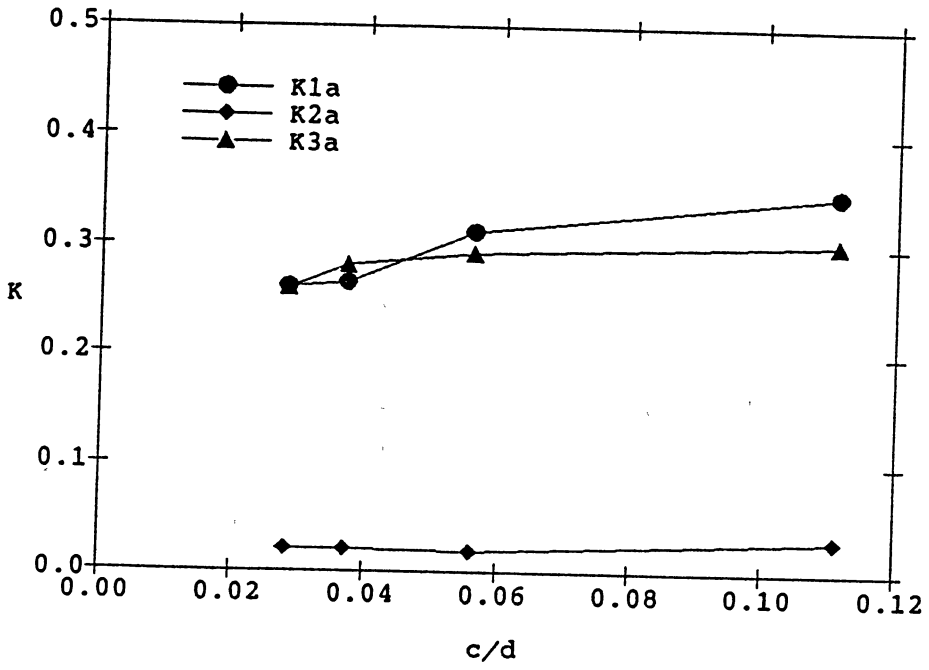

Figure 29. K_{ia} (i = 1, 2, 3) for Cracks of Constant Depth

Figure 30 shows the ratio R_k of equivalent stress intensity factor at the crack front center to that at the crack left end. The equivalent SIF is defined from equal energy release rate of a fully mixed mode in a plannar propagation, to consider the contribution of each mode. This curve is for cracks with constant depth (a = 6.67 mm) but different crack lengths. For $R_k < 1.0$, these saddle cracks tend to grow faster along the weld toe than along the wall-thickness direction.

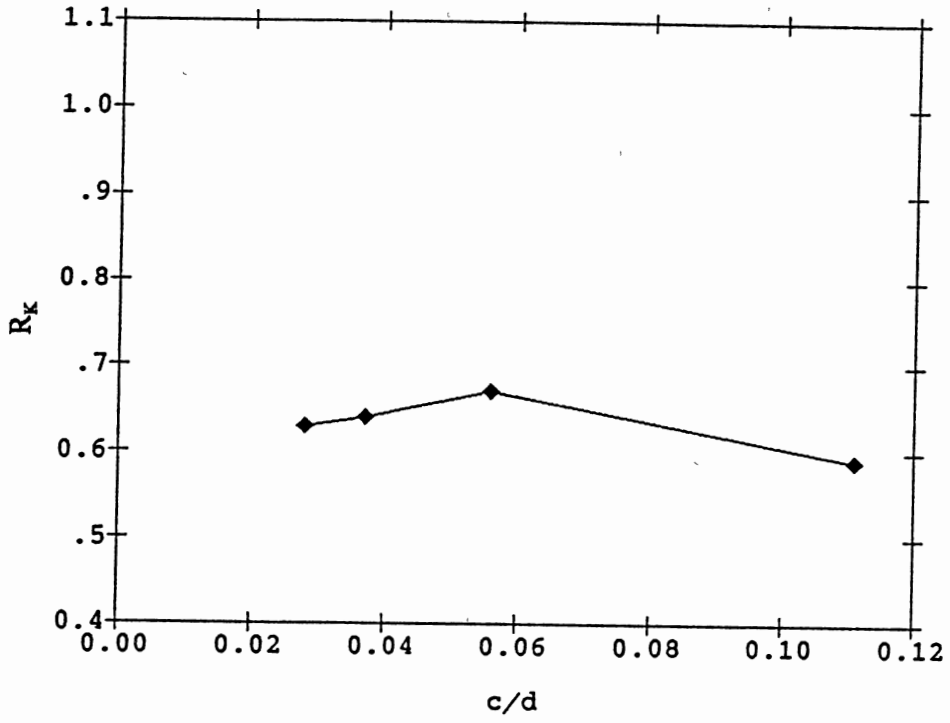

Figure 30. Trend of R_K versus Relative Crack Half Length (c/d)

In an actual crack growth situation, both length (2c) and depth (a) increase simultaneously. Figures 31 and 32 show the normalized (using a = 6.67 mm) SIF values at the crack front deepest point. Each curve corresponds to a specific a/c ratio. The

trends in Figure 31 indicate that for shallow cracks (a/T < 0.20), K_{1a} increases with a/T, and for deep cracks (a/T > 0.20), K_{1a} may increase or decrease with a/T. The shape ratio a/c has a strong effect on the SIF trend. As in the brace axial tension, both the crack sizes (a and c) and the applied stress field near the crack area contribute to the value of the stress intensity factor. A low ratio a/c (e.g., 0.20) has a greater c size effect on K_{1a} than a high ratio a/c (e.g., 0.40). For deep cracks, the combined effect of crack depth and the applied stress field through the wall-thickness is to reduce K_{1a}. The K_{2a} is not significant compared to K_{1a} (dash lines). Except for shallow cracks (e.g., a/T < 0.20), K_{3a} in Figure 32 increases much faster than K_{1a} (dash lines) and becomes dominant.

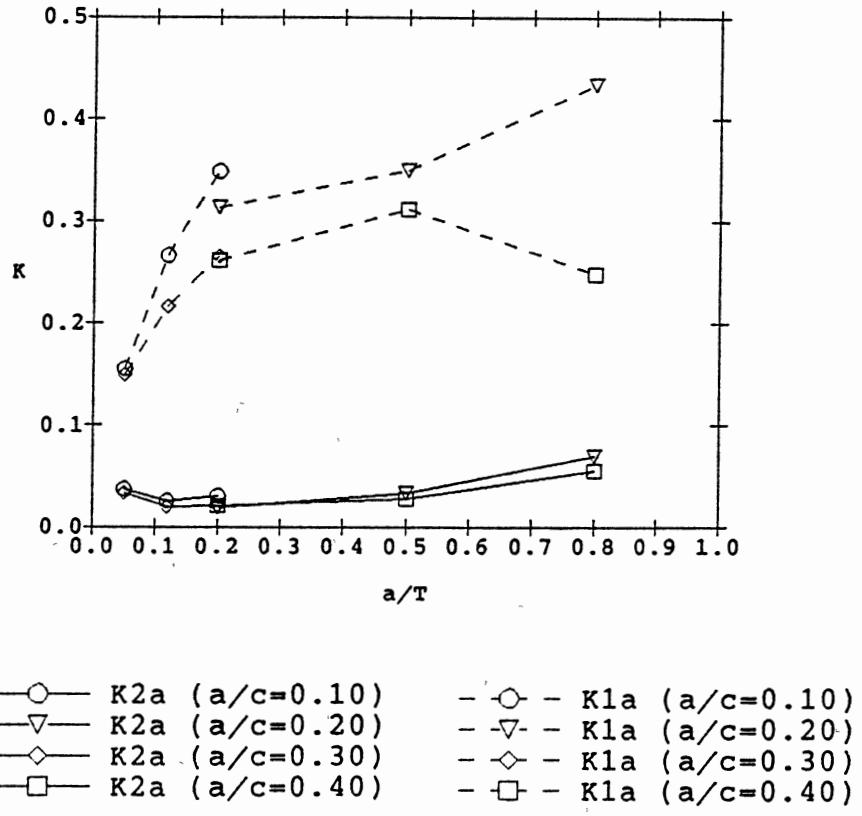

Figure 31. K_{1a} and K_{2a} versus a/T under IPB

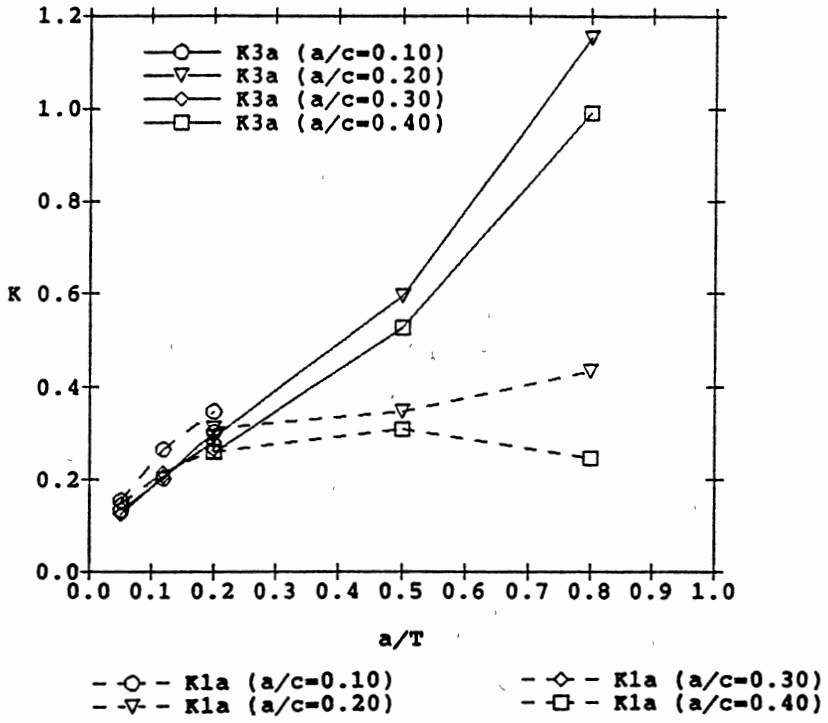

Figure 32. K_{1a} and K_{3a} versus a/T under IPB

The behavior of the normalized SIF (using a= 6.67 mm) at the crack left surface end is shown in Figures 33 and 34. For a constant a/c ratio, an increase in a leads to an increase in 'c'. A greater 'c' makes the crack left end come closer to the joint crown region, the hot-spot area under in-plane bending. This causes K_{1cL} (Figure 33) to increase with a/T. The absolute values of K_{2cL} (Figure 33) are of comparable order of K_1cL and increase with a/T. The effect of a/c ratio on K_{3cL} seems not significant, as shown in Figure 34.

In summary, for saddle cracks under in-plane bending, modes III and I at the deepest point are of similar order in shallow cracks, and mode III becomes dominant in deep cracks, while at the crack surface end, modes I and II appear to be significant.

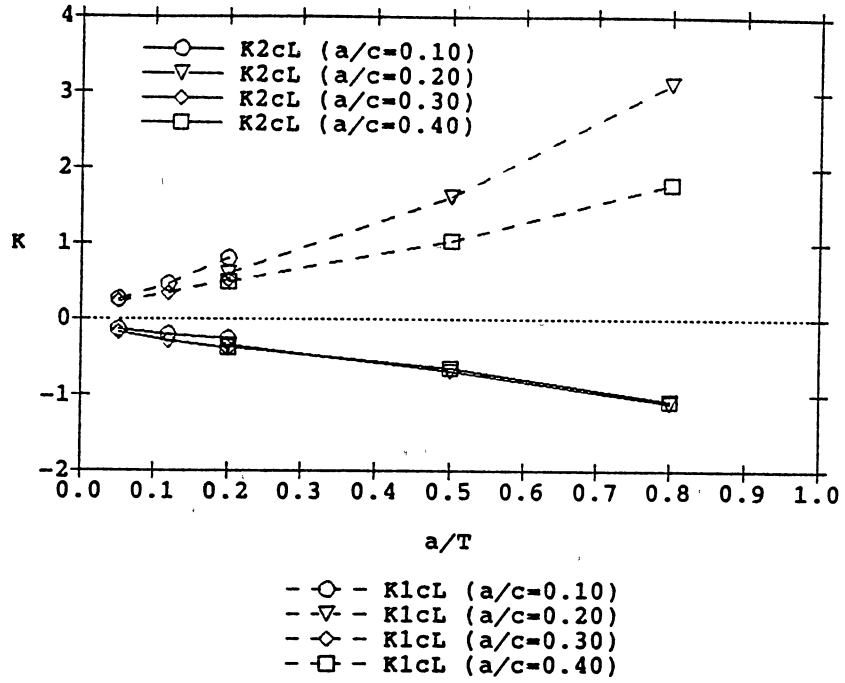

Figure 33. K_{1c} and K_{2c} versus a/T under IPB

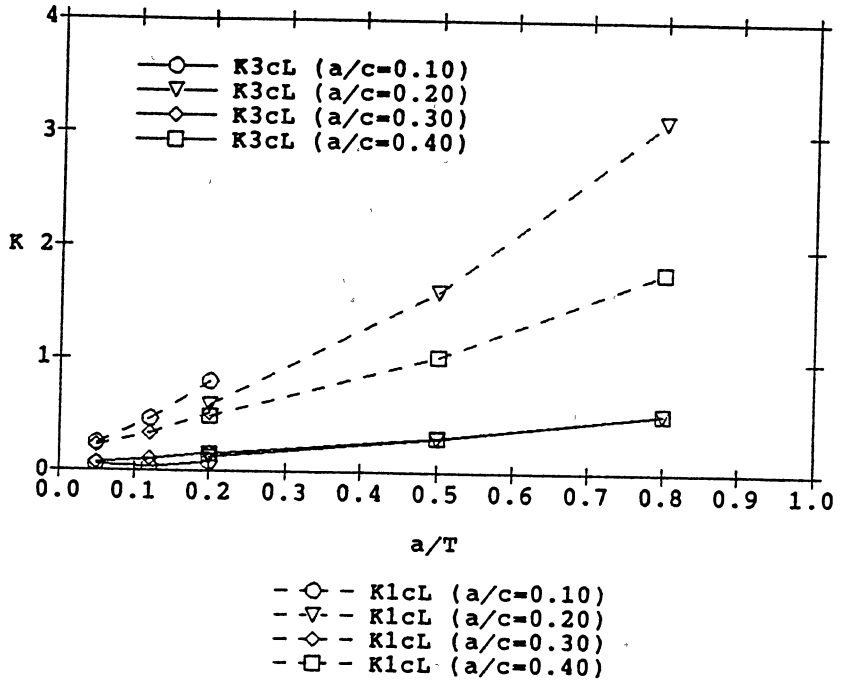

Figure 34. K_{1c} and K_{3c} versus a/T under IPB

Chord Side Crack versus Brace Side Crack

Six Y tubular joint models (Table 5), each with a saddle surface crack were studied, two for the chord crack and four for the brace crack, as illustrated in Figure 35. The Y-joint with dimensions shown in Figure 19 was used for joint models with $\beta = 0.60$. To study the effect of brace diameter on the SIF, the brace diameter was modified to 800 mm for Y-joint models, with $\beta = 0.80$. Both ends of the chord were fixed as the boundary conditions. The SIF solutions under axial brace tension will be discussed.

TABLE 5

MODELS FOR CHORD SIDE AND BRACE SIDE CRACKS

β	Chord Crack (mm)		Brace Crack (mm)	
0.60	a/c = 4.0/40.0 (S5)	a/c = 6.67/33.35 (L4)	a/c = 4.0/40.0 (BY2SF)	6.67/33.35 (BY1F)
0.80			a/c = 4.0/40.0 (BY4F)	6.67/33.35 (BY3F)

In general, the SIFs for crack on the chord side are higher than those of the brace side cracks. Figure 36 shows the normalized SIF solutions along the crack front (from right to left) with a/c = 4.0/40.0 (mm) from two models (i.e. S5 and BY2SF). Three curves of square symbols are the SIF for the crack on the chord side, the other three curves of diamond symbols are the SIF for the crack on the brace side, under brace axial tension. The trends from other two Y-joint models with saddle crack a/c = 6.67/33.35 mm on the chord and on the brace sides are similar to those in this figure. These results are consistent with the SCF trends shown in Figure 17.

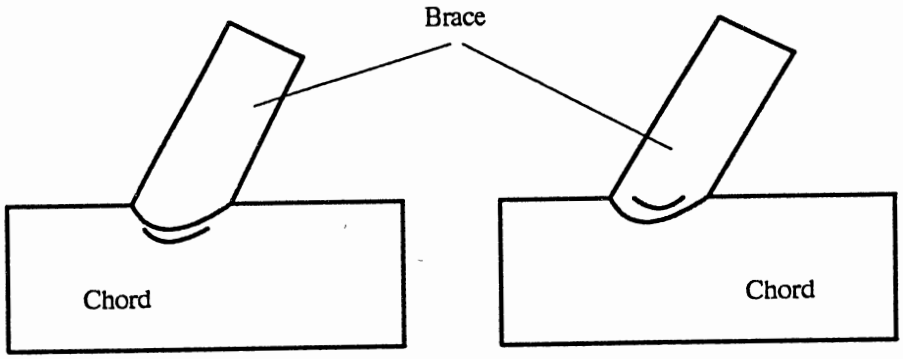

Figure 35. Crack on Chord and on Brace Side

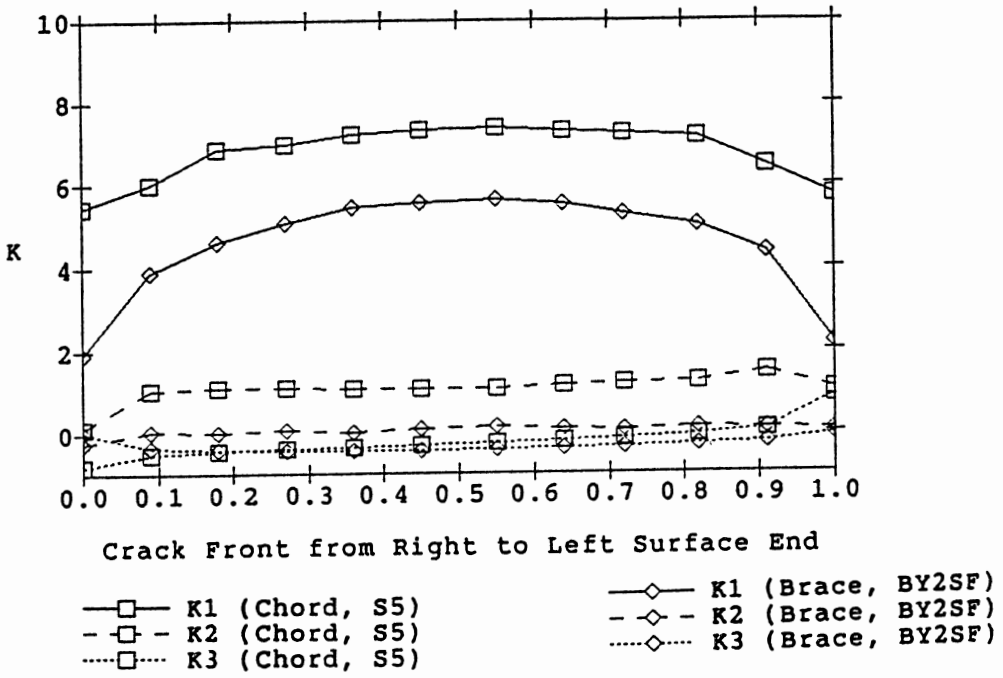

Figure 36. SIF Distributions for Cracks on Chord and on Brace

The SIF for the smaller brace diameter has higher values. Figure 37 shows two sets of normalized SIF curves, one for a saddle crack (a/c = 4.0 mm/40.0 mm) on the surface of the brace with β = 0.60, the other for the same crack on the brace with β = 0.80. The mode I SIF is dominant. Similar trends were found for another saddle crack with size a/c = 6.67 mm/33.35 mm, since the stress at the saddle of a small brace diameter is greater than that of a larger brace diameter (Figure 18).

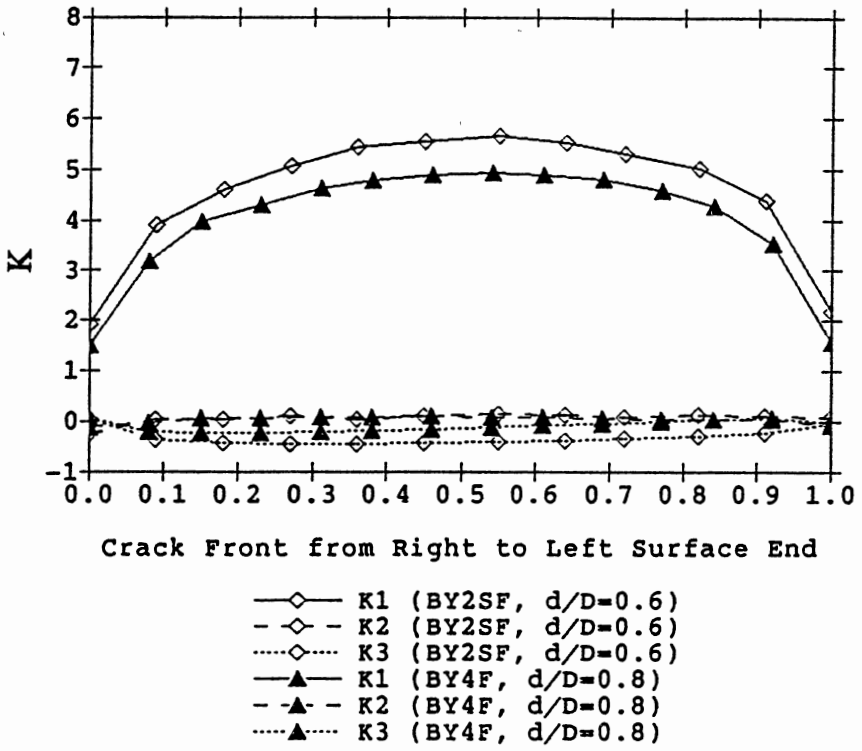

Figure 37. SIF Distributions of Brace Cracks

In summary, both stress distributions in the wall-thickness direction and on the weld toe surface affect the SIF solutions. The SIF is generally higher on the chord side. This is consistent with the fact that a fatigue crack initiates more likely along the weld toe on

the chord side. It also indicates that the SCF distribution on the joint surface has a significant effect on the SIF for a crack, since the SCF partially represents the local stress on the tube surface.

Single versus Double Cracks on Saddle Point

Four cracked Y-joint models (Table 6) were analyzed. The Y-joint geometry is as shown in Figure 19. The locations of the single crack and the double cracks are illustrated in Figure 38. The sizes of the chord surface crack are a/c = 16.67 mm/200 mm. This is a rather large crack, covering about 40 percent of the weld toe length on one side of the Y joint. Both ends of the chord were fixed as the boundary conditions. Two loading modes, brace axial tension (AT) and in-plane bending (IPB), were applied separately. Owing to symmetry of the Y-joint model with double cracks, only half of the Y-joint was modelled for the analyses.

TABLE 6

Y-JOINTS WITH SINGLE CRACK OR DOUBLE CRACKS

Crack	No Rigid Ring	Rigid Ring at Brace End
Single Crack	SYC	SYCR2
Double Crack	DBC	DBC2

The normalized SIFs (K_1, K_2, K_3) for double cracks (Model DBC) under AT are shown with circled lines in Figure 39. The lines with triangles are for the single crack model (SYC). K_1 of the double cracks is about 4.2 percent lower than that for the single

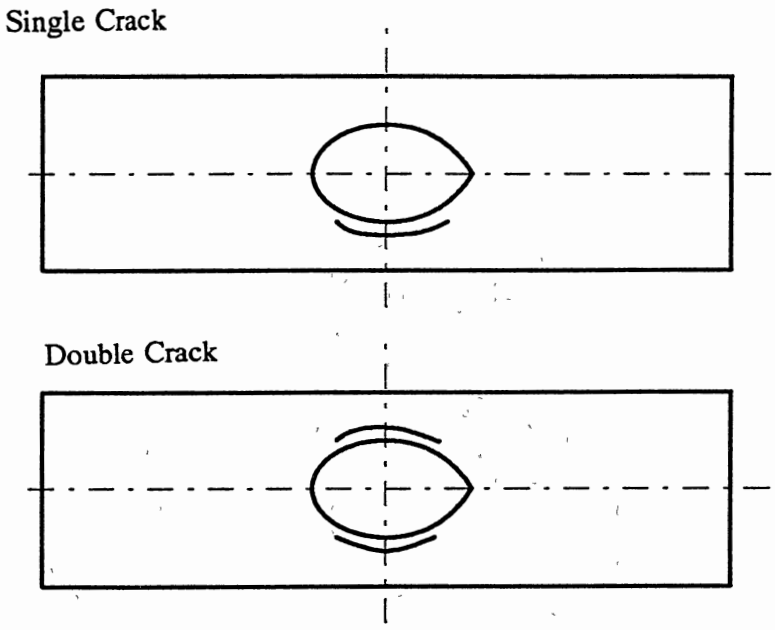

Figure 38. Illustration of Single and Double Cracks

crack at the crack front center. This is because of the out-of-plane bending effect due to lack of symmetry in the single saddle crack model. This effect was confirmed by analyzing another single crack model (SYCR2) in which "rigid ring" was used at the brace end where the out-of-plane bending freedom was removed. The new SIF results from model SYCR2 are shown in pointed lines.

Under the condition of no global out-of-plane bending, K_1, from single crack (the lines with points) is 2.5 percent lower than that for the double cracks (the lines with circles) at the crack front center. The out-of-plane bending effect increases K_1 by 6.7 percent. To check the effect of the rigid ring, another model for double cracks with the rigid ring at the brace end was analyzed using FEM. The results indicated that the effect of the rigid ring on SIF solutions was negligible. Therefore, double saddle cracks may

produce higher or lower SIF than single crack, depending on the brace end displacement conditions. However, the double crack effect on the SIF appear not to be very significant. Under in-plane bending, the effect of one saddle crack on the other is not significant, as shown in Figure 40.

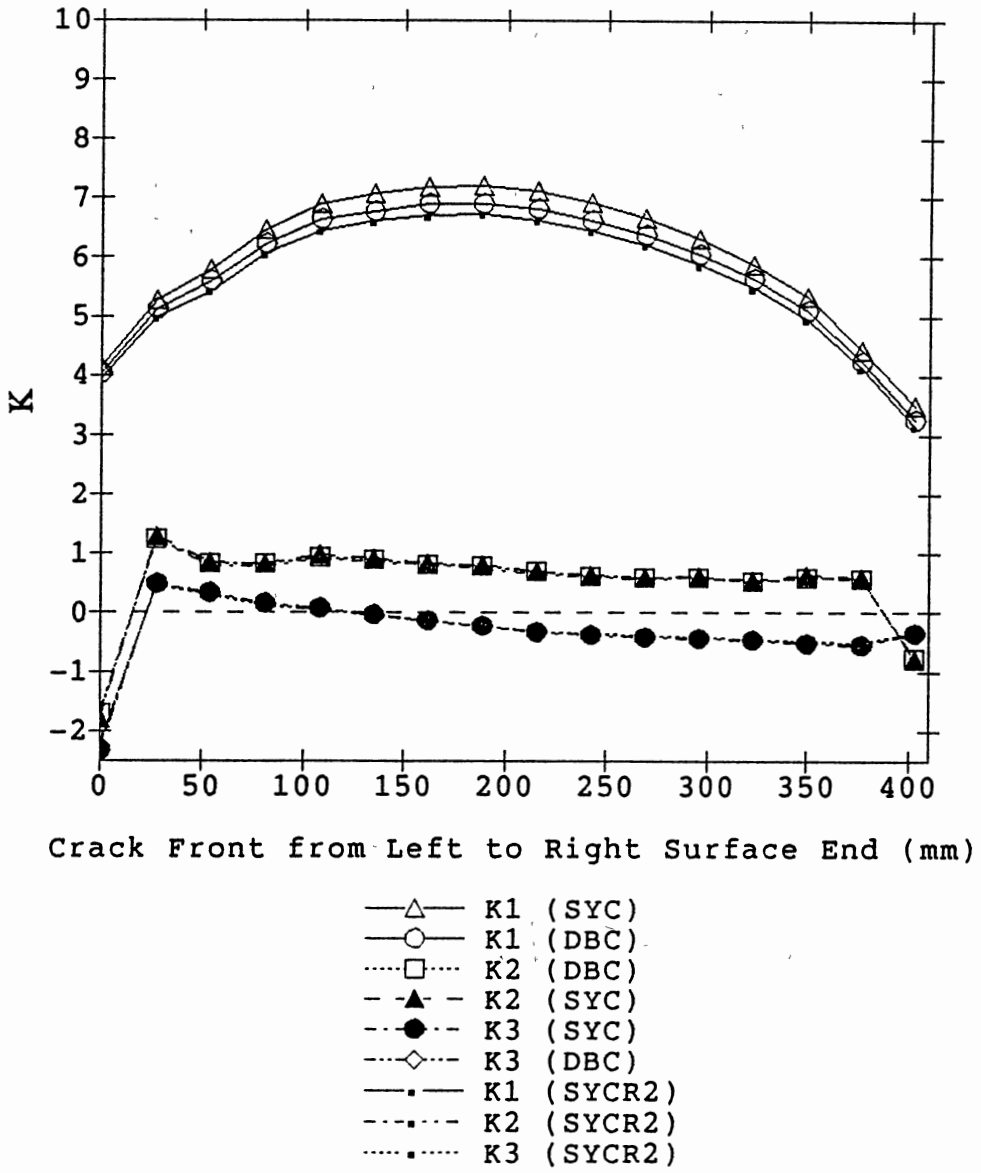

Figure 39. SIF Distributions for Single and Double Cracks

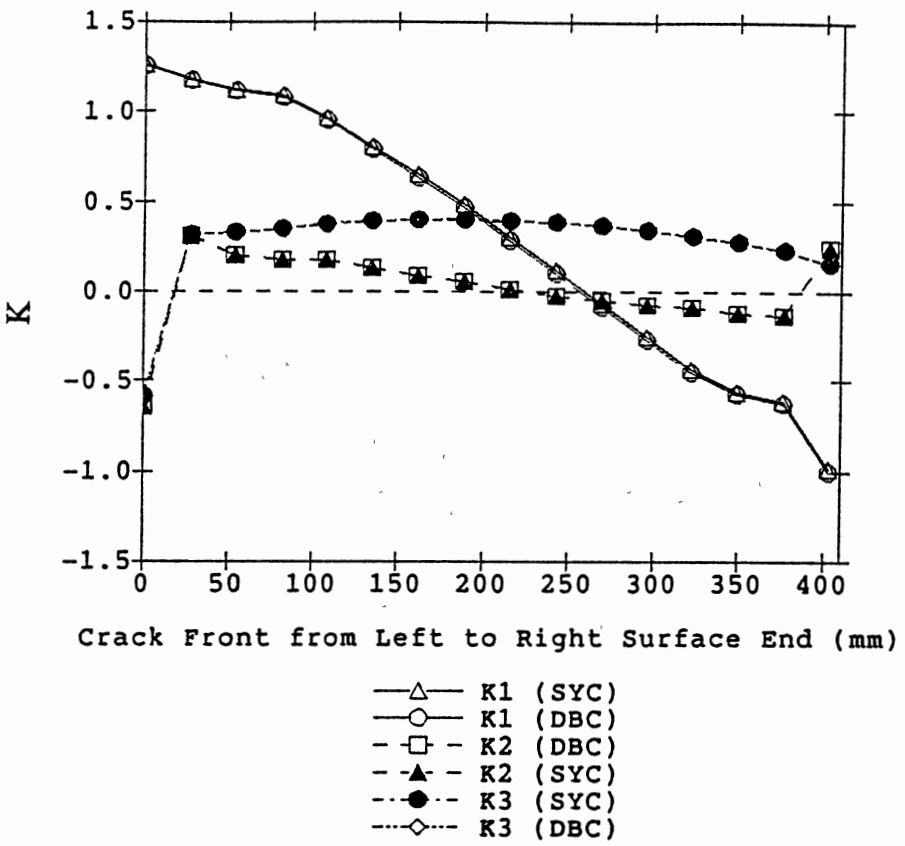

Figure 40. SIF Distributions of Single and Double Cracks under IPB

Crack Location Effect

A crack with the same nominal sizes (a and c) will behave differently at different locations along the chord/brace intersection, because of the effects of local stress and geometry. To study these effects, six Y-joint models, each having a crack on one of the three locations (Figure 41), were used to calculate the SIF solutions. These six models consist of two sets of Y-joint dimensions as given in Table 1.

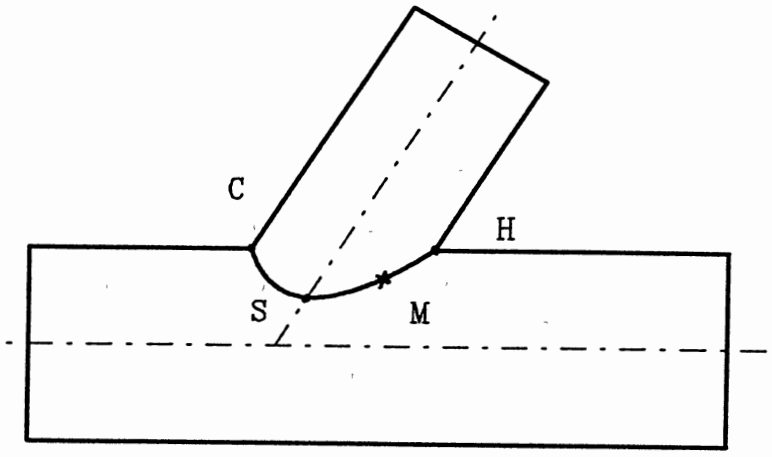

C: Crown-toe
S: Saddle point

H: Crown-Heel
M: Middle point between S and H

Figure 41. Definition of Crack Locations

Figure 42 shows the trends of the SIF at the deepest point factored by the brace nominal stress under axial tension. Modes II and III are not significant. The trends of mode I for cracks on these two joints are consistent with those of the SCF shown in Figure 13. At locations with greater SCF, the SIF is also greater. Figure 42 also indicates that it is more convenient to use the brace nominal stress than the brace total load to study the weld toe cracks. Similar trends are shown in Figure 43 for the factored SIF at the crack left surface ends. Since the crack sizes (mm) used here are not very long and deep, a/T = 0.20 for a/c= 6.67/33.35, the effect due to change in local geometry and stress over chord thickness from location to location is not significant for this crack of

relative small sizes. Under brace in-plane bending, the factored SIFs at the deepest point, $K_{ia}/(M_i\ d/2I)$, for these cracks are shown in Figure 44. These trends are consistent with those of the stress shown in Figure 14. The factored SIF at the crack left surface ends for these cracks are given in Figure 45. This figure also indicates that for the same crack sizes, local stress is the only dominant factor affecting the SIF solutions.

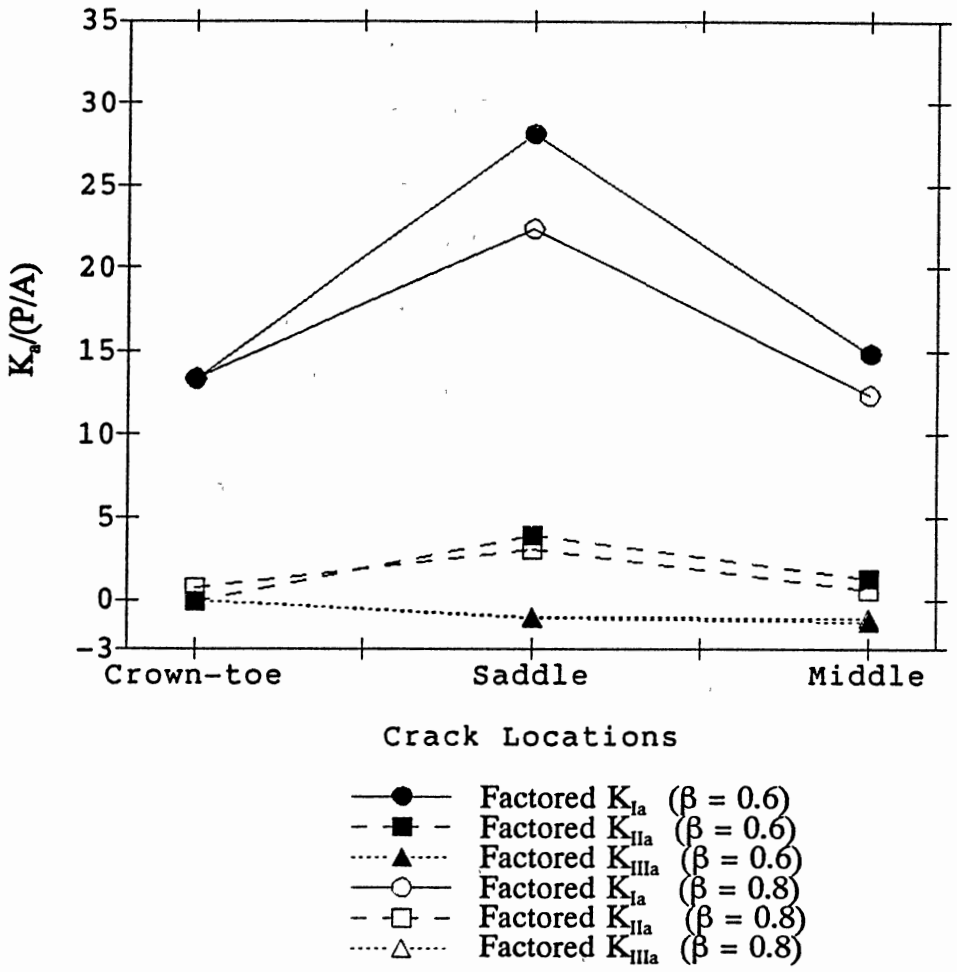

Figure 42. Factored SIF at the Deepest Crack Point under AT

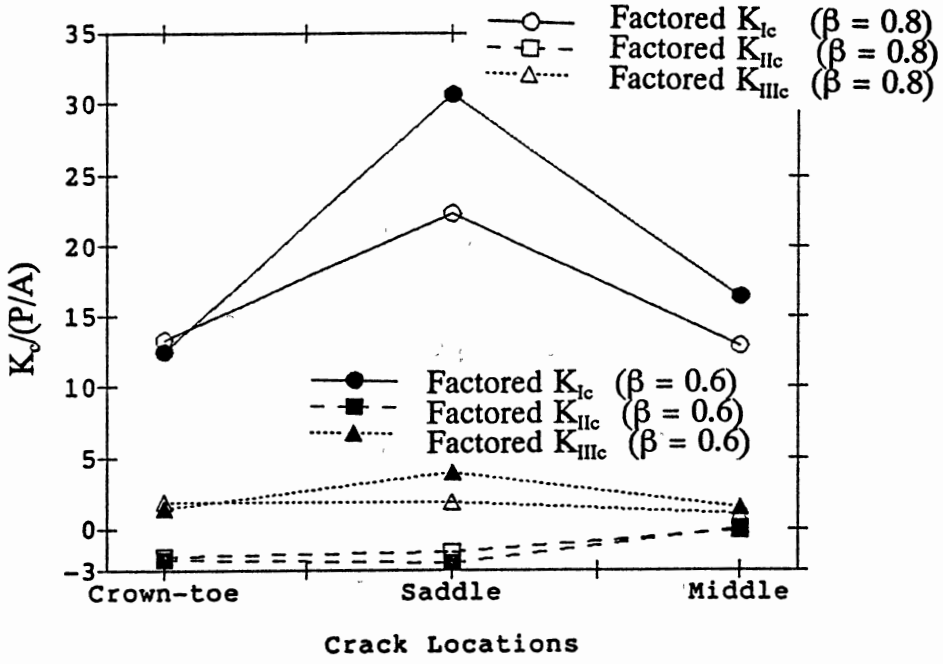

Figure 43. Factored SIF at the Left Crack Surface End under AT

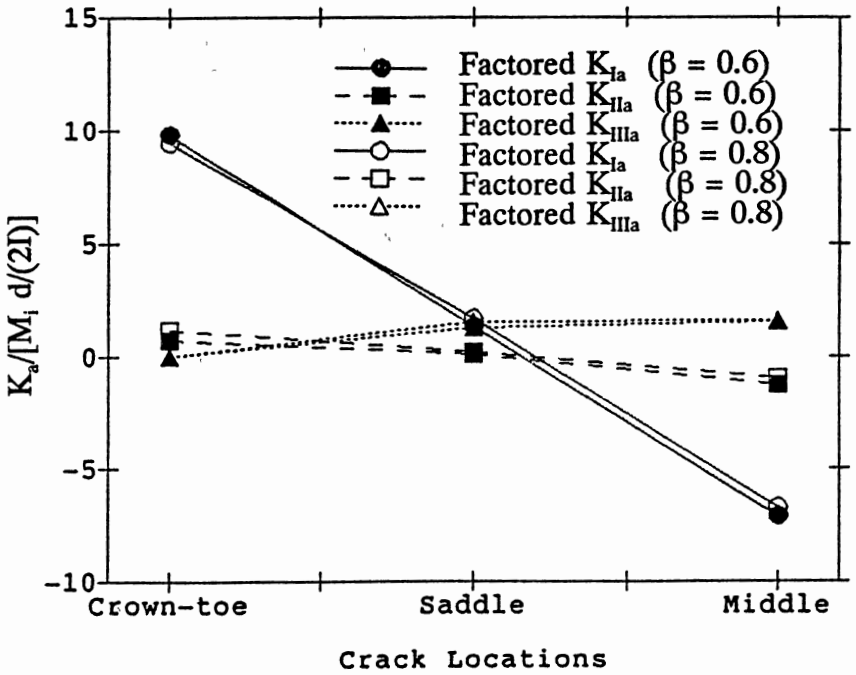

Figure 44. Factored SIF at the Deepest Crack Point under IPB

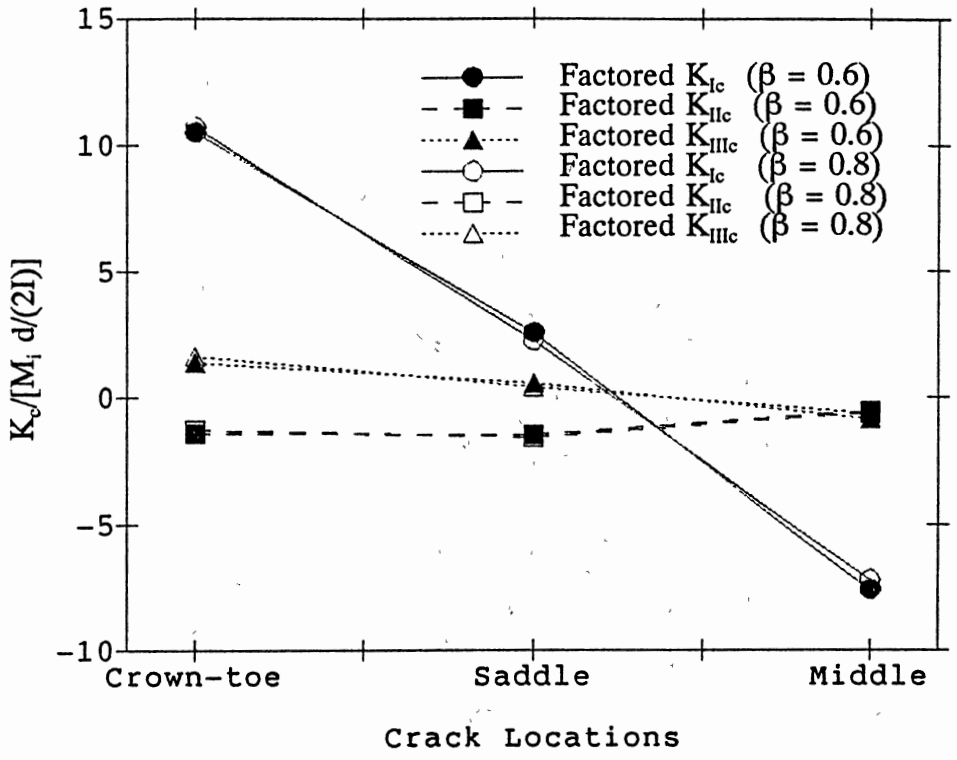

Figure 45. Factored SIF at the Left Crack Surface End under IPB

Joint Dimension Effect

Previously, various cracks on a tubular joint have been investigated to understand the effect of crack sizes on the crack fracture behavior. To study the effect of tubular joint dimensions on the SIF behavior of a crack, twenty-seven different cracked Y-joints (Table 7) with β = 0.4, 0.6, 0.8, γ = 10, 15, 20, τ = 0.3, 0.65, 1.0, and θ = 60° were analyzed using the 3-D finite element procedure. The parameters are defined as β = d/D, γ = D/(2T), and τ = t/T, with D and T being the chord outer diameter and wall-thickness, and d and t being defined in Table 2. A surface crack of sizes (mm) a/c = 6.67/33.35 is located at the saddle of each tubular joint in Table 7.

TABLE 7

Y-JOINTS WITH A SADDLE CRACK

Model	β	γ	τ
YS1		10.0	0.30
YS2		20.0	1.00
YS3		15.0	0.30
YS4		15.0	0.65
YS5	0.40	10.0	1.00
YS6		10.0	0.65
YS7		15.0	1.00
YS8		20.0	0.65
YS9		20.0	0.30
YS10		15.0	0.30
YS11		20.0	0.65
YS12		10.0	0.30
YS13		20.0	0.30
YS14	0.60	15.0	1.00
YS15		15.0	0.65
YS16		20.0	1.00
YS17		10.0	0.65
YS18		10.0	1.00
YS19		15.0	0.65
YS20		20.0	0.30
YS21		10.0	1.00
YS22		15.0	1.00
YS23	0.80	10.0	0.65
YS24		10.0	0.30
YS25		15.0	0.30
YS26		20.0	1.00
YS27		20.0	0.65

The real dimensions (in mm) of these joints are listed in Table 8.

TABLE 8

DIMENSIONS (mm) OF THE 27 Y-JOINTS

	D = 1000,	T = 50.0	
t	15.0	32.5	50.0
d			
400	YS1	YS6	YS5
600	YS12	YS17	YS18
800	YS24	YS23	YS21
	D = 1000,	T = 33.3	
t	10.0	21.7	33.3
d			
400	YS3	YS4	YS7
600	YS10	YS15	YS14
800	YS25	YS19	YS22
	D = 1000,	T = 25.0	
t	7.5	16.3	25.0
d			
400	YS9	YS8	YS2
600	YS13	YS11	YS16
800	YS20	YS27	YS26

Figure 46 shows the mode I SIF at the deepest crack point, K_{Ia}, under axial tension AT = 10000 N, for cracked Y-joints with $\beta = 0.60$. This figure contains the combined effects of joint dimensions in terms of local stress and relative crack sizes. Relatively deep cracks (a/T = 0.27) have higher SIF solutions than shallow cracks (a/T = 0.13). Joints with greater τ (or t/T) cause higher SIF solutions due to the higher local stressening

along the chord/brace intersection [3]. Factored SIFs at the deepest crack point, $K_{Ia}' = K_{Ia}/[\sigma_N(a/T)(c/d)]$, is used to measure the joint dimension effect on the SIF behavior.

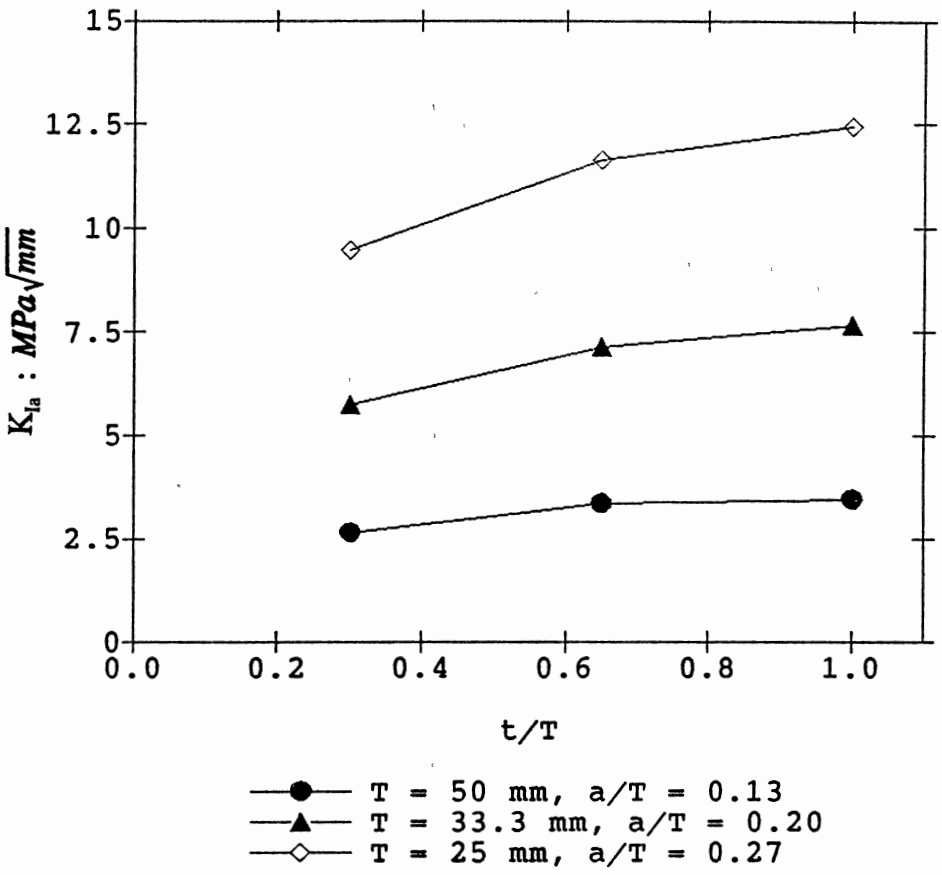

Figure 46. Joint Dimension Effect on K_{Ia} under AT = 10^4 N (β=0.6)

Figure 47 shows K_{Ia}' for joints with β = 0.60. Only τ effect is significant. This figure indicates that γ does not generally affect the factored SIF. Joints with β = 0.4 and 0.8 yield this similar trends, which are shown in Figure 48. The first number in the legend is γ value, and the second is the τ value. For the "same" relative cracks and the same nominal stress, large joints (d/D = 0.8) cause higher SIFs than those of small joints

(d/D = 0.40 and 0.60). This appears to corroborate the size effect commonly mentioned in experimental investigation of tubular joint fatigue behavior.

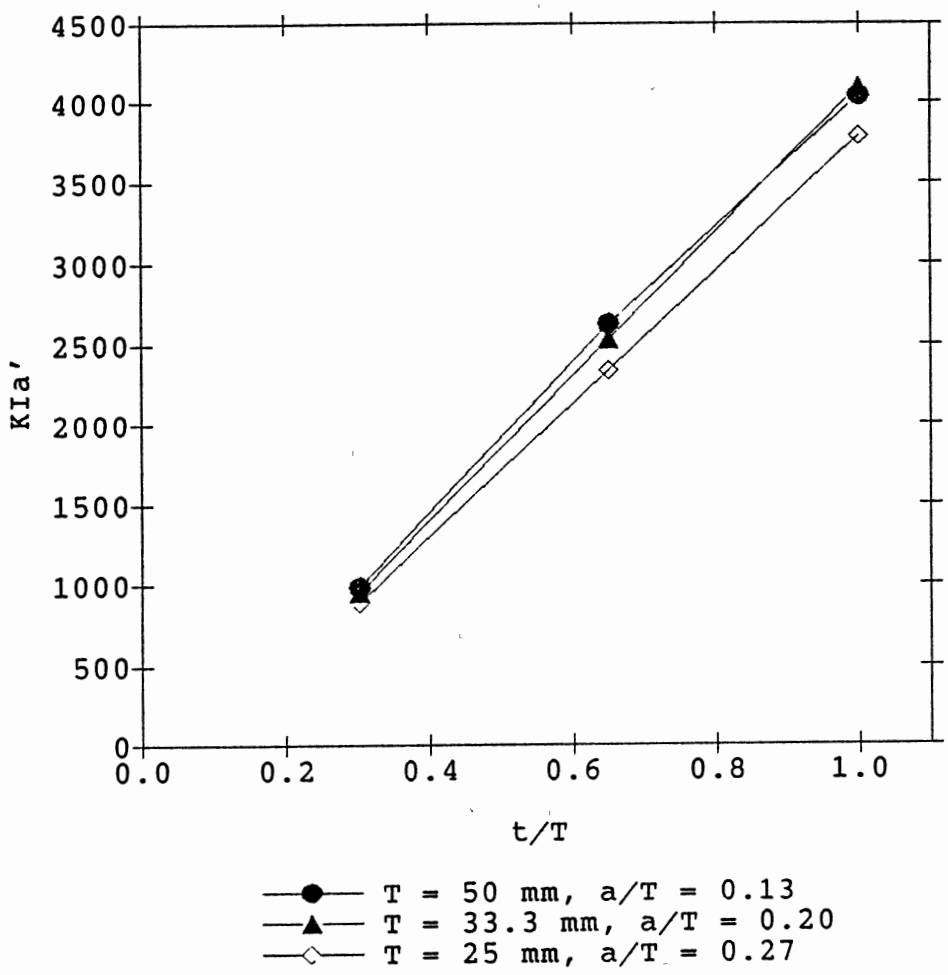

Figure 47. K_{Ia}' for Y-Joints with $\beta = 0.6$ under AT

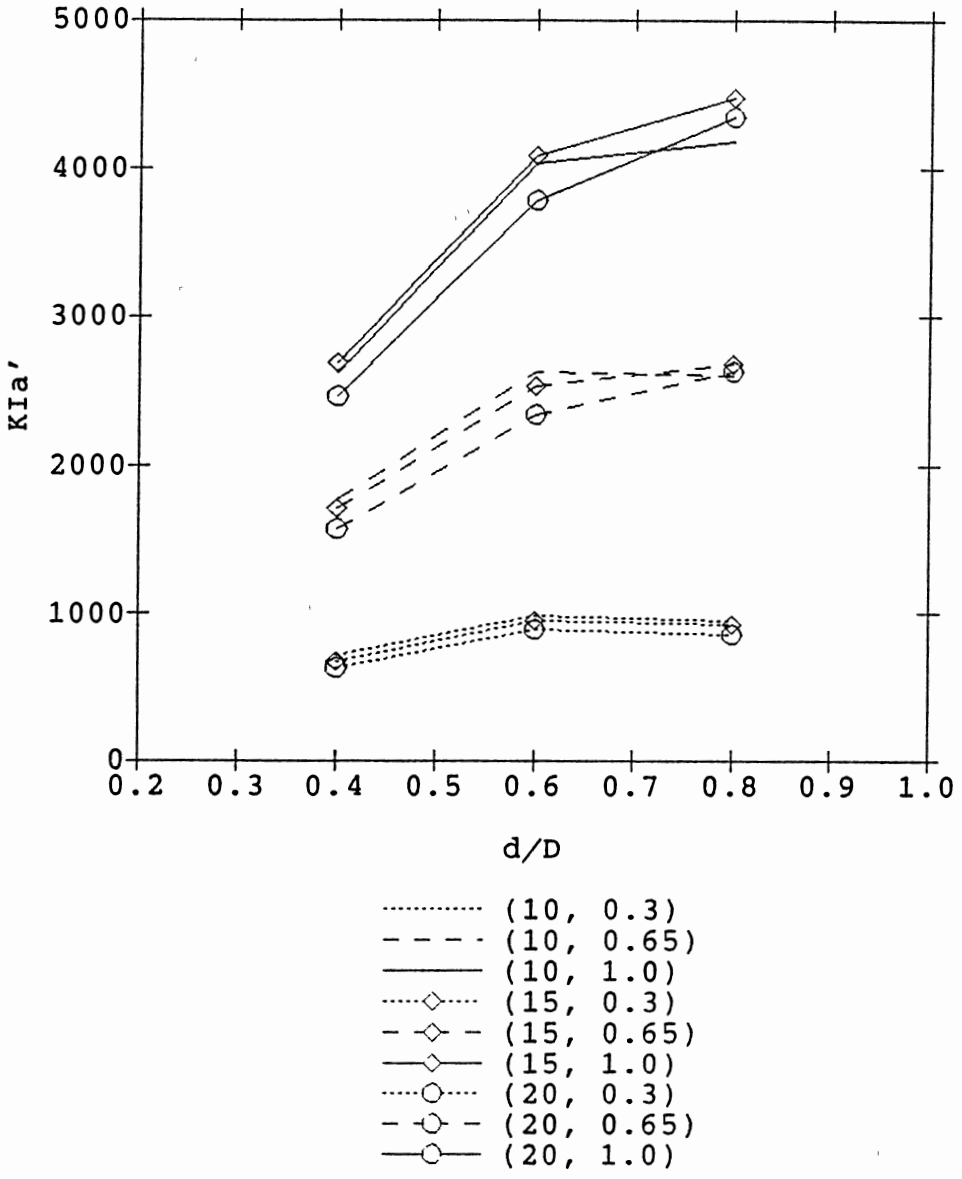

Figure 48. K_{Ia}' versus β = d/D for Joints under AT

Relative to the t/T effect, the chord wall-thickness T still has a strong effect on SIF. The factored SIFs, K_a', under IPB are shown in Figure 49 for joints with $\beta = 0.6$. This strong effect, probably due to the difference in stress distribution in the chord wall, is also shown on K_c' in Figure 50. The similar trends can be seen for other different joints, as shown in Figures 51 and 52. In general, the factored SIF for IPB is much less than that for AT, since the saddle crack is far away from the stress hot spot under IPB loading.

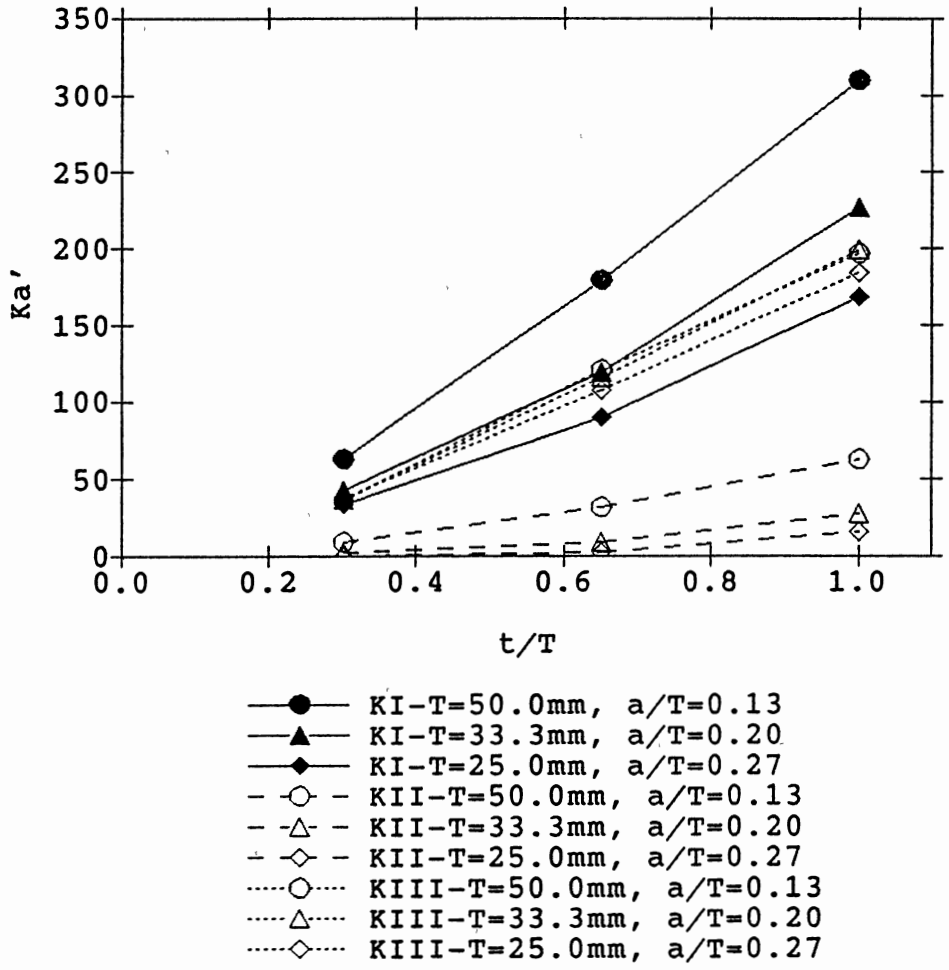

Figure 49. K_a' for Y-Joints with $\beta = 0.6$ under IPB

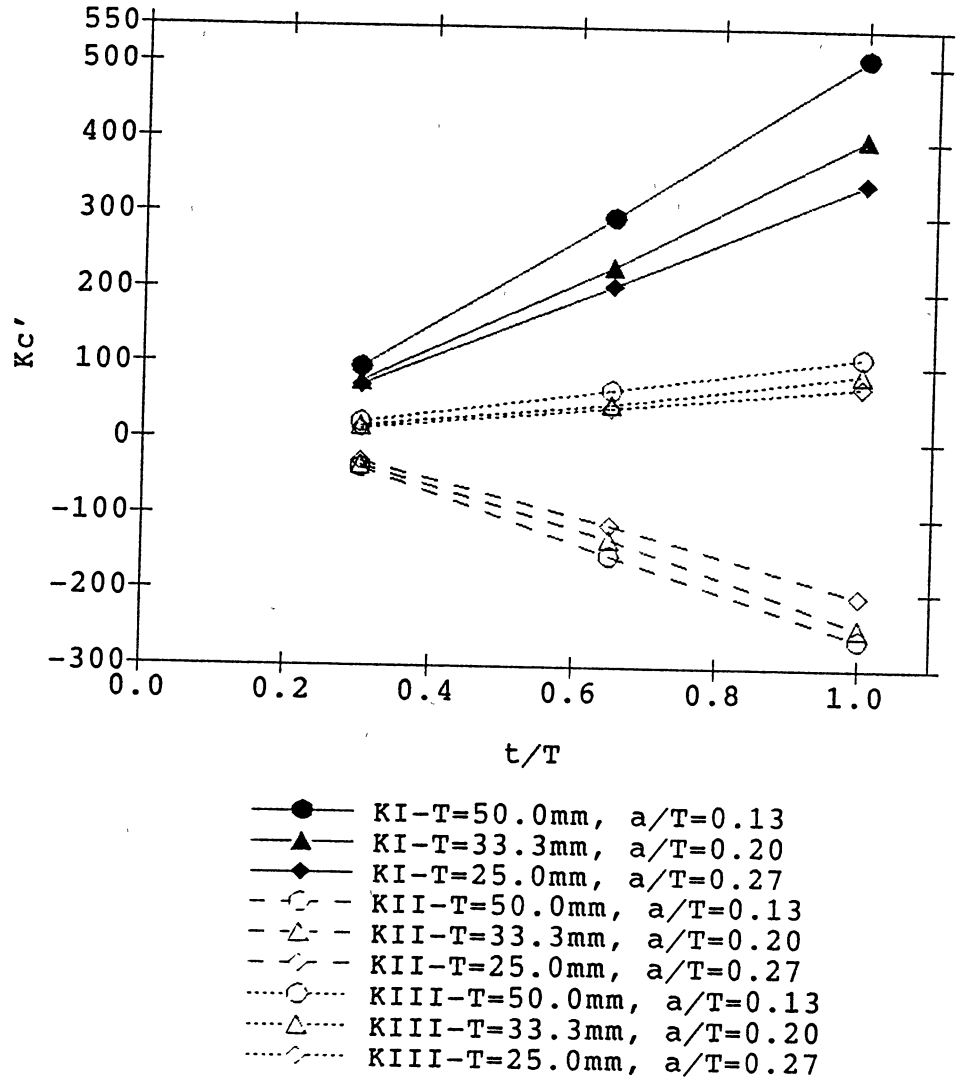

Figure 50. K_c' for Y-Joints with $\beta = 0.6$ under IPB

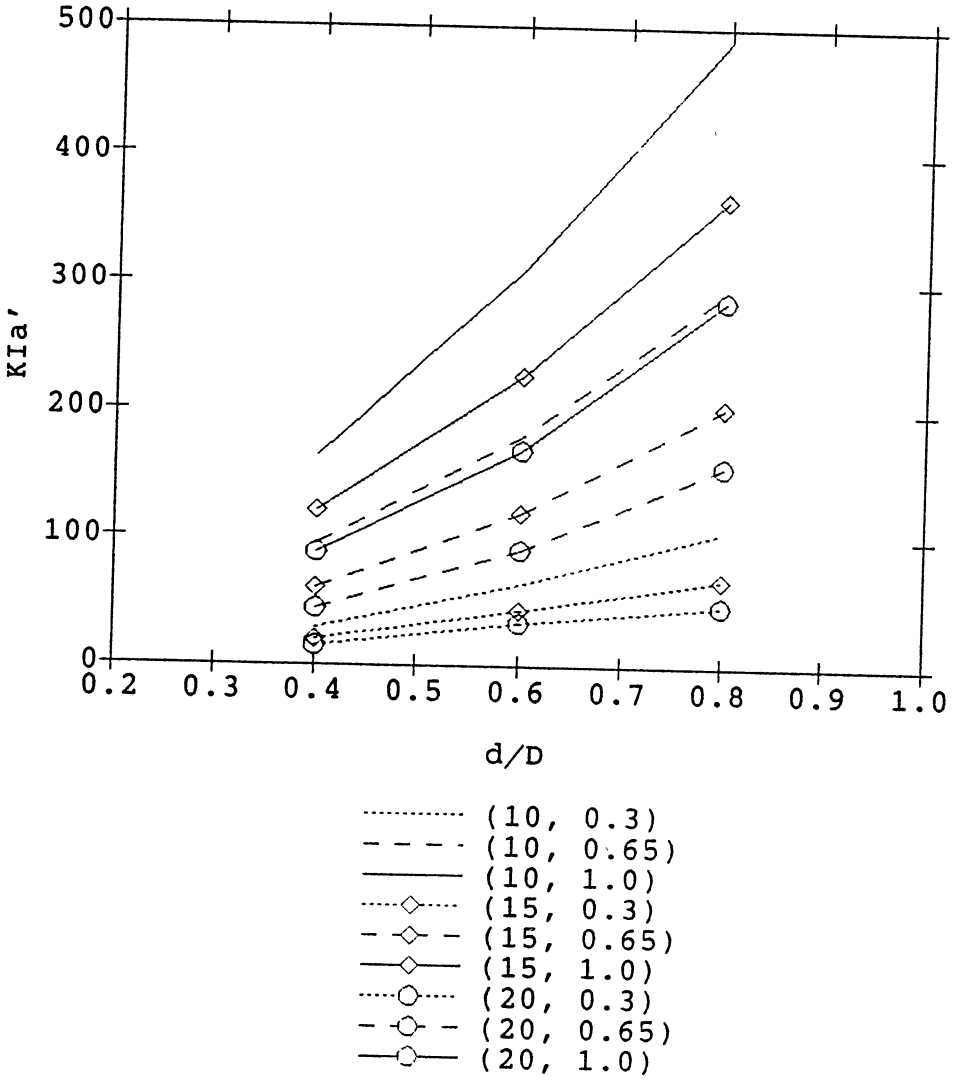

Figure 51. K_{Ia}' versus β = d/D for Joints under IPB

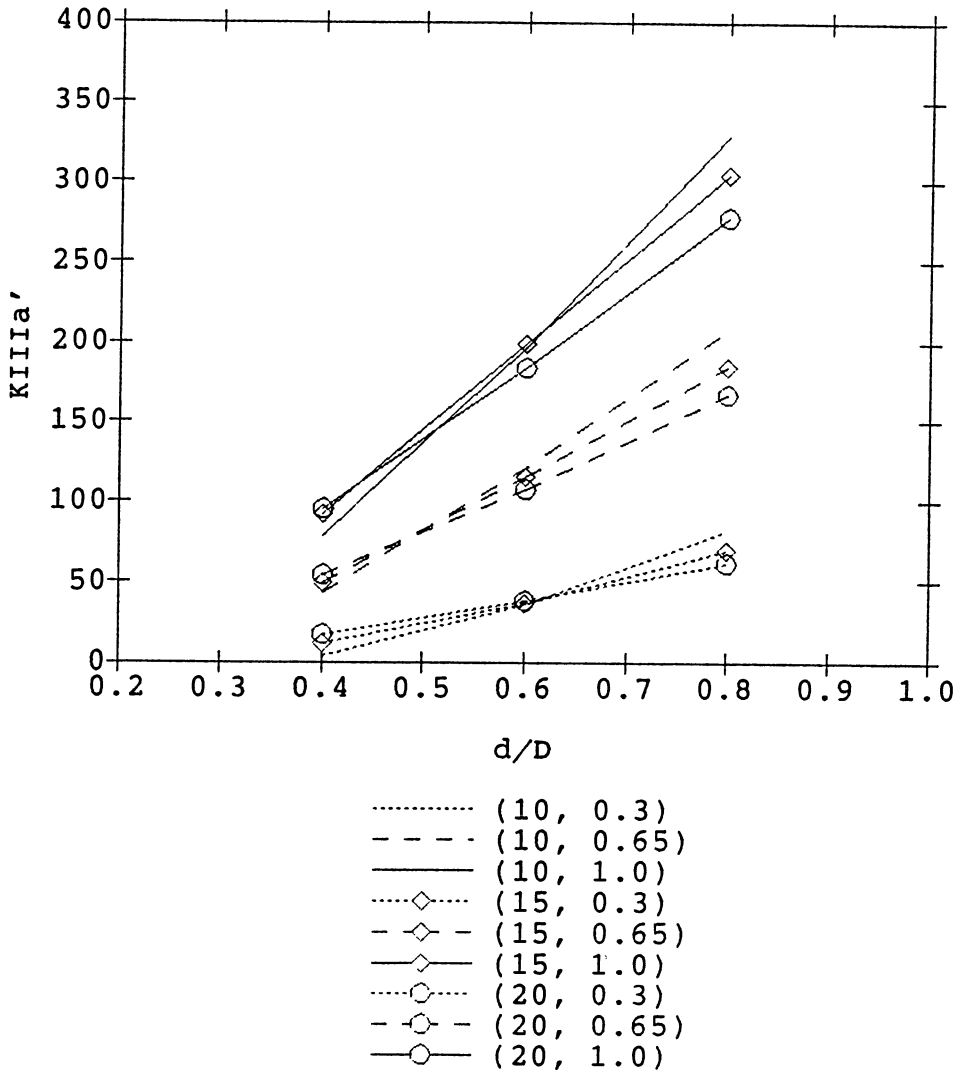

Figure 52. K_{III}' versus β = d/D for Joints under IPB

Mixed Mode Behavior of Weld Toe Cracks

In general, the three modes of relative movement between the two crack surfaces can exist for a Y-joint saddle surface crack. It is difficult to justify the assumption that a saddle crack has only relative crack opening movement due to the complicated geometry and stress distribution in the weld toe area, especially in the real ocean environment. The significance of the mixed mode behavior depend on the loading conditions, the crack location, and size.

The modeled crack surfaces are curved along the weld toe, and straight normal to the tube surface. Such a crack could be an initial defect. For relative shallow cracks, the models may represent fatigue cracks which were observed growing normal to the tube surface and only later in life turning curved in the weld [84]. The mixed mode behavior at two particular locations (the deepest point and the left surface end) on the crack front have been mentioned. This section will present the SIF along crack front where the mixed mode is possible.

Figure 53 shows the SIF solutions of model L1, L2 and L3 of Table 3, under axial brace tension. For a short and deep crack shown by the lines with points, the K_1 values in the deepest region may be very close to the K_2 values there. Under in-plane bending at brace end, the values of K_1, K_2, and K_3 for a small crack (Model S3) are shown in Figure 54. The SIF values of these three modes are rather close. This implies that even under simple loading, the mixed mode behavior may be significant. Further study is needed to understand how a crack growth direction affects the SIF, and how, in turn, the mixed-mode SIF influences the crack propagation behavior physically.

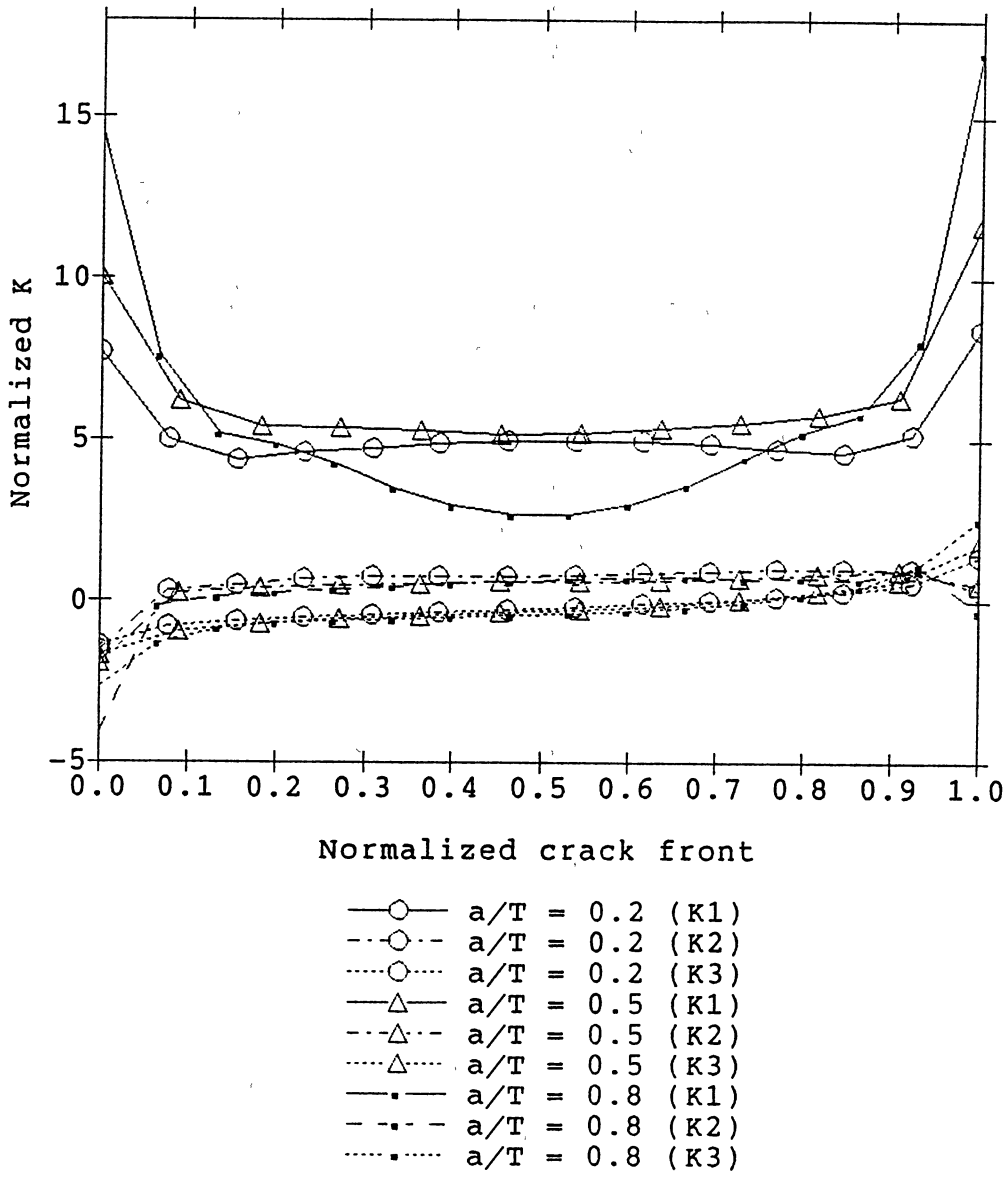

Figure 53. SIF Distribution Along Crack Front under AT

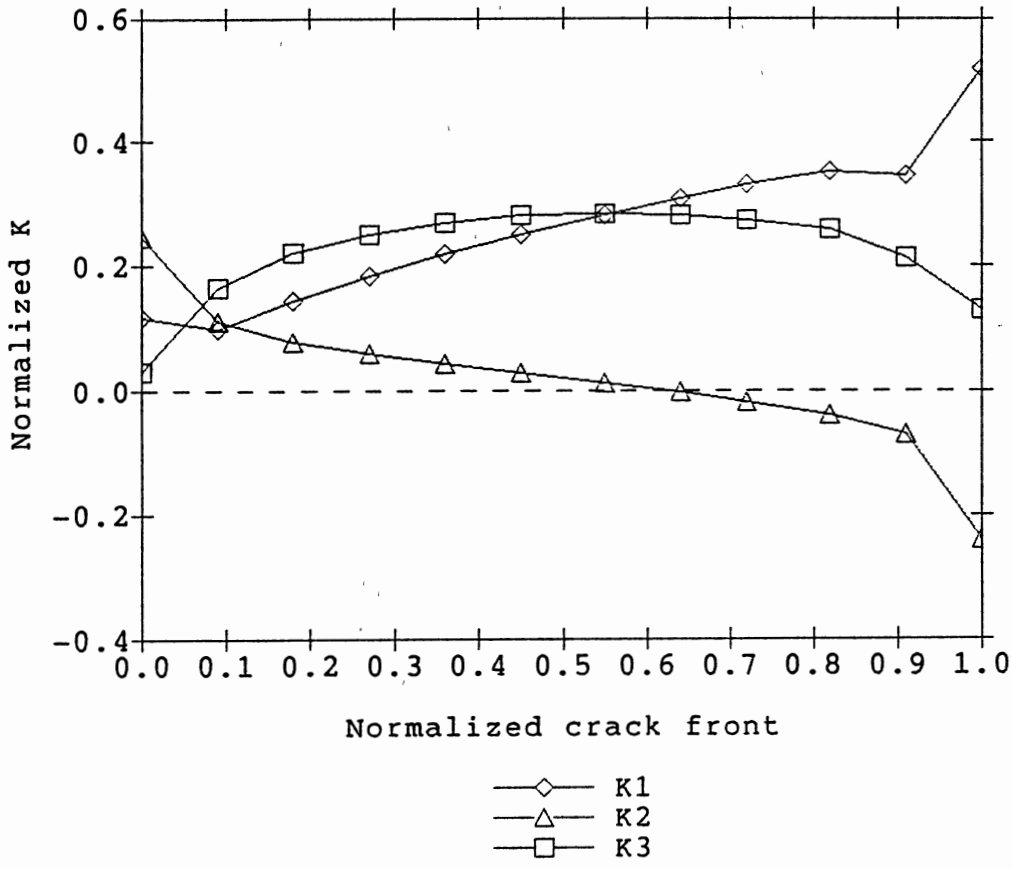

Figure 54. SIF Distribution Along Crack Front under IPB

Through-Wall Cracks in K-Joint

In a simple geometry, such as a plate with an inclined central crack, an initially mixed mode crack grows into a Mode I crack under stable fatigue loads by changing the crack growing direction [8]. This mode transformation may not be possible for a through-wall crack along the weld toe of a tubular joint because of the complex geometry and loading conditions.

Tubular joint weld toe cracks usually grow along the chord/brace intersection, and at the final statge of crack propagation they intend to grow on the chord away from the intersection [28]. To investigate the fatigue and fracture behavior of tubular joint defects after the wall penetration due to fatigue crack propagation, three K joint models, each with a through-wall crack of different size, as in Figure 55, were analyzed. The three K joints have the same dimensions as those shown in Figure 56. The sizes of the three through-wall cracks are c = 41.67 mm (model RK2F), c = 83.35 mm (model RK3F), and c = 160.0 mm (model K4F2), respectively.

A typical cracked K-joint FE model away from the crack region is shown in Figure 57 with boundary conditions. The through-wall crack was assumed on the chord side, with the two crack fronts straight and normal to the chord outer and inner surfaces. The mesh pattern near the crack front and opening is shown in Figure 58 with local coordinate systems along the two crack fronts.

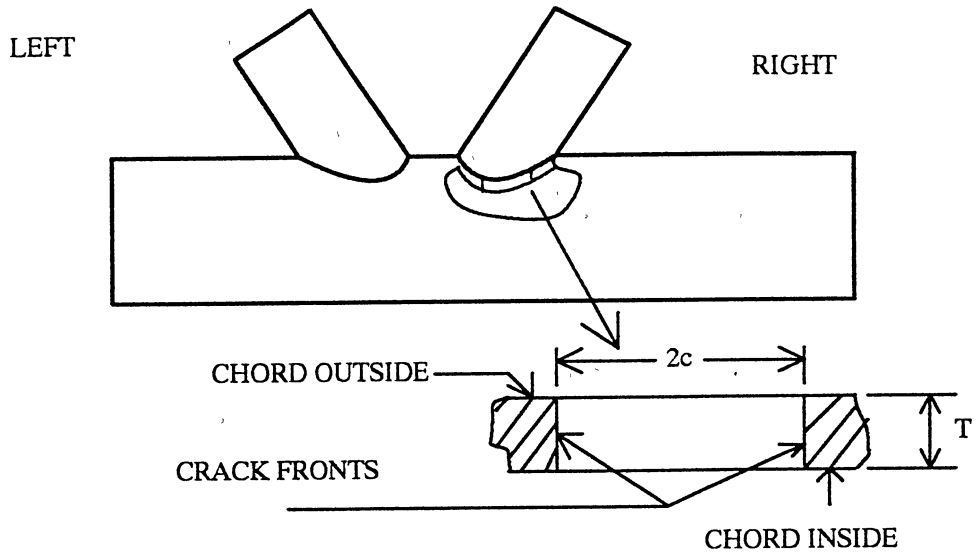

Figure 55. Through-Wall Crack in K-Joint

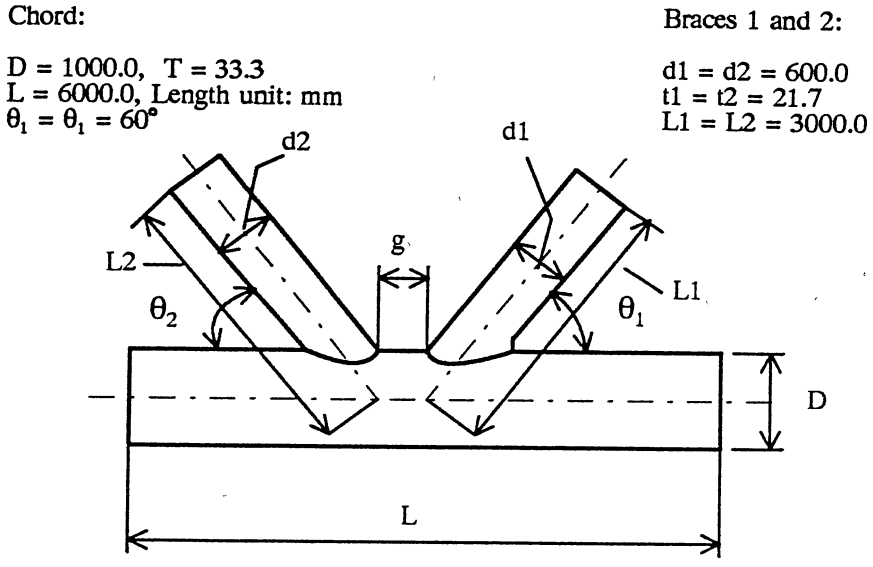

Figure 56. K-Joint Dimensions

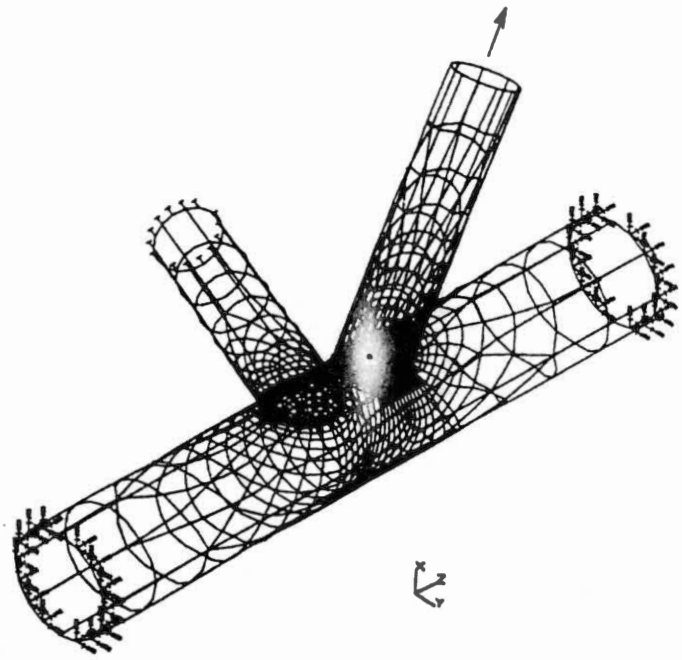

Figure 57. Finite Element Model of a K-Joint

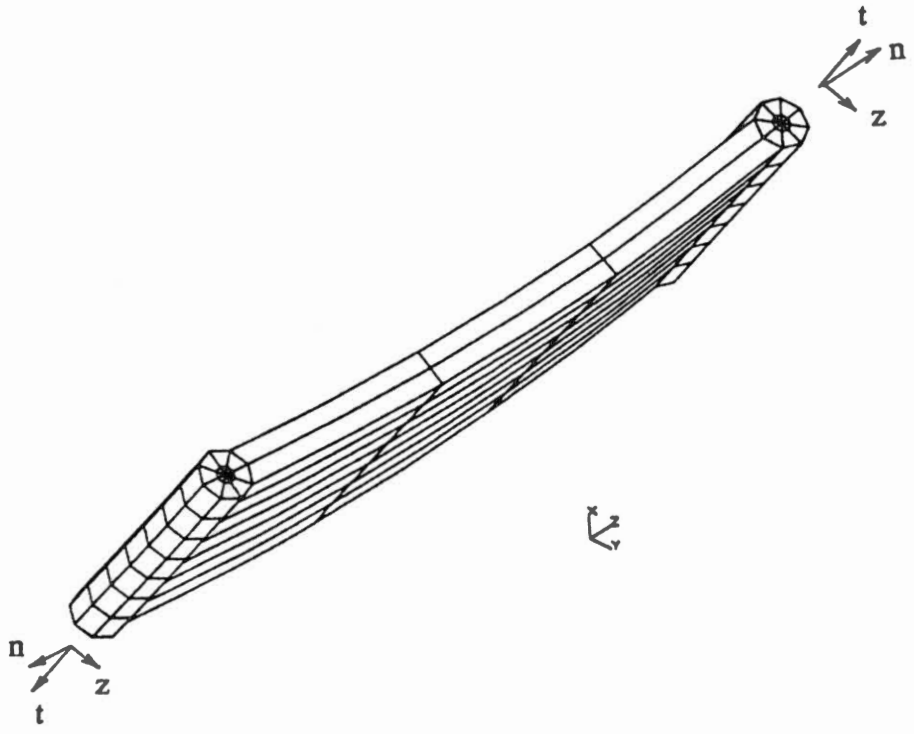

Figure 58. Local Coordinate Systems Along Crack Fronts

The SIFs at the left outer and inner crack tips on the chord surface versus crack half length c, under axial tension on brace 1, are shown in Figures 59 and 60, respectively. Normalized SIFs, using a = T, have been used. Symbol K_{1LO} denotes K_1 at the left crack end outside chord surface; K_{1Li} represents K_1 at the left crack tip of the inner chord surface, and other symbols have similar meaning. Model I (i.e. K_1) is dominant for short cracks (c < 80 mm), while mixed mode behavior appear to exist for long cracks (Figure 59). The mixed mode SIF seams to be more significant at the inner surface left crack tip, as shown in Figure 60.

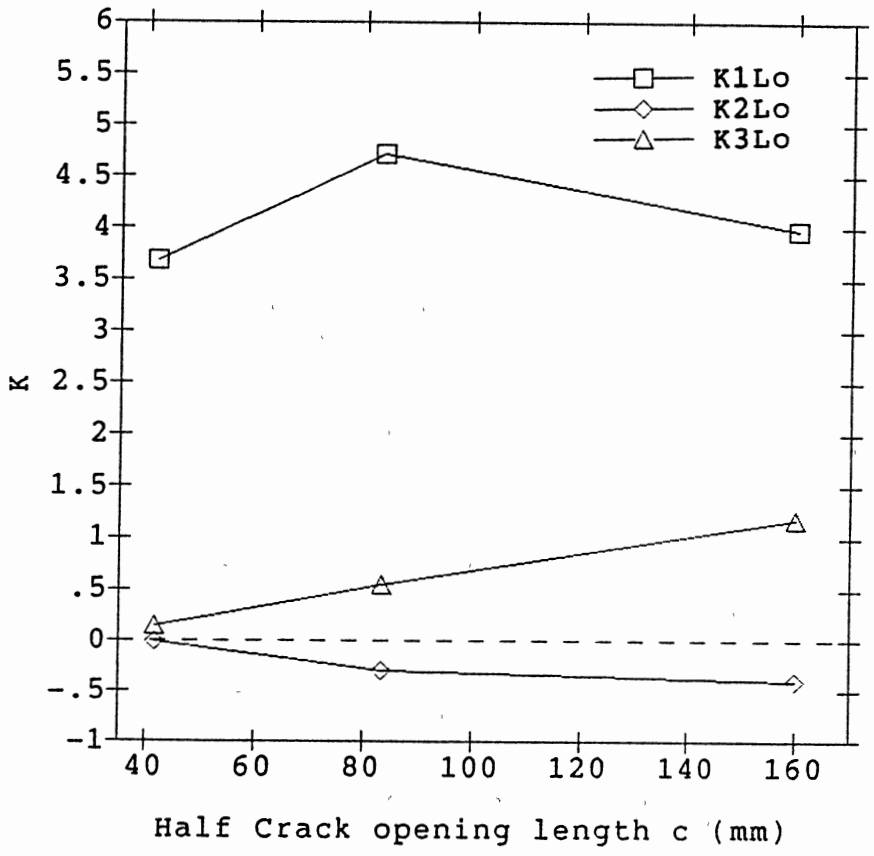

Figure 59. Normalized SIF at Left Outside Crack Tip

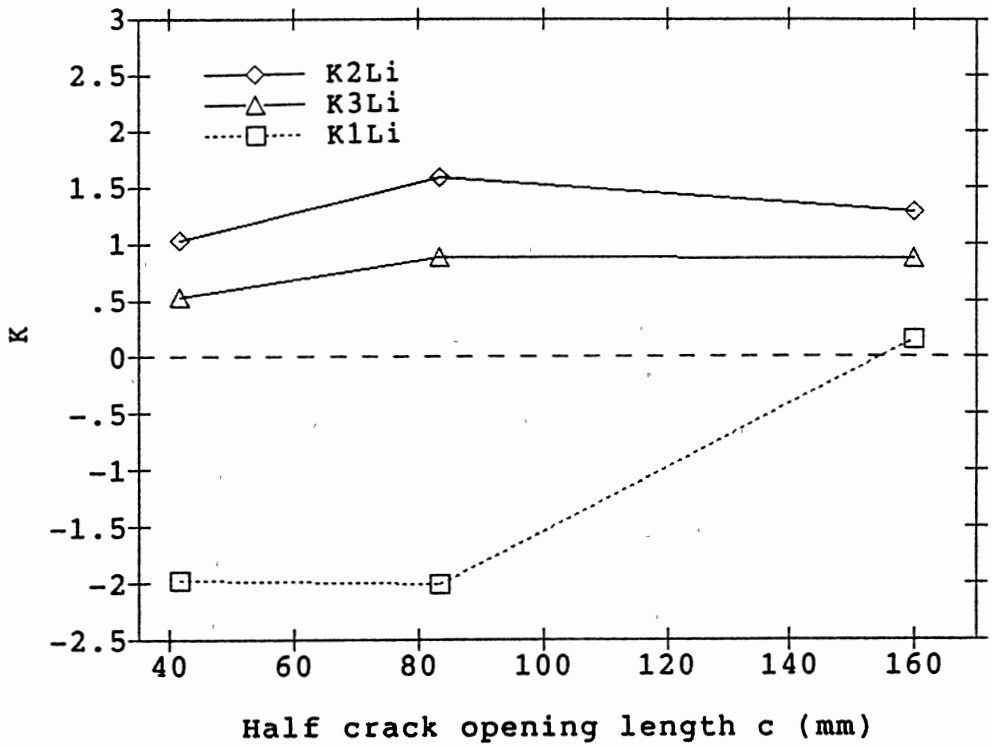

Figure 60. Normalized SIF at Left Inside-Surface Crack Tip

The dashed lines indicate that mode I is negative, implying that contact and penetration of the crack model surfaces occurred during the loading. Contact behavior of crack surfaces is very complicated because of its highly nonlinear nature and the surface friction involved. The subject of surface contact is beyond the scope of this work. A preliminary study of a cracked K-tubular joint with friction-free contact element indicates that the K_I solutions in the contact region are zero, and solutions away from the contact region are close to the K_I solutions without using contact element. Mode II and III SIFs are not affected significantly by the friction-free contact. Further studies are needed to understand the contact effect on the SIF. The effects of modes II and III in

Figure 59 increase with crack length. For the K-joint models under discussion, it seems that mixed mode SIF behavior may also occur and becomes significant at some crack front locations.

Multi-Axial Load Effects on K-Joint Weld Toe Crack

Various combinations of loading magnitudes and directions from marine environments produce many complicated load situations in a tubular joint. It is important to have systematic procedures to calculate the stress intensity factors efficiently for a crack under multi-axial loading conditions, so that minimum number of finite element analyses is performed. In the following discussion, a K-joint was used to demonstrate a superposition procedure which is efficient to calculate SIF solutions under multi-axial loads. The geometry dimensions of the joint are given in Figure 56. Only the chord right end was fixed as the model boundary condition. The other two brace and chord ends were subjected to loads.

The original joint can be treated as the superposition of three K joints, each having a single axial load, as illustrated in Figure 61. The three K-joint models in this figure were named MK1, MK2, and MK3, respectively. Each of these three models yields the stress intensity factors (K_I, K_{II}, K_{III}) at a point along the crack front. For example, the SIF solution at the crack front center (i.e. the deepest point) from Model MK1 under axial brace tension can be written as

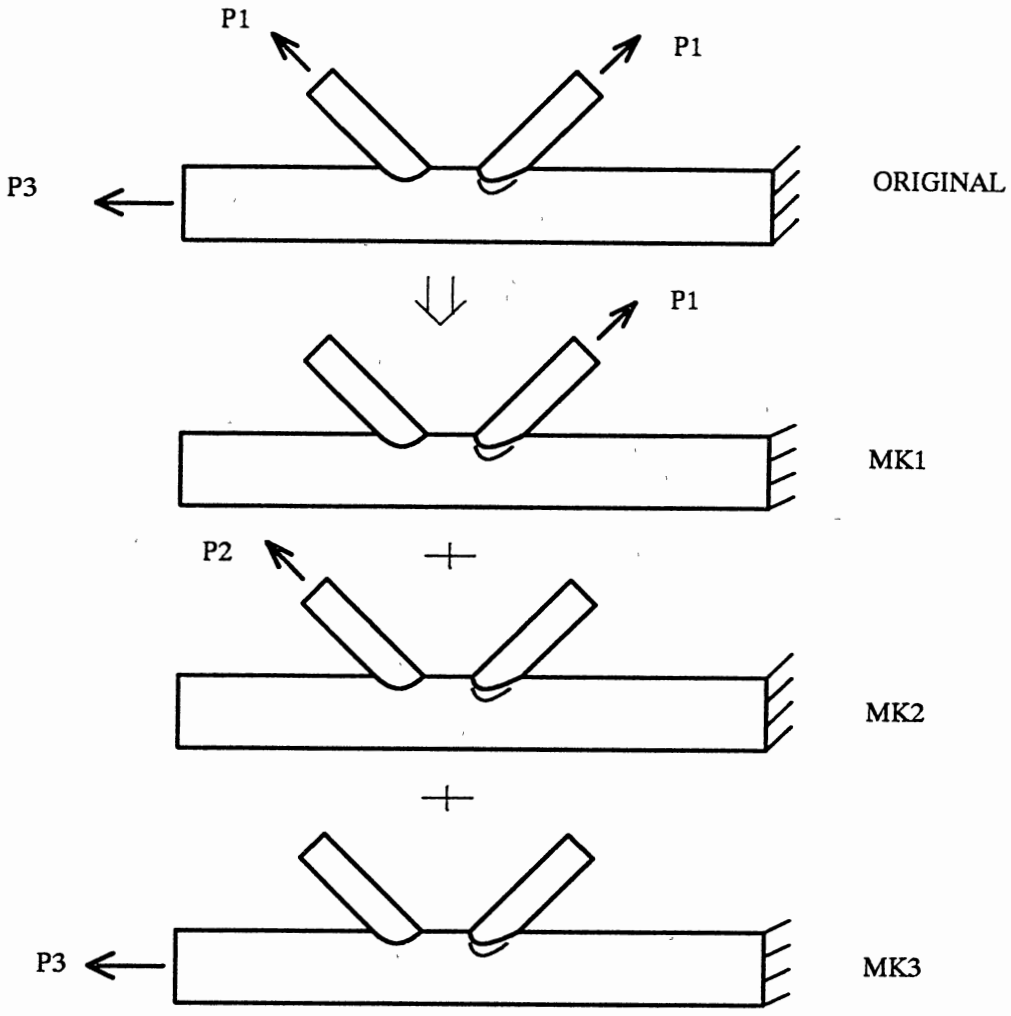

Figure 61. Superposition Procedure for Multi-Axial Load Effect

$$K_I = C_{11} P_1$$
$$K_{II} = C_{21} P_1 \qquad (21)$$
$$K_{III} = C_{31} P_1$$

where coefficients C_{11}, C_{21}, and C_{31} represent the contribution of unit load of P_1 to K_I, K_{II},

and K_{III} at the crack front center, respectively. These coefficients are called influence coefficients at crack front center from load P_1. The finite element method was used to obtain these coefficients. Similarly, the SIFs at the same location as above for models MK2 and MK3 can be written as

$$\begin{aligned} K_I &= C_{12} P_2 \\ K_{II} &= C_{22} P_2 \\ K_{III} &= C_{32} P_2 \end{aligned} \tag{22}$$

and

$$\begin{aligned} K_I &= C_{13} P_3 \\ K_{II} &= C_{23} P_3 \\ K_{III} &= C_{33} P_3 \end{aligned} \tag{23}$$

respectively, where C_{i2} and C_{i3} (i = 1, 2, 3) are the influence coefficients at the crack front center due to tension loads P_2 and P_3, respectively. Therefore, total SIFs at the crack front center of the original K-joint are obtained by combining the above components, i.e.,

$$\begin{aligned} K_I &= C_{11} P_1 + C_{12} P_2 + C_{13} P_3 \\ K_{II} &= C_{21} P_1 + C_{22} P_2 + C_{23} P_3 \\ K_{II} &= C_{31} P_1 + C_{32} P_2 + C_{33} P_3 \end{aligned} \tag{24}$$

One of the advantages of this procedure is that once the influence coefficients C_{ij} are obtained for the K tubular joint with the saddle crack from FE analyses, the SIFs for any load combinations can be readily obtained without using FE analysis. These equations

can be generalized for other crack front locations, and for any other load combinations. This procedure can also be generalized for other tubular joints with more complicated configurations. The superposition procedure is applicable as long as there is no crack surface contact under the final combined loads.

The first row in Table 9 lists influence coefficients C_{ij}^{L} in the above equations. The superscript symbol L indicates loading mode, L = 1 for AT, axial tension. Results for the other five loading modes are also given in these two tables. The load directions corresponding to C_{ij}^{L} in Table 9 are given in Table 10. The positive directions for each tube are shown in Figure 62. A positive sign (+) indicates that the applied load is in the same direction as the corresponding positive coordinate system direction. A negative sign (-) indicates that the applied load is in the opposite direction.

To examine the accuracy and reliability of the proposed superposition procedure, several different loading cases on the K-joint have been applied in the following two examples.

Table 11 shows the SIF results (K_{Ia}), of example 1, with the K joint under multiple axial tensions P1 = 34000 N, P2 = -34000 N, and P3 = 60000 N as shown in Figure 61, from the superposition procedure using the influence coefficients of load AT in Table 9, and the direct FEM on the original model (with all the forces applied at the same time), respectively. The two sets of SIF solutions are in very good agreement, with slight difference due to rounding errors of the coefficients in Table 9.

Table 12 shows SIF results (K_{Ia}), of example 2, for the K-joint with six modes of loading at each of the three tube ends. The superposition and the direct FEM analysis also provide very close SIF solutions. The load vector applied at joint end i relative to

TABLE 9

SIF INFLUENCE COEFFICIENTS AT THE
DEEPEST CRACK FRONT POSITION

Models	MK1			MK2			MK3		
Load	C_{11}^L	C_{21}^L	C_{31}^L	C_{12}^L	C_{22}^L	C_{32}^L	C_{13}^L	C_{23}^L	C_{33}^L
AT	7.0564×10^{-4}	0.8540×10^{-4}	0.0326×10^{-4}	3.4956×10^{-4}	0.4215×10^{-4}	0.6528×10^{-4}	-0.3488×10^{-6}	1.1627×10^{-6}	-1.7440×10^{-6}
OPB	4.2857×10^{-6}	0.4774×10^{-6}	-0.0858×10^{-6}	1.4897×10^{-6}	0.1321×10^{-6}	0.0687×10^{-6}	0.0833×10^{-8}	0.2916×10^{-8}	-0.4582×10^{-8}
IPB	1.5788×10^{-7}	0.0500×10^{-7}	2.7286×10^{-7}	3.6661×10^{-7}	0.6096×10^{-7}	0.4885×10^{-7}	0.1795×10^{-7}	-0.0376×10^{-7}	0.0543×10^{-7}
TOR	2.4992×10^{-6}	0.2906×10^{-6}	0.2572×10^{-6}	0.6626×10^{-6}	0.0548×10^{-6}	0.0525×10^{-6}	0.1229×10^{-7}	0.0312×10^{-7}	1.1122×10^{-7}
OPS	1.0131×10^{-2}	0.1141×10^{-2}	-0.0118×10^{-2}	0.3426×10^{-2}	0.0308×10^{-2}	0.0301×10^{-2}	0.6685×10^{-5}	1.3487×10^{-5}	6.5632×10^{-5}
IPS	-1.5661×10^{-4}	-0.5778×10^{-4}	6.1121×10^{-4}	7.6667×10^{-4}	1.3696×10^{-4}	0.8453×10^{-4}	0.5383×10^{-4}	-0.0872×10^{-4}	0.7987×10^{-4}

Units: For AT, OPS and IPS: C_{ij}^L unit is MPa $\cdot \sqrt{mm}/N$

For OPB, IPB, and TOR: C_{ij}^L unit is MPa $\cdot \sqrt{mm}/N \bullet mm$

TABLE 10

CHORD AND BRACE LOADING DIRECTIONS

Model	Load					
	IPS	OPS	AT	OPB	IPB	TOR
MK1	-	-	+	+	-	-
MK2	-	+	+	-	-	+
MK3	+	-	-	-	-	-

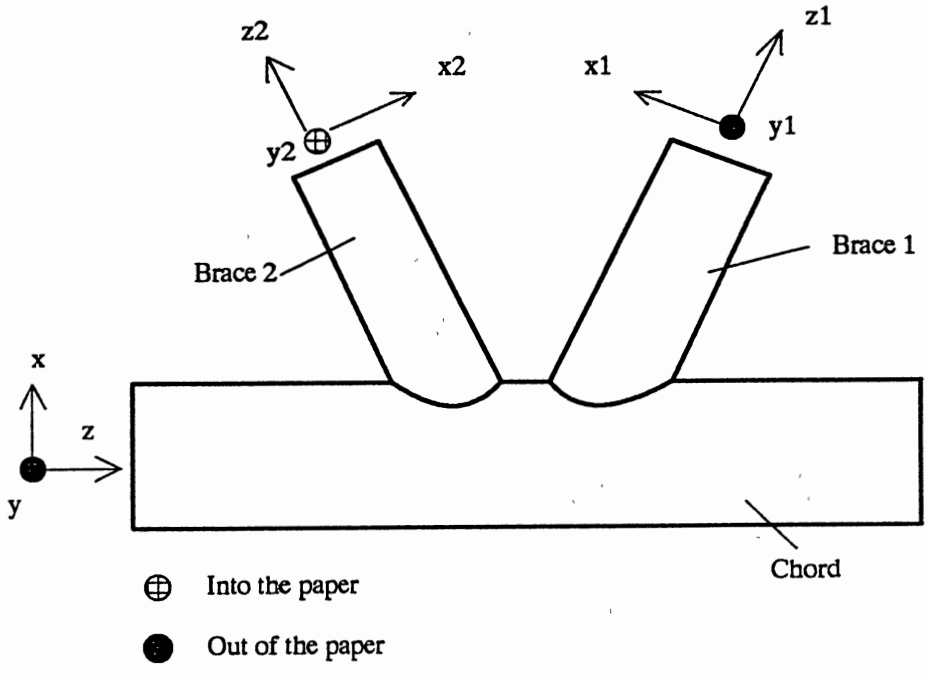

Figure 62. Brace Local Coordinate Systems of the K-Joint

the local coordinate axes are written as:

$$\underline{F}_i = \{P_x, P_y, P_z, M_x, M_y, M_z\}^T = \{P_i^6, P_i^5, P_i^1, P_i^2, P_i^3, P_i^4\}^T$$

TABLE 11

K_{Ia} UNDER MULTIPLE AXIAL TENSION

Units: MPa$\sqrt{}$mm

Method	K_I	K_{II}	K_{III}
Superposition	12.0858	1.5403	-2.2133
FEM Analysis	12.1235	1.5984	-2.2160
Difference	-0.31%	-3.63%	-0.12%

TABLE 12

K_{Ia} UNDER COMBINED LOADING AT MULTIPLE ENDS

Method	K_I	K_{II}	K_{III}
From Superposition	15.6427	1.9263	-1.4574
From FEM Directly	15.6834	1.9805	-1.4579
Difference	-0.26%	-2.74%	0.03%

The SIF (K_I, K_{II}, K_{III}) unit is MPa$\sqrt{}$mm

The loads used for the SIF solutions in Table 12 are given by:

$$\underline{F}_1 = \{-850.0, -220.0, 34000.0, 65000.0, -360000.0, -4600.0\}^T$$

$$\underline{F}_2 = \{-700.0, 120.0, -34000.0, -25000.0, -250000.0, 1600.0\}^T$$

$$\underline{F}_3 = \{430.0, -320.0, -60000.0, -85000.0, -620000.0, -7600.0\}^T$$

The units of force and moment are N and N•mm, respectively.

CHAPTER IV

SENSITIVITY STUDY OF FINITE ELEMENT MODELS

Introduction

The effects of model dimensional sizes and the finite element mesh are important issues for experimental and numerical studies of tubular joint weld toe cracks. Proper chord and brace lengths are needed to eliminate end effects on joint strength. However, insufficient test data are available to evaluate the effects of chord length for T/Y joint strength [3]. Previous work [90] on stress concentration factors (SCF) along tubular joint weld toe indicates that the chord length effect can be ignored when the ratio of chord length to chord diameter (2L/D) is greater than 13.1. However, no data are available to assess the effects of chord length and brace length on the SIF solution of tubular joint weld toe defects.

Reliable SIF solutions and computing cost considerations from the finite element method require a reasonable distribution of the finite element mesh over the tubular joint. To assess the effects of chord/brace length and element mesh on the SIF solutions, twenty-one cracked Y-joint models have been studied using 3-D finite element method. The results will be discussed in the following sessions.

Chord and Brace Length Effect

Various joint models of different chord lengths with crack sizes (in mm) a/c = 6.67/33.35 were studied. Six FE analysis results of the SIF for Y joints with saddle surface cracks were calculated. Symbols KIa, KIIa and KIIIa (or K_{Ia}, K_{IIa}, and K_{IIIa}) represent the SIF at the deepest crack point, while KIc, KIIc and KIIIc (or K_{Ic}, K_{IIc}, and K_{IIIc}) represent the SIF at the left crack end. The SIF under AT increases with chord length or α (Figures 63 and 64), since longer chord results in greater bending moment for a constant brace axial tension. Under constant OPB, the SIF increases slightly but similarly to that in Figure 63 with the chord length.

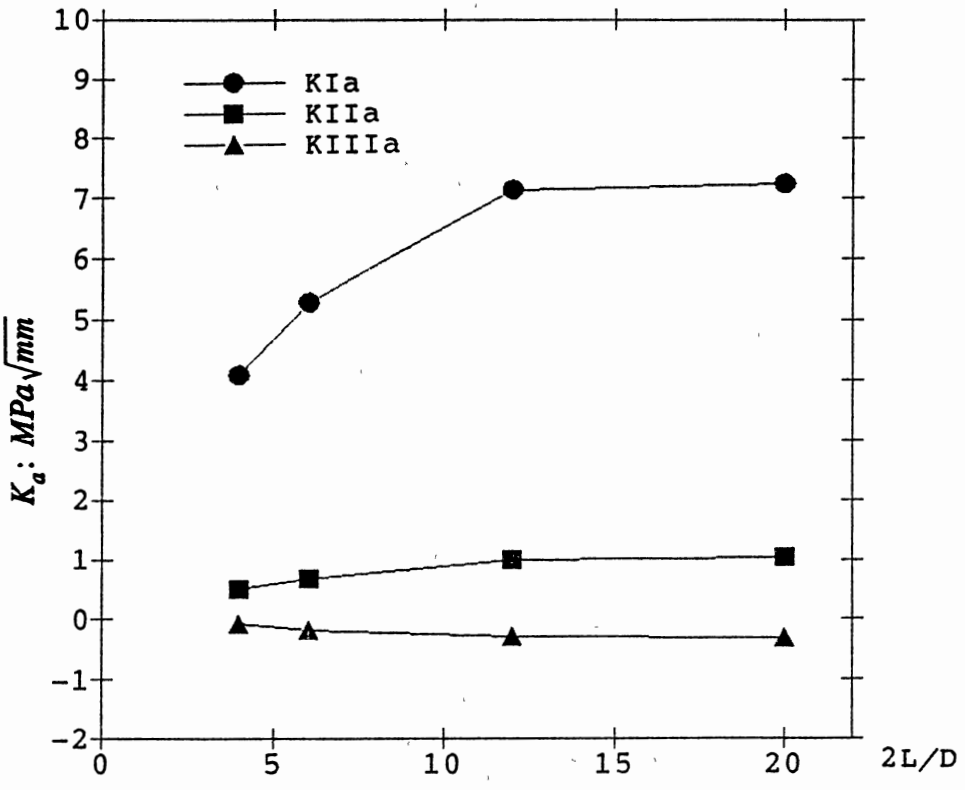

Figure 63. K_{ia} (i = I, II,III) versus α = 2L/D under AT = 10^4 N

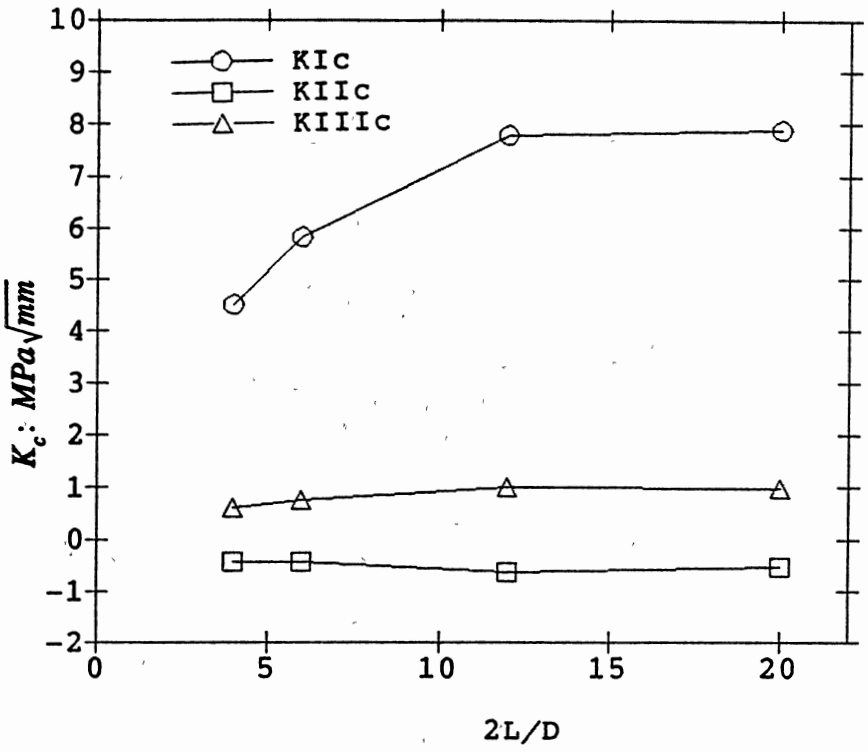

Figure 64. K_{ic} (i = I, II,III) versus α = 2L/D under AT = 10^4 N

For constant IPB, the SIF decreases with chord length (Figures 65 and 66), since longer chord releases the in-plane bending stress in the joint intersection area. In general, the chord length of a tubular joint affects the SIF solution of a weld toe defect. However, the effect is not significant for all these loading modes when $\alpha > 12.0$.

The effect of brace length on the SIF of cracks on chord side is not significant for a brace long enough to allow its external applied end force distribution to "smooth out", since the brace primarily transfer load to the chord. For the two Y joint models with saddle cracks in Figure 67, the SIF versus brace length (L_b/D) under AT is shown in Figure 68. The effect of brace length on the SIF solutions under OPB and IPB have also

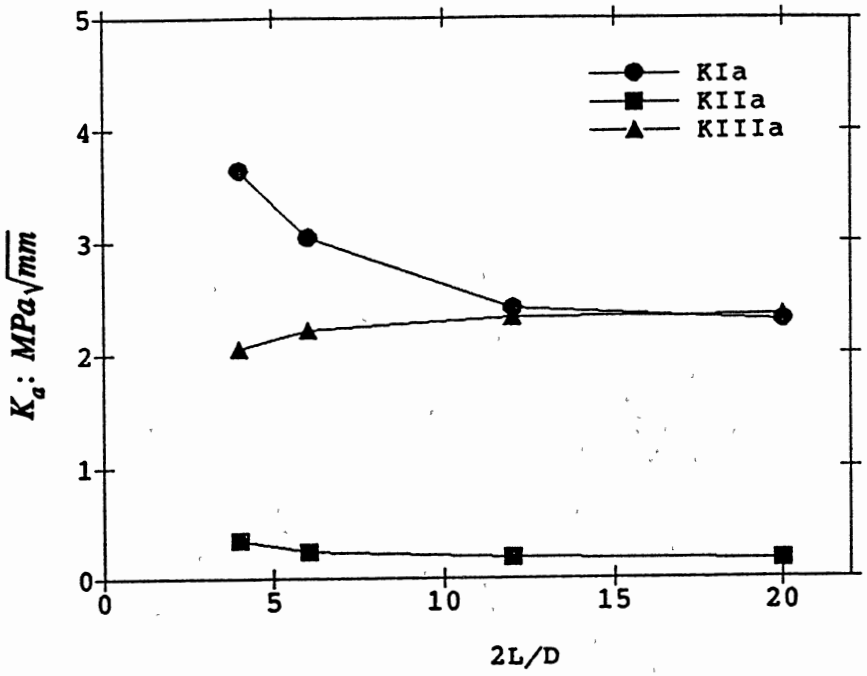

Figure 65. K_{ia} (i = I, II, III) versus α = 2L/D under IPB = 10^7 N mm

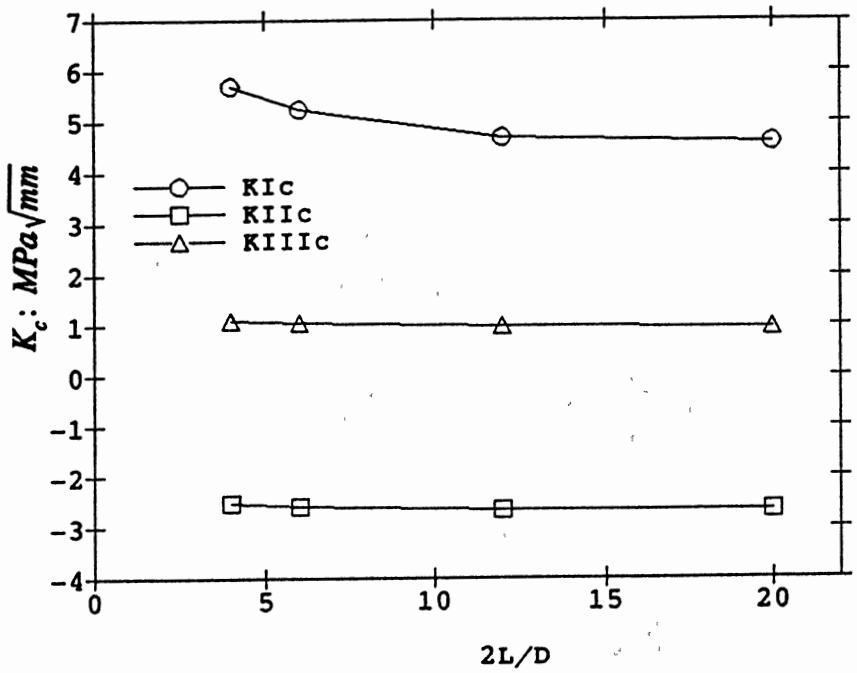

Figure 66. K_{ic} (i = I, II, III) versus α = 2L/D under IPB = 10^7 N mm

been examined and similar trends exist. These solutions indicate that the effect of brace length is not significant even for $L_b/D > 1.5$.

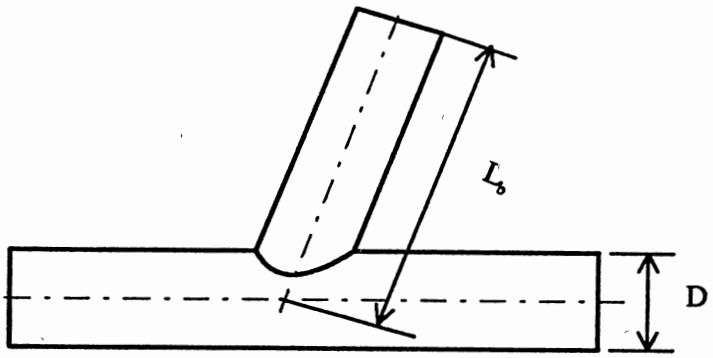

Figure 67. Y-Joints with Different Brace Length

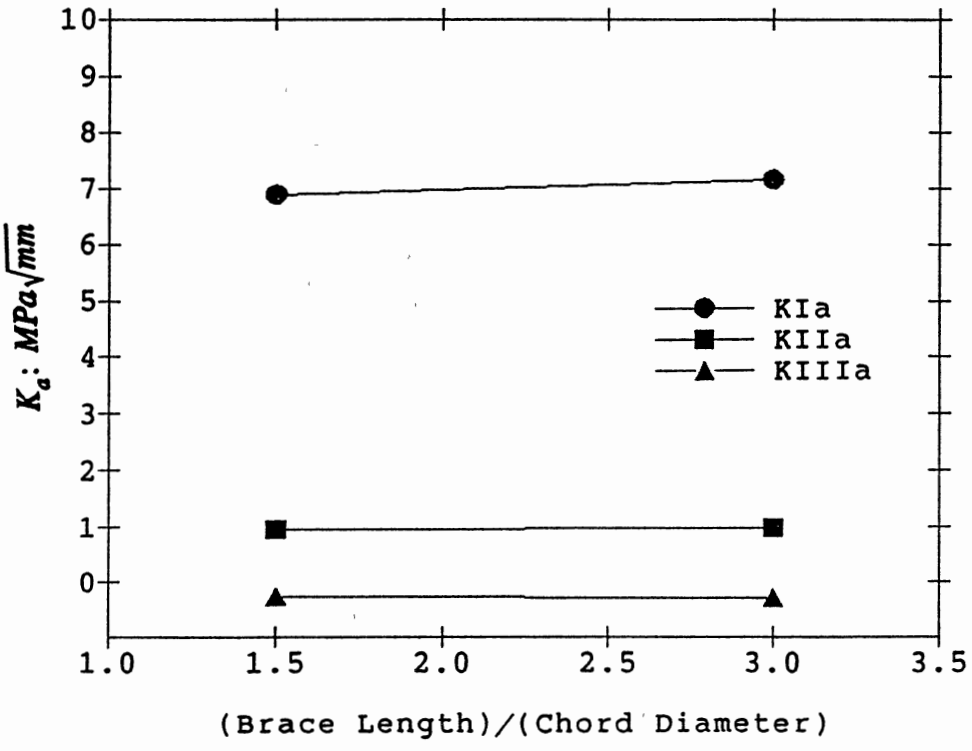

Figure 68. Brace Length Effect on K_{ia} (i = I, II, III) under AT = 10^4 N

Finite Element Mesh Effect

The finite element mesh density generally affects the accuracy of solutions. For a conventional structural analysis (i.e., without a crack), the smaller element sizes yield better accuracy. This may not be true for FEM solutions of a cracked structure. Previous research by others [83] on a simple standard configuration (the ASTM E399 standard three-point bend) indicates that the optimum 3-D crack tip quarter-point element size (L_e) for that problem appears to be about $L_e/a = 0.06$. However, the optimum crack tip element size is controlled by the size of the K dominant zone, which is problem dependent.

For the sensitivity study of the FEM for tubular joints with cracks, the finite elements were classified as two groups: one group (Local elements) consists of the elements in the crack region where cubic solid elements and quarter-point 3-D elements were used. The other group (Global elements) consists of the elements away from the crack region, where thick-shell elements for the tubes and cubic solid elements for the weld, as well as transition elements, were used. To isolate the mesh effect from each group, mesh in one group was modified while the other group unchanged. Fifteen FE models of the Y joint YS15 in Table 8 have been analyzed to investigate the sensitivity effect. The combinations of the local and the global elements are listed in Table 13, where G_e represents the number of global elements, and SEN1S, SEN2S, ... etc., are model names. The sizes (in mm) of the crack are a/c = 6.67/33.35. In the following, the results under brace axial tension (AT) will be discussed.

TABLE 13

Y-JOINT MODELS WITH VARIOUS GLOBAL AND LOCAL ELEMENTS

G_e	L_e/a 2.5%	5%	10%	15%	20%
750	SEN3S	SEN2S	SEN1S	SENB1	SENB2
1200	SEN6S	SEN5S	SEN4S	SENB3	SENB4
1593	SEN9S	SEN8S	SEN7S	SEN10	SEN11

Figure 69 shows the solutions of the normalized SIFs at the crack deepest point. The horizontal axis represents the ratio L_e/a. The symbol G_e in the figure represents the number of the global elements. This figure indicates that for L_e/a between 0.025 and 0.20, the global element effect (G_e = 750 to 1593) on the SIFs is not significant. By comparison, the effect of crack-tip element size is more significant than that of global element sizes. A similar plot for the normalized SIFs at the left crack end were also obtained.

The SIF values at the crack front center were the average of the SIF solutions from the 9 directions (θ = -180°, -135°, -90°, -45°, 0°, 45°, 90°, 135°, 180°) along the crack-tip radial lines. A typical set of normalized SIF solutions along Y-Joint weld toe crack front under AT (Model YS19 in Table 7) is given in Figure 70. They are consistent with each other for most of the radial directions throughout the crack front, except for crack front points at the tubular surface where the normal plane cannot be defined and the crack tip radial lines are curved [10]. These solutions would be the same if the FEM

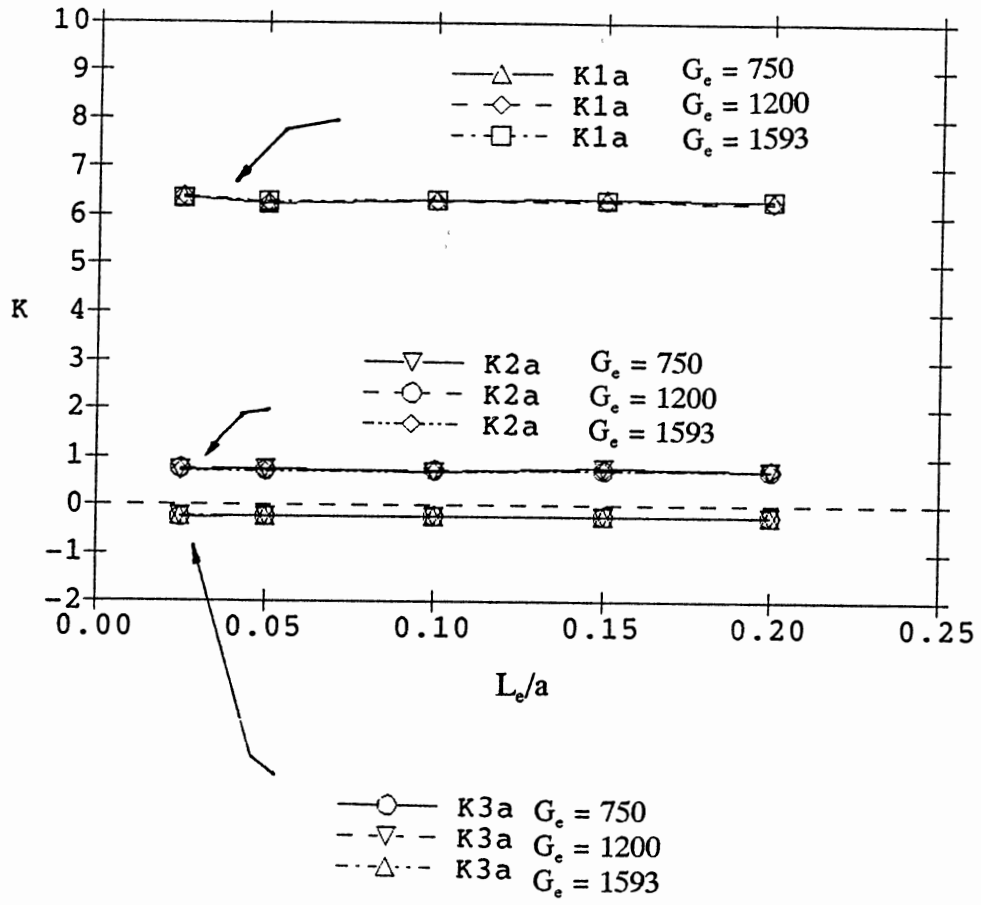

Figure 69. Sensitivity of K_{1a} under Axial Brace Tension

were exact. Therefore, the scatter (standard deviation) of the solutions about the average can be used as another alternative measurement of accuracy and reliability of SIF solutions.

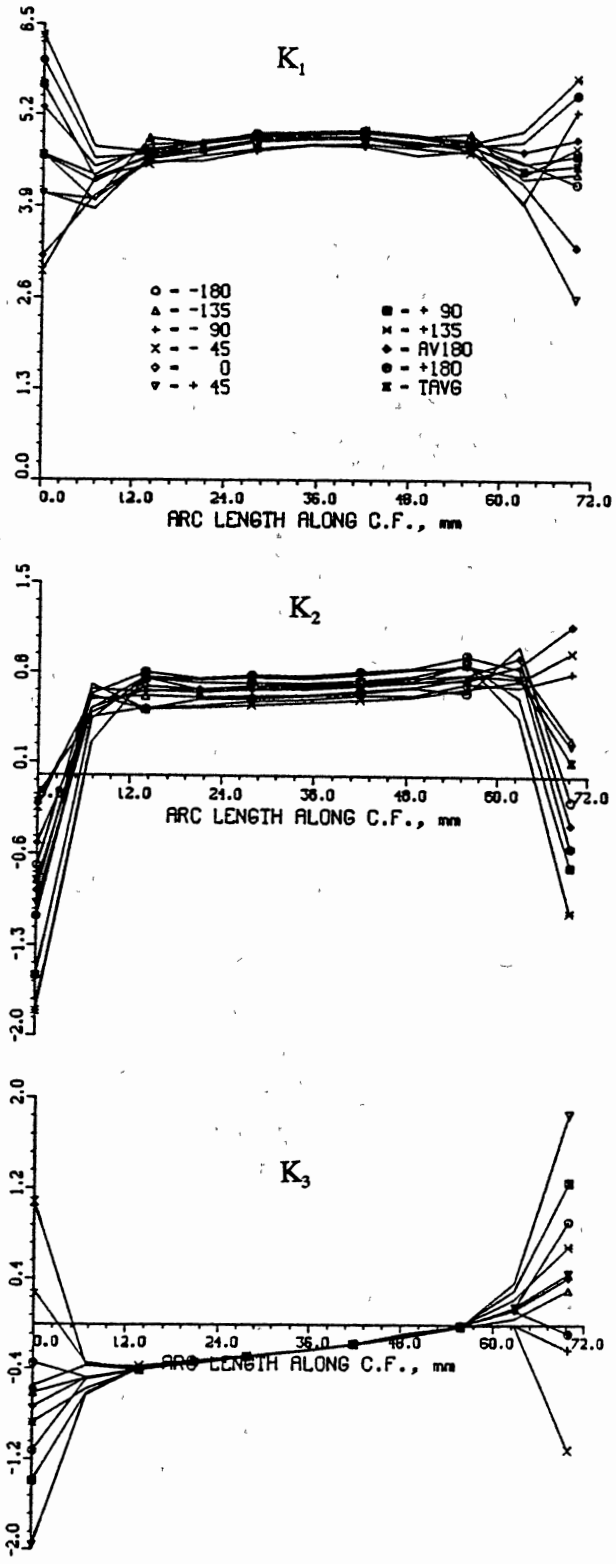

Figure 70. Normalized SIF from Different Radial Directions

Figure 71 shows averaged K_1-scatter (or the standard deviation, STD_K1) on the five-points near the crack front deepest point. Lower scatter implies better results of K_1. The curves in Figure 72 are the K_2-scatters (i.e. STD_K2) of K_2 around the crack deepest point. The K_3-scatters around the crack deepest point are less than 10% of the K_1-scatters. K_2-scatters are generally less than K_1-scatters, but the relative scatter (i.e., relative error, or deviation coefficient) of K_2 is often slightly greater than those of K_1 and K_3, respectively. This is due to the fact that mode I is dominant under AT.

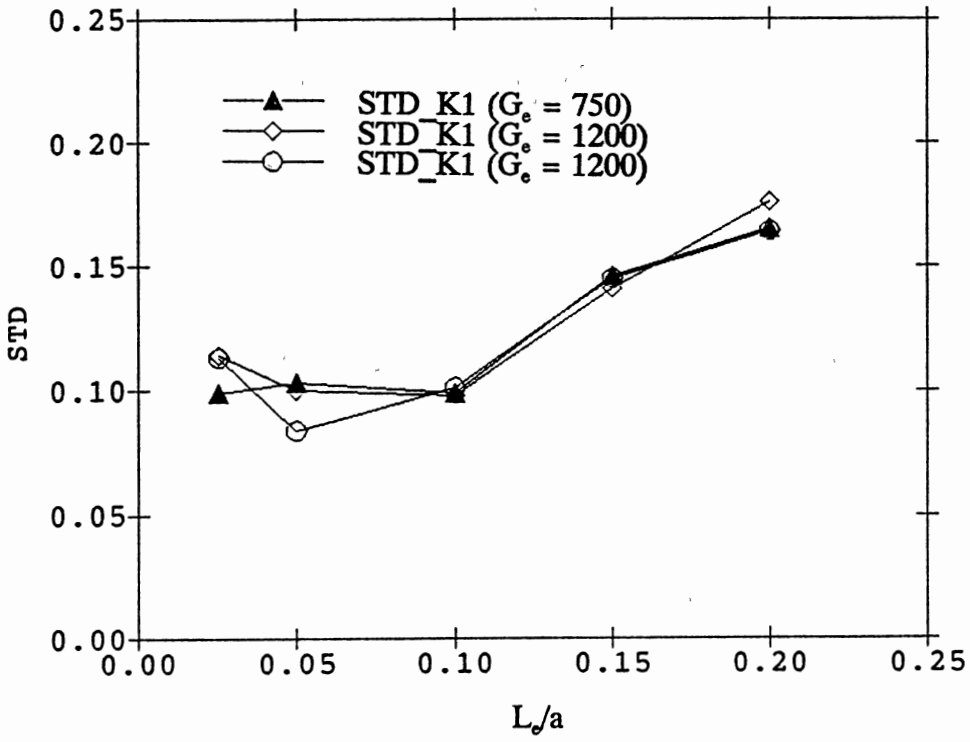

Figure 71. Standard Deviation of K_1 around Crack Front Center

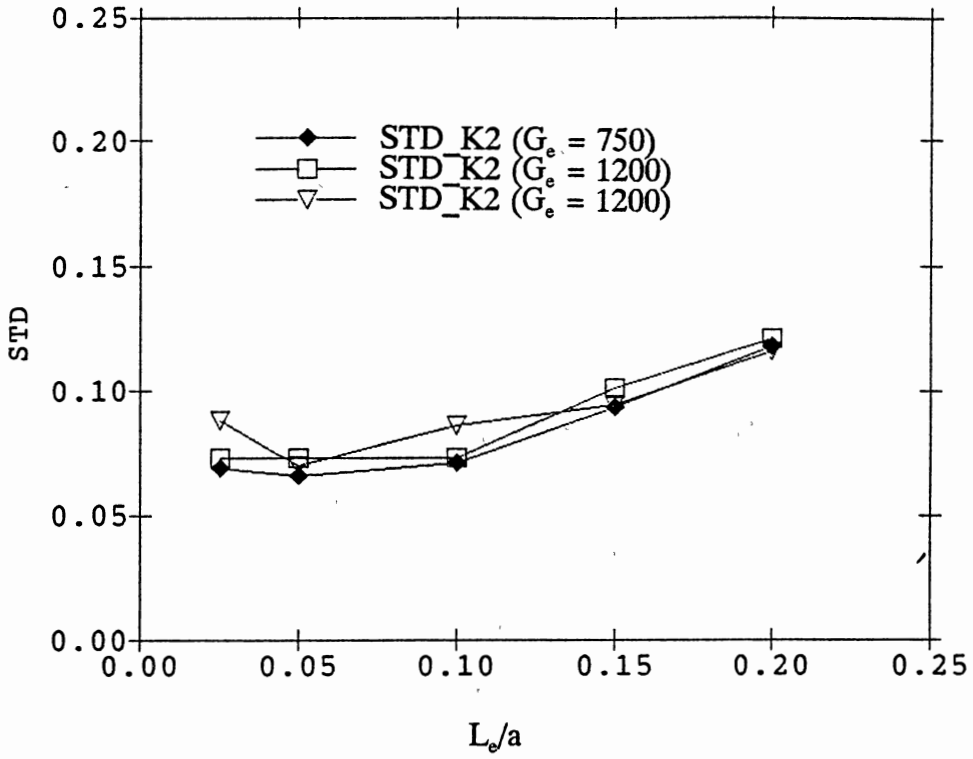

Figure 72. Standard Deviation of K_2 around Crack Front Center

Concluding Remarks

The crack-tip element size in the previous chapter were around L_e/a = 0.05 to 0.10, and the number of the global element (G_e) were generally greater than 900. These results in this chapter indicate that for L_e/a = 0.05 to 0.10, the SIFs have the least scatter for the 15 analyses performed. The sensitivity study provides confidence in the three-dimensional finite element models used in this work.

CHAPTER V

EMPIRICAL FORMULAS FOR THE STRESS INTENSITY FACTORS OF T-TUBULAR JOINTS

Introduction

Empirical formulas of the SIF solutions for tubular joint weld toe surface cracks are useful in the fatigue crack growth simulation analysis or crack instability analysis. Unlike the situation for stress concentration factors, it is impractical to determine the SIF solutions required for such empirical formula development through experiments. The use of simplified methods is not reliable for this purpose, since the trends of such solutions, as well as the accuracy of isolated solution data, are not certain. The three-dimensional finite element procedures appear to be the only practical approach at this time [91].

For the first time, these SIF empirical formulas were developed for weld toe surface cracks at the saddle points of T-joints, covering a wide range of practical joint dimensions of existing jackets. The considered loading conditions are the brace axial tension (AT) and in-and out-of-plane bending (IPB and OPB) loads. The procedures for the development include:

- An experimental design to select a set of crack and joint dimensions to be analyzed for SIF data required for statistical curve fitting of empirical formulas.
- The calculation of SIF data for this selected set through three-dimensional finite

element analyses.

- Regression analyses to fit the SIF data into the selected formulas.
- The validation and discussion of the developed formulas.

The factor ranges for the empirical SIF formulas are given as: $0.4 \le \beta \le 0.8$, $10.0 \le \gamma \le 20.0$, $0.30 \le \tau \le 1.00$, $0.05 \le a' \le 0.80$, and $0.05 \le c' \le 1.20$, where $\alpha = 2L/D$, $\beta = d/D$, and $\gamma = D/(2T)$. The parameter $a' = a/T$, and c' is defined as $3c/d$ for numerical convenience. Details of each step will be explained in the following sections.

Experimental Design and Data Base Generation

The experimental design was carried out to minimize the data need and optimize the accuracy of the empirical equations. Classical design methods are simple and recommended when the conditions of an experiment are suitable. However, classical designs have constraints on the number of factor settings, the position of sample cases, and the number of sample size. For this experimental design, D-Optimal method in the general purpose statistical analysis program, RS/DISCOVER [92] was used. The D-Optimal design is a computer generated design that maximizes the determinant $\mathbf{X}^T\mathbf{X}$ for a given prediction model, over specified factor ranges, and in a fixed sample size. Each row of the design matrix, $\mathbf{X}$, is created by using the proposed model to expand the setting for each factor in each sample case (i.e., experimental run). As a result, D-Optimal designs minimize the region of uncertainty of the unknown coefficients in the model [92].

To create a D-Optimal design, a set of factors and their settings, as well as a design model have to be identified. On the basis of understanding of the tubular joint weld toe defects, five setting levels of a' and c', and three setting levels of β, γ, and τ were

selected as,

β: 0.40, 0.60, 0.80

γ: 10.0, 15.0, 20.0

τ: 0.30, 0.65, 1.00

a′: 0.05, 0.10, 0.20, 0.40, 0.80

c′: 0.05, 0.10, 0.35, 0.70, 1.20

The value of parameter α is set at 12 which is considered great enough to neglect the effect of the chord length as shown in Chapter IV.

The stress intensity factor K_e is a function of the load and geometry. For the weld toe crack of T-joints, the K_e solution can be expressed by

$$K_e = F(\beta, \gamma, \tau, a', c')\sigma_N\sqrt{\pi a} \tag{25}$$

The logarithms of the F function was approximated with

$$Ln(F) = P(q) + H(p) \tag{26}$$

where P(q) is a quadratic polynomial of the logarithms of all factors β, γ, τ, a′, and c′, respectively. Symbol H(p) represents some combined polynomial terms of C^i, A^i, (i = 3, 4), and the other factors, where C = Ln(c′), and A = Ln(a′). About five terms were selected for H(p). Unknown coefficients in Equation 26 were determined by statistical regression. The selected form of the empirical formulas (i.e. design models) is in a modified power law form, since a power law can generally fit experimental data with reasonable accuracy. Table 14 lists the 40 cracked joints selected by D-Optimal design

method [93] for data generation.

The finite element modeling and analysis procedures are similar to those mentioned in Chapter III. The post-processor, KAARL, was used to calculate the SIF solutions. Both ends of the chord were fixed as boundary conditions. The surface crack is semi-elliptical on the rectangular strip, which results from mapping the plane defined by the brace-chord intersection and the chord thickness along the normal to the chord surface. In this work, the cracks are placed at the joint saddle only. The crack surface in the crack depth direction is flat and normal to the chord wall surface while in the longitudinal direction, the crack surface is along the weld toe.

Figure 73 presents the SIF solutions along the crack front (from left to right) of Case 4 of Table 14 under IPB. The horizontal axis of the figures is the crack front length in mm. The vertical axis of each plot represents the non-dimensional SIF, $K_i/(\sigma_N\sqrt{\pi a})$, where K_i is the Mode i SIF (i=I, II, and III), a is the crack depth, and σ_N is the nominal stress defined as in Table 2.

Negative K_I solutions of Figures 73a under IPB load occurred due to the fact that a contact algorithm was not utilized in the finite element analysis. Consequently, the crack surface contacted and penetrated each other due to compressive stresses. As mentioned in the section on through-wall cracks in K-tubular joints (Chapter III), SIF solutions away from the contact region will not be affected significantly. In the contact region, K_I is zero, K_{II} and K_{III} remains approximately the same as those of non-contact solutions. For AT and OPB loading, K_I and K_{II} solutions along the crack front are closely symmetric, and K_{III} solutions are closely anti-symmetric, which is consistent with the symmetric nature of the problem.

TABLE 14

DIMENSIONS (mm) OF ANALYZED CRACKS

Run No.	d	T	t	a	c
1	400.0	25.00	7.50	20.00	160.00
2	400.0	25.00	7.50	1.25	93.33
3	400.0	25.00	7.50	1.25	6.67
4	400.0	25.00	25.00	5.00	93.33
5	400.0	25.00	25.00	1.25	160.00
6	400.0	25.00	25.00	20.00	6.67
7	400.0	33.33	10.00	26.67	13.33
8	400.0	33.33	33.33	3.33	13.33
9	400.0	50.00	15.00	40.00	6.67
10	400.0	50.00	15.00	2.50	160.00
11	400.0	50.00	15.00	10.00	93.33
12	400.0	50.00	32.50	20.00	46.67
13	400.0	50.00	50.00	40.00	160.00
14	400.0	50.00	50.00	2.50	6.67
15	600.0	25.00	7.50	10.00	70.00
16	600.0	25.00	7.50	2.50	10.00
17	600.0	25.00	25.00	1.25	20.00
18	600.0	33.33	21.67	6.67	20.00
19	600.0	33.33	21.67	6.67	70.00
20	600.0	33.33	21.67	3.33	190.00
21	600.0	33.33	21.67	6.67	70.00
22	600.0	33.33	21.67	20.00	190.00
23	600.0	33.33	21.67	3.33	70.00
24	600.0	50.00	15.00	2.50	70.00
25	600.0	50.00	50.00	20.00	20.00
26	800.0	25.00	7.50	1.25	320.01
27	800.0	25.00	7.50	20.00	13.33
28	800.0	25.00	16.25	20.00	26.67
29	800.0	25.00	25.00	2.50	93.34
30	800.0	25.00	25.00	1.25	13.33
31	800.0	25.00	25.00	20.00	320.01
32	800.0	33.33	10.00	1.67	26.67
33	800.0	33.33	33.33	13.33	13.33
34	800.0	50.00	15.00	2.50	13.33
35	800.0	50.00	15.00	20.00	320.01
36	800.0	50.00	15.00	40.00	186.67
37	800.0	50.00	32.50	5.00	26.67
38	800.0	50.00	50.00	2.50	186.67
39	800.0	50.00	50.00	2.50	320.01
40	800.0	50.00	50.00	40.00	13.33

Note: Chord Diameter D = 1000.000

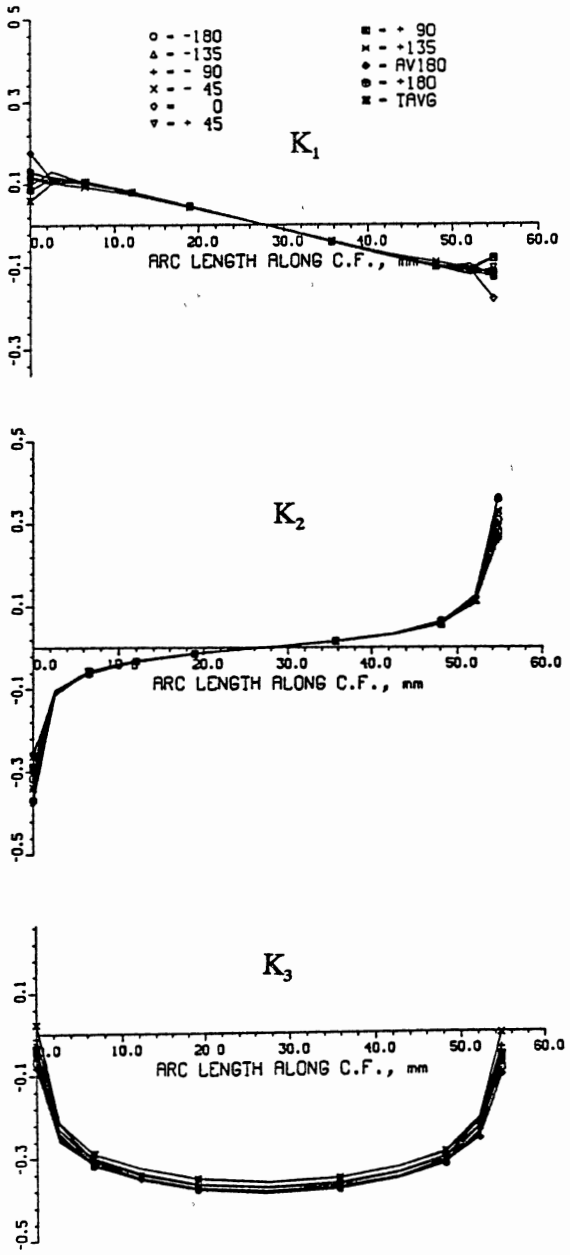

Figure 73. Distribution of Normalized SIF Along Crack Front under IPB

An equivalent SIF based on the energy release rate is defined as, $K_e = [K_I^2 + K_{II}^2 + K_{III}^2/(1 - \nu)]^{1/2}$, which is assumed as a crack driving force parameter for a mixed mode fracture problem. For all load cases, the SIF empirical formulas were developed for K_e. For T-Joints under IPB, a 20 percent increase of the K_I at the crack surface end was incorporated into K_e to consider the effects of partial crack surface contact on the solutions. At the surface crack front point where solution curves have a large scatter, the inside solutions were extrapolated, guided by the data distribution at the location, to obtain the corresponding SIF solution.

Curve Fitting by Regression Analyses

The modified power law curve fitting of the 40 equivalent SIF solutions was performed with computer software RS/EXPLORE [94], using the logarithmic values of these solutions as

$$Ln\left(\frac{K_e}{\sigma_N\sqrt{\pi a}}\right) = f(Ln\beta,\ Ln\gamma,\ Ln\tau,\ Lna',\ Lnc') \tag{27}$$

to determine the f functions. This equation is equivalent to

$$\begin{aligned} K_e &= \sigma_N \sqrt{\pi a}\ e^{f(Ln\beta,\ Ln\gamma,\ Ln\tau,\ Lna',\ Lnc')} \\ &= F(\beta,\ \gamma,\ \tau,\ a',\ c')\ \sigma_N \sqrt{\pi a} \end{aligned} \tag{28}$$

where $F = F_g F_s F_t$, with F_g being a joint geometry factor, F_s being a crack size factor

and F_i being joint and crack coupling factor, and σ_N being nominal stress, as defined previously. The f functions of Equation 27 were grouped and converted into three F functions of Equation 28. The validation of the developed empirical formulas was carried out using the RS/EXPLORE programs.

Depending on the K_e value used in curve fitting of Equation 27, the resulting F_g, F_s, and F_i have different expressions for the empirical formulas. For each of the three load cases, two crack front points were selected to develop the K_e expression of Equation 28 to result in a total of six empirical formulas. One is the deepest crack front point K_a and the other is the surface crack front point K_c. Since the cracked joint is symmetric for symmetric loading, the two surface crack front solutions should be identical. When the load is anti-symmetric (IPB), the higher K_e value was selected as the surface crack front point solutions. Figures 74 through 76 present the expressions of functions F_g, F_s, and F_i at the deepest and surface crack front points for all three load cases.

$$K_e = \sigma_N F_g F_i F_s \sqrt{\pi a}$$

Model AKA1 : Deepest Crack Front Point (K_a)

$F_g = 0.2749\beta^{-0.6225-1.2685\ln\beta}\ \gamma^{1.3191-0.1661\ln\tau}\ \tau^{1.6621+0.3704\ln\beta}$

$F_i = \beta^{0.3561A-0.0956C}\ \gamma^{0.0983A+0.2298C+0.0817C^2}\ \tau^{-0.0762A}$

$F_s = (a')^p(c')^r$

$p = -0.8669-0.2198A-0.0162A^2-0.4750C^2-0.1667C^3-0.0193C^4$

$r = 0.0777+1.0531A+0.5820A^2+0.0810A^3-0.7001C-0.0604C^2+0.0060C^3$

$A = \ln a'$ and $C = \ln c'$

Model AKC2 : Surface Crack Front Point (K_c)

$F_g = 204.08\beta^{-0.5858-0.7492\ln\beta}\ \gamma^{-2.6713-0.2884\ln\beta+0.5646\ln\gamma}\ \tau^{1.1491-0.2936\ln\gamma-0.5043\ln\tau}$

$F_i = \beta^{0.0680A}\ \gamma^{0.0478A-0.5344C-0.1218C^2}\ \tau^{-0.1299A-0.0370C}$

$F_s = (a')^p(c')^r$

$p = 1.0787+0.6397A+0.1569A^2+0.0186A^3-(0.0770+0.0478A+0.0099A^2)C^2$

$r = 0.8617+0.4888A+0.1816A^2+0.0123A^3-0.3252C\ -0.2210C^2-0.0275C^3$

$A = \ln a'$ and $C = \ln c'$

Figure 74. SIF Empirical Formula of T-Joint under Brace Tension

$$K_e = \sigma_N F_g F_i F_s \sqrt{\pi a}$$

Model OKA2: Deepest Crack Front Point (K_a)

$F_g = 0.1718\beta^{0.9626-0.5003\ln\beta}\ \gamma^{1.5274}\ \tau^{0.6488+0.3353\ln\beta-0.2962\ln\tau}$

$F_I = \beta^{0.3066A-0.0598C}\ (a')^{0.1315\ln\gamma-0.0775\ln\tau}$

$F_S = (a')^p(c')^r$

$p = -1.3130-0.4253A-0.0584A^2+0.9843C-0.3278C^2-0.0308C^3$

$r = 0.7184+0.5401A^2+0.0889A^3-0.4186C-0.0496C^2-0.04210A^2C$

$A = \ln a'$ and $C = \ln c'$

Model OKC1: Surface Crack Front Point (K_c)

$F_g = 4.7016\beta^{0.7362-0.9523\ln\beta}\ \gamma^{0.2227-0.7169\ln\beta}\ \tau^{0.6663-0.1040\ln\gamma-0.3802\ln\tau}$

$F_i = \beta^{0.1388A-0.2143C}\ \gamma^{0.0573A-0.5026C-0.1175C^2}\ \tau^{-0.1548A}$

$F_S = (a')^p(c')^r$

$p = 1.5044+0.8350A+0.1258A^2+0.6624C-0.0202C^2$

$r = 0.2954+0.3328A^2+0.0453A^3-0.6990C-0.3648C^2-0.0473C^3$

$A = \ln a'$ and $C = \ln c'$

Figure 75. SIF Empirical Formula of T-Joint Under OPB

$$K_e = \sigma_N F_g F_i F_s \sqrt{\pi a}$$

Model IKA5: Deepest Crack Front Point (K_a)

$F_g = 0.0887\beta^{1.3433-0.4798\ln\beta}\ {}_{\gamma}5.2247-0.5555\ln\beta-0.8310\ln\gamma\ {}_{\tau}0.6928-0.4302\ln\beta$

$F_i = 0.0887\beta^{-0.0758A-0.2391C}\ {}_{\gamma}0.1406A+0.4341C+0.1543C^2\ {}_{\tau}-0.1771A$

$F_s = 0.0887(a')^p(c')^r$

$p = 1.8586+2.2859A+0.9035A^2+0.1215A^3-1.0918C-0.4785C^2$

$r = -1.3298-0.3040A^2+0.4834C+0.7030C^2+0.1130C^3-0.1207A^2C$

$A = \ln a'$ and $C = \ln c'$

Model ICK3: Surface Crack Front Point (K_c)

$F_g = 0.1395\beta^{-0.6498-1.1883\ln\beta}\ {}_{\gamma}1.0779-0.3414\ln\beta\ {}_{\tau}0.8168-0.2149\ln\beta$

$F_i = \beta^{0.0422A-0.2452C}\ {}_{\gamma}1.4558A+0.4173A^2-0.9276C-0.3297C^2\ {}_{\tau}-0.0905A-0.0338C$

$F_s = (a')^p(c')^r$

$p = -2.4921-0.0063A+0.2056A^2+0.9804C+0.3916C^2+0.0620C^3-0.0110C^4$

$r = 2.8298+0.5682A^2+0.0704A^3+0.6562C-0.0453C^2+0.0022C^3+A^2C(0.1621+0.0384C)$

$A = \ln a'$ and $C = \ln c'$

Figure 76. SIF Empirical Formula of T-Joint Under IPB

Figure 77 (or 78) shows the error plot of developed empirical formula for K_a under the brace tension (or in-plane bending) load, in the form of Equation 27, when it is compared with the 40 input data. The residual Δ is defined as

$$\Delta = Ln\left(\frac{K}{\sigma_N\sqrt{\pi a}}\right) - Ln\left(\frac{K_o}{\sigma_N\sqrt{\pi a}}\right) = Ln\left(\frac{K}{K_o}\right)$$

where K is the equivalent SIF from the empirical formulas AKA1 and IKA5, and K_o is the SIF computed from the FEM for the 40 cases listed in Table 14. The relative error

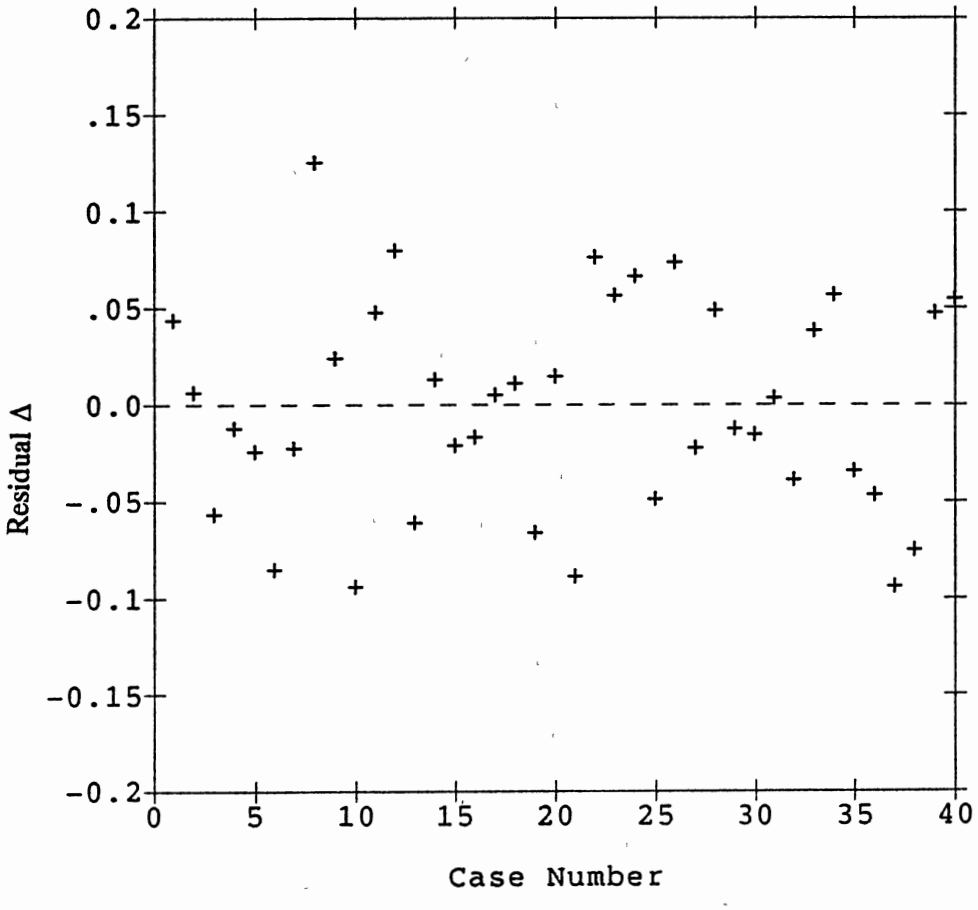

Figure 77. Error Residual of Formula AKA1

is obtained by $\varepsilon = (K - K_o)/K_o = e^{\Delta} - 1$. The maximum fitting error on the worksheet is within 14 percent (or 16 percent), while the majority of the errors are within 10 percent for both cases. Although the error plots of other formulas are not presented, Figure 78 shows the worst case.

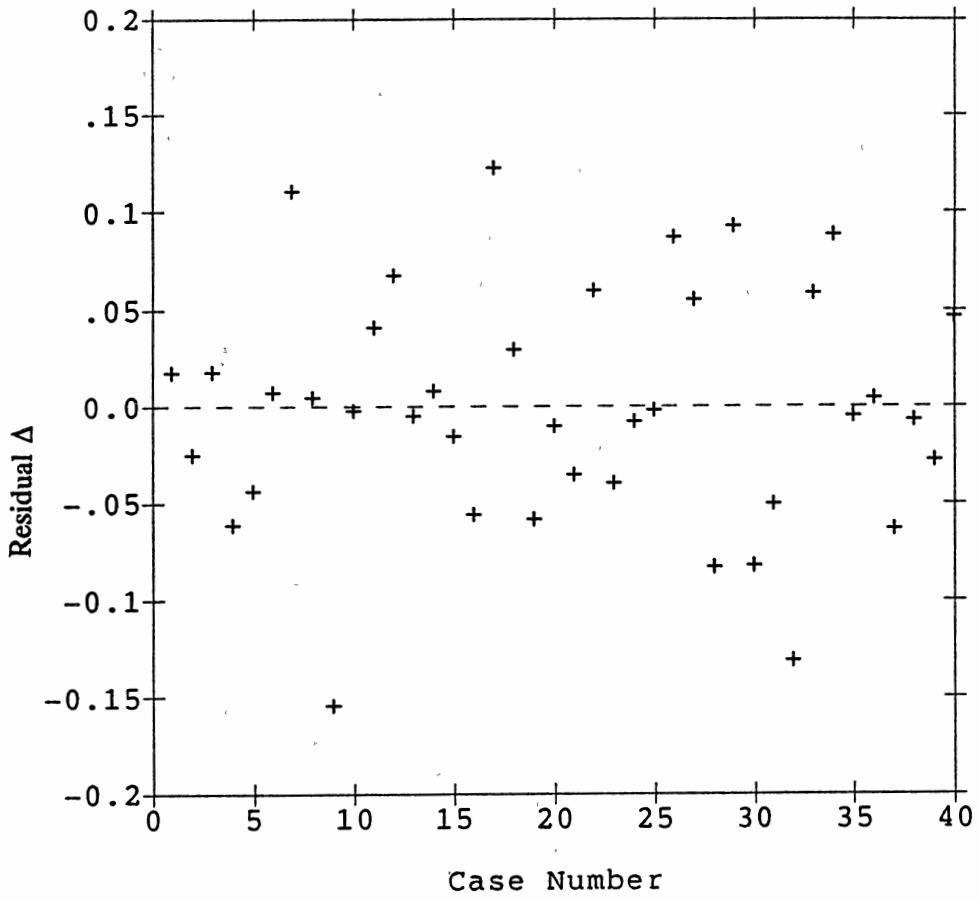

Figure 78. Error Residual of Formula IKA5

Discussion of the Empirical Formulas

The developed six SIF formulas have been analyzed to assess their reliability, using a joint with the following dimensions: $\beta = 0.60$, $\gamma = 15.00$, $\tau = 0.65$, $T = 33.3$ mm, and

d = 600 mm. The load is AT = 10^3 N, OPB = IPB = 10^6 N•mm. With the aid of computer program MACSYMA [95], the equivalent SIF solutions, K_a and K_c, were calculated from the empirical formulas for cracks with depths, a = 3.33, 6.67, and 13.33 mm and lengths, c = 20, 70, and 190 mm, and their trends were examined. The non-dimensional crack size parameters of these cracks are: a′ = 0.1, 0.2, and 0.4; and c′ = 0.1, 0.35, and 0.95. The SIF results of finite element analyses for several identical cracks from the 40 cases which were analyzed for the data generation, were compared with the empirical solutions. The finite element solutions are presented with various symbols in the plots for comparison. Most of the cases agree well with the corresponding empirical formula solutions.

The plots of equivalent SIF K_a versus crack depth for the joint under the brace axial tension, from formula AKA1, are presented in Figure 79. There are two contradicting factors to control the magnitude of the stress intensity factor as the crack grows deeper with fixed crack length. The stress intensity factor tends to increase with the crack depth, while the predominantly bending stress distribution along the chord wall of the T-joint tends to reduce the stress intensity factor as the crack grows deeper. For this reason, the trend of the stress intensity factor with respect to the crack depth depends on the crack tip location in the joint. Figure 79 indicates that, for shallow cracks K_a increases with the crack depth. However, from a certain crack depth, the trend reverses to decrease with crack depth. This effect is especially apparent with shorter cracks. Figure 79 also shows that an increase in crack length will result in an increase in the value of K_a which is physically reasonable.

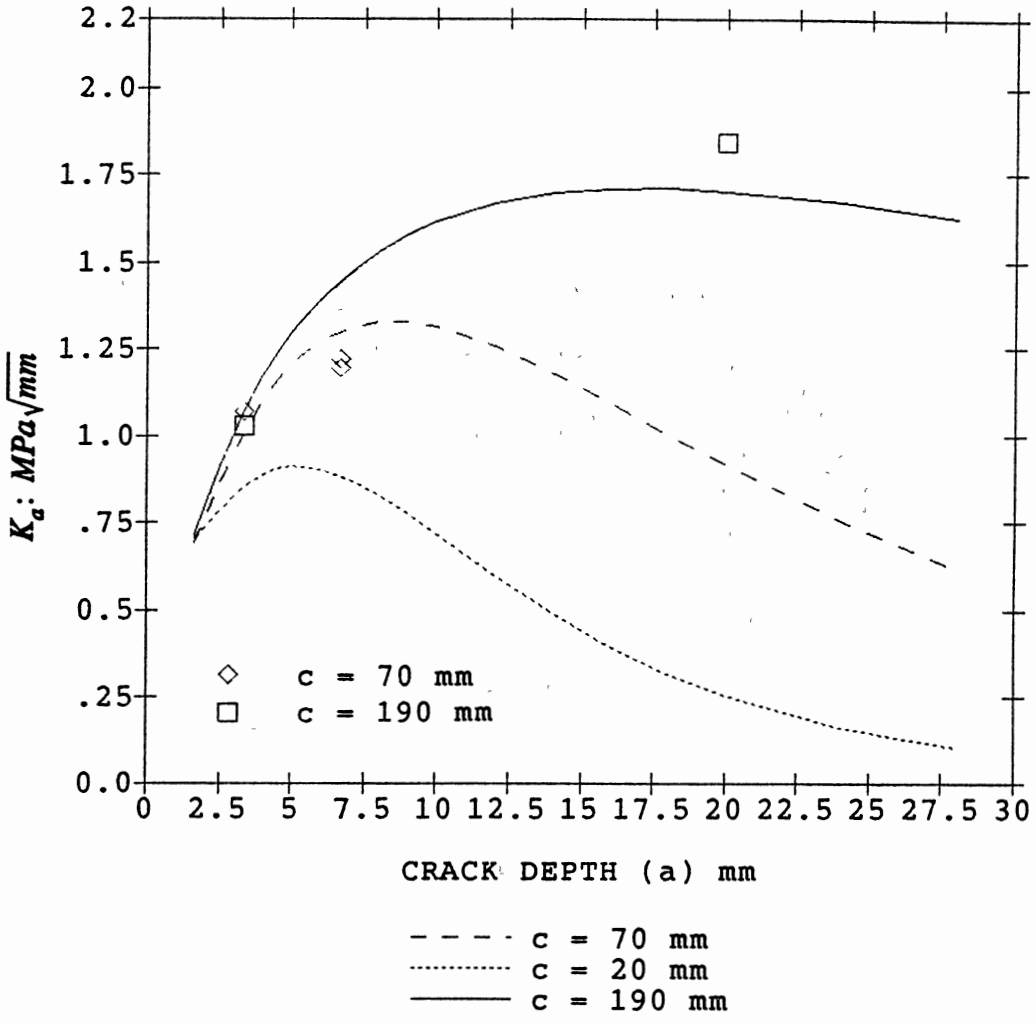

Figure 79. K_a versus Crack Depth from Formula AKA1

The equivalent SIF K_a versus crack length of the solutions, from formula AKA1, is plotted in Figure 80. The equivalent SIF K_a increases with the crack length, when the crack tip location is fixed in depth. When the cracks are short, SIFs for cracks with the largest depths are lower than those with the medium depth, since the crack tip stresses of deeper cracks are lower than those of shallow ones. However, the size effects on the SIF overcome those of the stress to make SIFs greater for the deeper cracks as cracks grow longer.

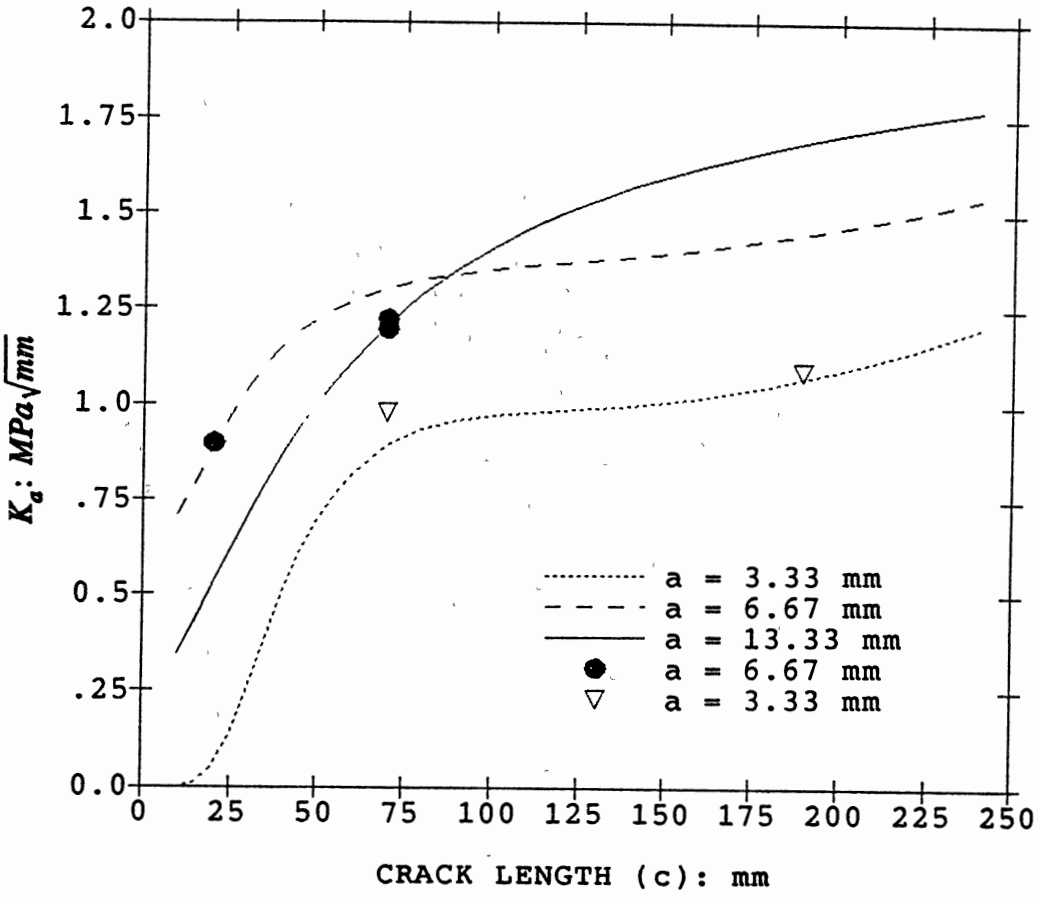

Figure 80. K_a versus Crack Half Length from Formula AKA1

The plots of equivalent SIF K_c versus the crack depth for the joint under the brace axial tension from formula AKC2 are shown in Figure 81. The monotonic increase of SIF with the crack depth, while the crack length is fixed, is consistent with the size effects on the SIF magnitude. Because of the higher stress concentration near the saddle point, the shortest crack has the highest SIF when the crack depth is small. As the crack grows deeper, the size effects on the SIF magnitude overcome those of the stress and the gradients of K_c for longer cracks (e.g., c = 70 and 190 mm) exceed those of the shortest crack.

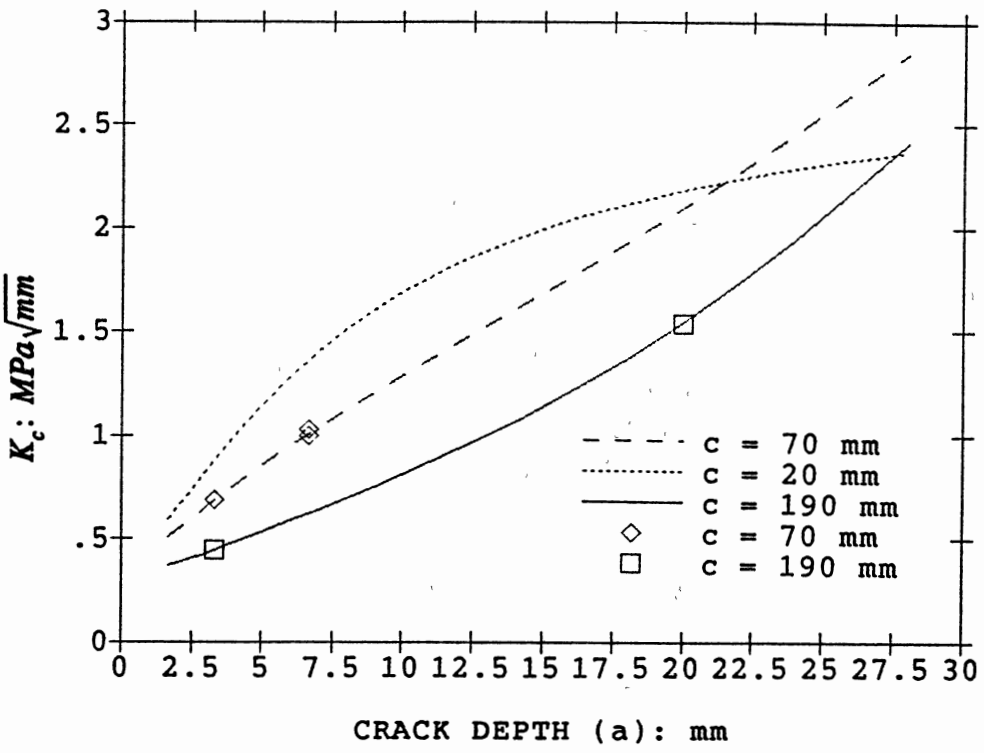

Figure 81. K_c versus Crack Depth from Formula AKC2

The equivalent SIF K_c versus half crack length for the three crack depths under the axial tension (AKC2) are plotted in Figure 82. All these curves indicate that K_c decreases as the crack grows in length. This is due to the fact that, as the crack grows longer, the surface crack front moves away from the hot spot region, resulting in a reduced stress at the crack tip location. The size effects on the SIF magnitude cannot overcome those of stress for the SIF at the surface crack front point.

Since the stress patterns of a T-joint under the OPB loading are similar to those of the brace axial tension loading, the general trends of the SIF (i.e., from formulas OKA2 and OKC1) of these two load cases are also similar. Detailed discussions about OPB cases are omitted for this reason.

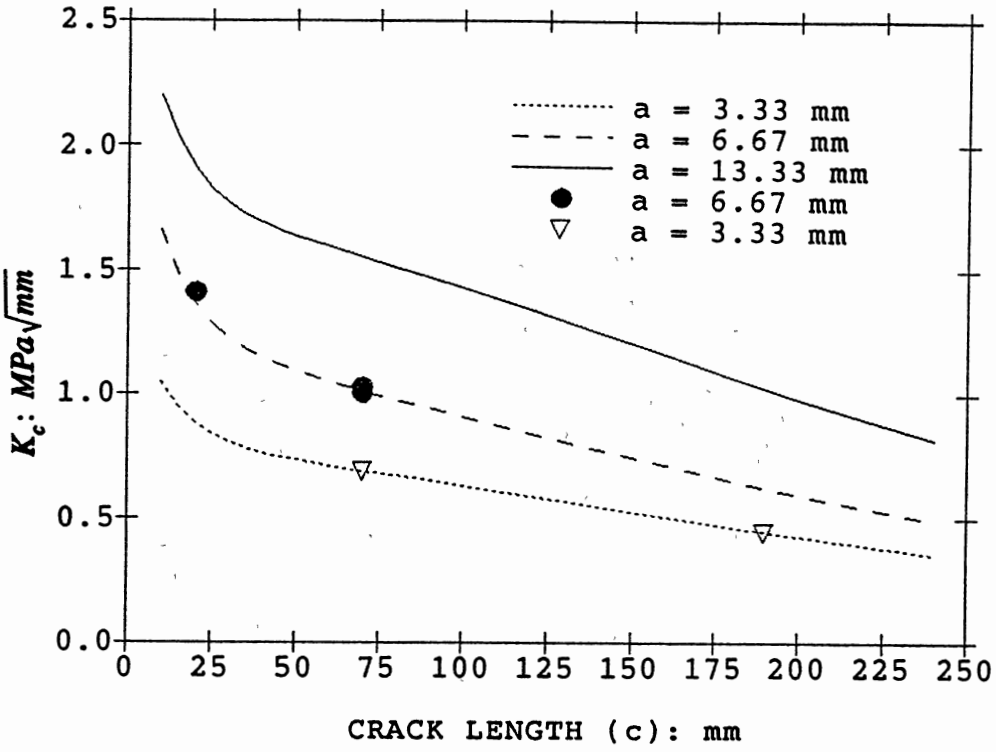

Figure 82. K_c versus Crack Half Length from Formula AKC2

The SIF solutions K_a from formula IKA5 versus crack depth for the joint under the in-plane bending load are shown in Figure 83. It is apparent from Figures 73a and 73b that only the K_{III} component exists at the deepest crack front point for the IPB case. At this location, K_{III} generally increases with crack depth, when the crack length is fixed. In Figure 83, the longest crack has lower SIF than shorter cracks at all crack depth, except for the medium crack depth range. Such a possibility can exist due to the complex nature of the tearing mode of IPB loading, although it is not immediately clear whether it is a fact or the result of errors originating from statistical data analyses, particularly for small crack depths.

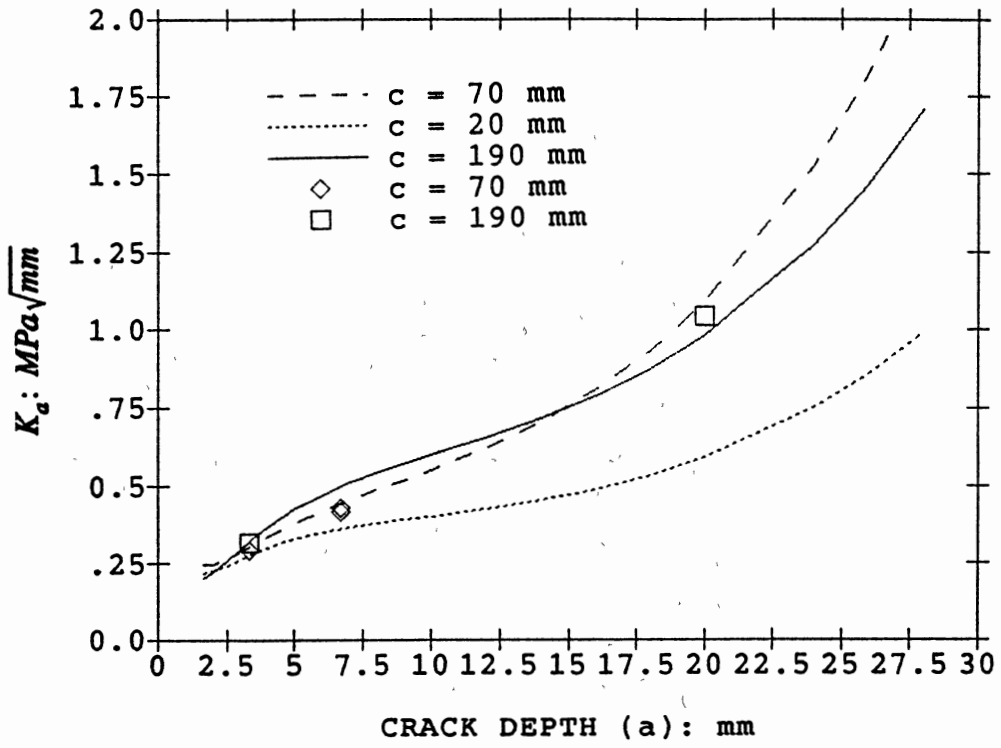

Figure 83. K_a versus Crack Depth from Formula IKA5

The plots of K_a versus the crack length from formula IKA5 are shown in Figure 84. The general trend of these plots is that the SIF increases with the crack depth. The mild fluctuation of the SIF with crack length increase can be considered to be unreasonable if the loading were AT or OPB, which is dominantly Mode I. However, for the IPB problem whose crack driving force is dominated by shear components (Modes II and III), it is not simple to determine intuitively the effects of crack size and shape on the SIF solutions. Although the crack size increases, the change in crack front line direction resulted by the change in crack aspect ratio can decrease the effects of a particular shear stress component on the SIF solutions. Differently from the Mode I, the SIF magnitude under Modes II and III loading can be affected by the crack front orientation with respect

to the load, as well as by crack size. Under the dominantly tearing mode of loading of IPB, the crack front orientation change originating from the crack aspect ratio change can result in unpredictable changes in crack driving force distribution along the crack front. Nevertheless, it requires further close examinations with more solution data to confirm this observation.

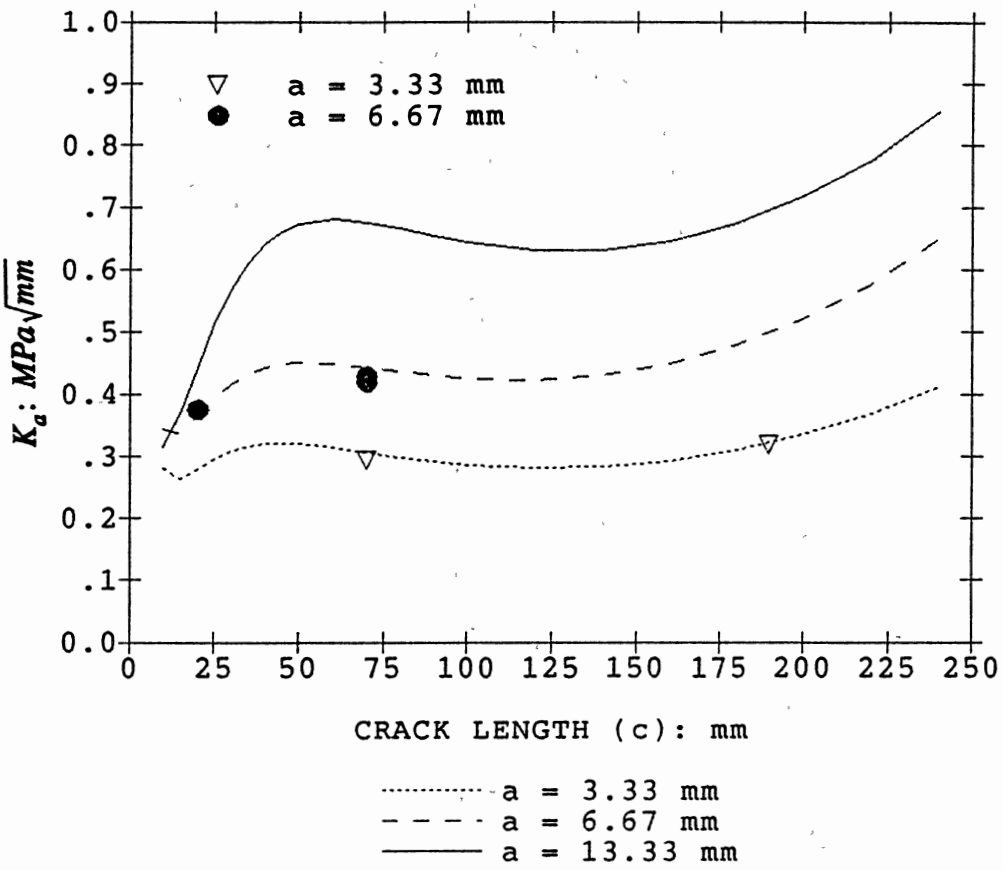

Figure 84. K_a versus Crack Half Length from Fomula IKA5

The K_c solutions from formula IKC3 for the same cracks under the IPB loading (Figures 85 and 86) consist of all three modes of SIF, with the sliding mode (Mode II)

contribution as the highest (Figure 73). For a mixed mode problem, this trend can be possible. Curves in Figure 85 show strong similarity to those in Figure 84, since K_{II} makes a significant contribution to K_e. The trend of the SIF solutions at the surface crack front point (K_e) that generally increases with crack size appears to be reasonable. As previously stated, it is necessary to investigate closely to further understand the behavior of mixed mode SIF solutions.

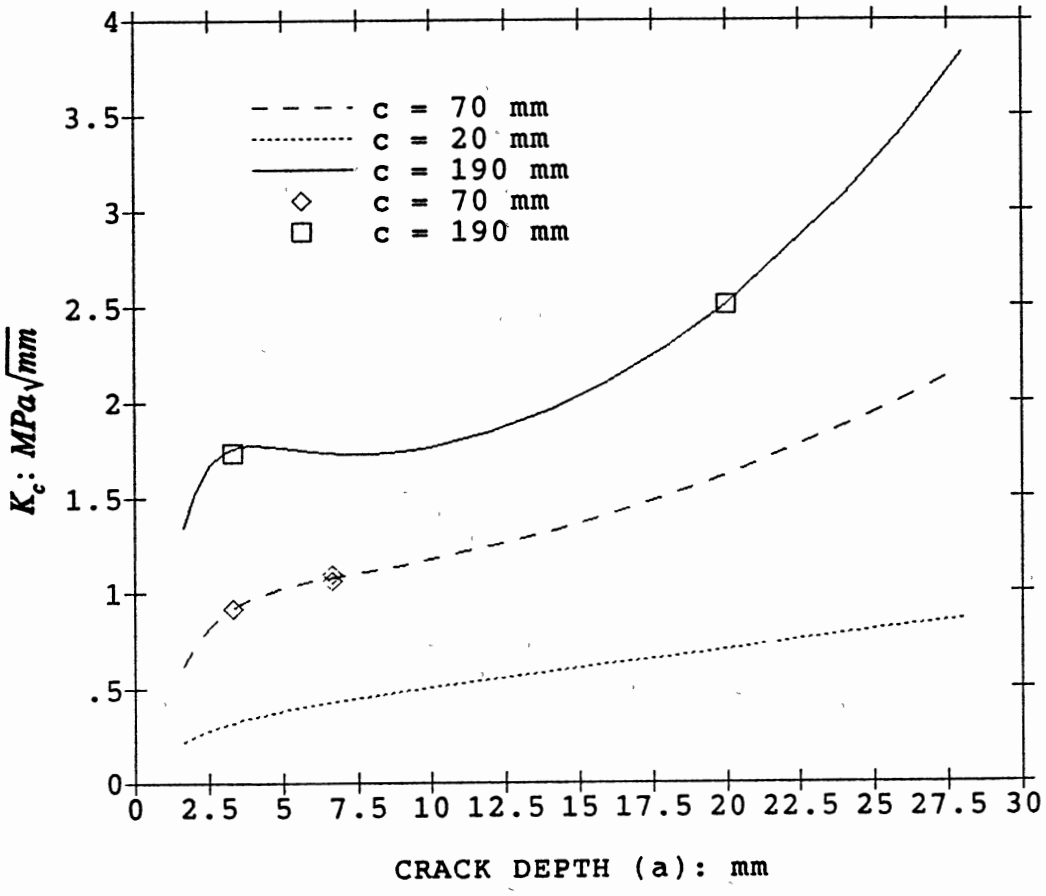

Figure 85. K_e versus Crack Depth from Formula IKC3

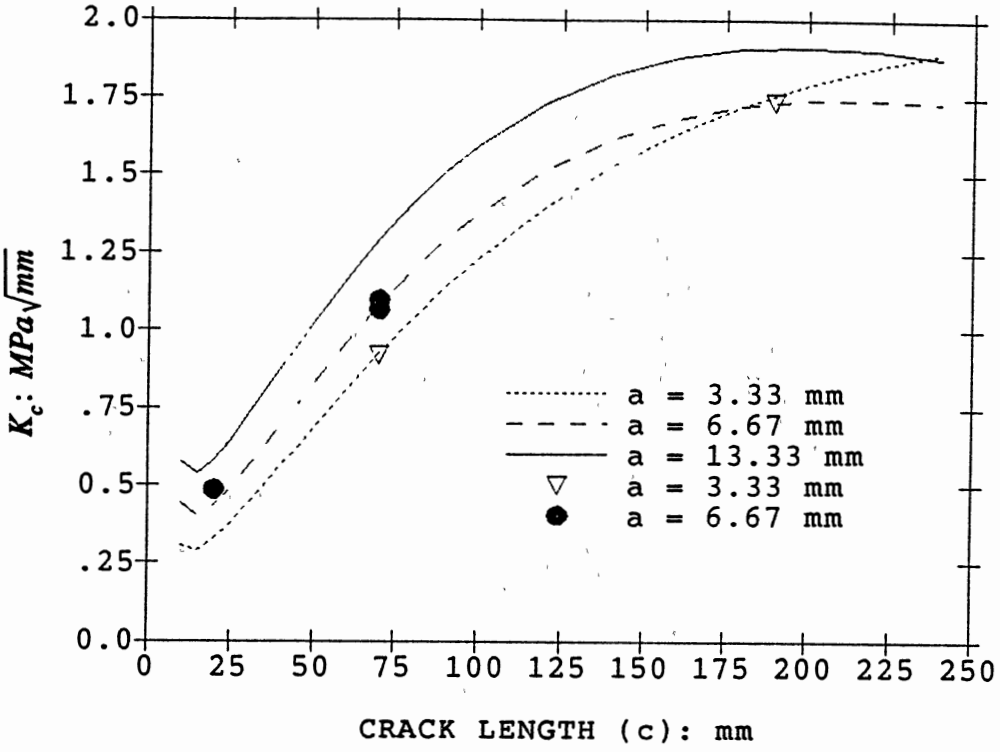

Figure 86. K_c versus Crack Half Length from Formula IKC3

Concluding Remarks

Focus was placed on the development of the stress intensity factor empirical formulas to make the fracture mechanics method efficient and inexpensive for tubular joint engineering. At the present time, for the lack of reliable approximate methods, the three-dimensional finite element method appears to be the only credible approach to generate data for the reliable defect assessment and development of stress intensity factor empirical formulas for tubular joints.

The use of SIF empirical formulas is not as simple as those of SCF, since the location of in-service fatigue crack development does not necessarily coincide with the crack location for which the formulas have been developed. For design analyses, if the dominant brace loading component is identified, the SIF empirical formulas based on the hot spot location can easily be developed following the procedures of the present work. In the general case where the critical location is uncertain, the development of the appropriate SIF empirical formulas is not a simple matter, even for a limited class of joint configuration. For this reason, a single set of SIF formulas will have limited applications. To be applicable to general problems of fracture mechanics in-service structural integrity assessment, many sets of SIF formulas have to be developed, as the offshore industry has invested in the development of SCF formulas for tubular joint engineering by the conventional approach. The SIF empirical formulas presented here are significant as a starting point of such development.

The conclusions of this chapter are summarized as follows:

- The empirical formulas of the stress intensity factors required for tubular joint fatigue life analyses can be developed by procedures similar to those of the stress concentration factors.
- Statistical data analyses can minimize the data required for the development of stress intensity factor empirical formulas of offshore tubular joints.
- The three-dimensional finite element method is suitable for the stress intensity factor solutions required for the empirical formula development.
- The empirical formulas obtained by curve fitting of 40 different crack solutions agree favorably with the physical behavior of weld toe cracks of T-joints and cover a wide

range of joint dimensions.

- The SIF empirical formulas can make the fracture mechanics fatigue life assessment of a tubular joint simple and inexpensive.

CHAPTER VI

CONCLUSIONS

Fracture Mechanics method is the only rational approach to assess the integrity of structural components with defects. For tubular joint weld toe defects in fixed offshore jacket platforms, closed-form stress intensity factor solutions are not available. It is difficult to calculate the SIF solutions due to the complexity of joint/crack geometry and loading conditions. Many simplified methods involve uncertainties. To develop rational and efficient fracture mechanics analysis procedures for tubular joint fatigue assessment, a sophisticated computer post-processor, KAARL, using Rhee's procedure [10], has been designed to obtain the SIF solutions from finite element analysis efficiently. A significant number of SIF solutions have been calculated and studied for a good understanding of the behavior of weld toe defects through accurate SIF solutions. The following conclusions can be drawn:

1. A simplified method to calculate the stress intensity factors of weld toe surface cracks of tubular joints involves uncertainties. Experimental methods can determine an effective crack driving force parameter of mixed mode tubular joint weld toe cracks, but it does not necessarily represent the crack tip singular stress magnitude as the stress intensity factors do.
2. The trends of the SIF solutions obtained through the finite element analyses are

consistent with the physical behavior of tubular joint weld toe cracks, as well as with the SCF distribution of an uncracked tubular joint.

3. The three-dimensional finite element method is reliable and practical for the calculation of the stress intensity factors of tubular joint weld toe cracks of various forms.
4. Finite element model sensitivity study indicates that relative crack tip element size L_e/a = 0.05 to 0.10 provide adequate SIF solutions.
5. Empirical formulas for the SIF of tubular joint weld toe defects can be developed through statistical design and 3-D finite element analyses. These formulas are useful for fracture and fatigue life assessment of tubular joint with crack-like defects.
6. The superposition procedure is efficient for the SIF calculation of a weld toe defect in a multi-brace joint subjected to combined multi-axial loads.
7. The mixed mode behavior is a possible mode of fatigue and fracture of tubular joint weld toe cracks. However, the modelling and practical aspects of the mixed mode behavior should be further studied through numerical and experimental investigations.

CHAPTER VII

RECOMMENDATIONS FOR FUTURE WORK

Introduction

Two major issues concerning tubular joint fatigue assessment are when the mixed mode behavior becomes too significant to be ignored and how to deal with it. Obtaining reliable and accurate SIF solutions of weld toe cracks is essential to the first issue. Solution of the second issue demands knowledge of crack instability criterion (for critical condition and growth direction), fatigue crack growth control parameter and growth model. The determination of these factors requires further experimental and analytical studies of material and structural behavior [96]. The recommendations in this chapter focus on the first issue.

SIF Over Realistic Fatigue Crack Profiles

Significant mode II and III components relative to mode I of the SIF in a planar crack would suggest that the crack should grow asymmetrically, forming a curved profile for the crack surfaces. The situation for weld toe defects of a tubular joint is much more complicated than the planar crack, because of the complex geometry and stress conditions.

Some crack propagation profiles of tubular joint weld toe defects are available from laboratory tests. Calculation of the SIFs for these realistic crack profiles using the 3-D

finite element procedure [10] is a feasible means to examine the mixed mode behavior. However, the option in TUJAP to model doubly curved cracks has not been validated. Future research to study the reliability of this option and to use it to investigate realistic crack profiles are required.

Multiple Boundary Condition Effect

As a member in an integrated jacket frame, the tubular joint is subjected to both multi-axial loads (forces and moments) and constraints (displacements and rotations) from neighboring structural members. Because of the complicated marine loading environment, various combinations of loading magnitudes and directions lead to many load and constraint combinations at the ends of a tubular joint. The multi-axial load effect can be treated using the superposition method discussed in Chapter III. A reliable and efficient method to treat the multi-axial end constraints are also needed for understanding and calculating the fatigue behavior of the tubular joint.

Consider a two-dimensional frame as shown in Figure 87, where a K-tubular joint is located at B. The loads and constraints at the ends of the joint are illustrated in Figure 88. This problem can be solved efficiently by first studying the models in Figures 89 and 90, and then combining the results from the two models.

In Figure 89, loads $\underline{F}_i'$ (i = 1, 2, 3) are to be determined later. Once these $\underline{F}_i'$ are known, this model can be solved using the multi-axial load method in Chapter III, i.e.,

$$\underline{K}' = \underline{C}_1\underline{F}_1' + \underline{C}_2\underline{F}_2' + \underline{C}_3\underline{F}_3' \tag{29}$$

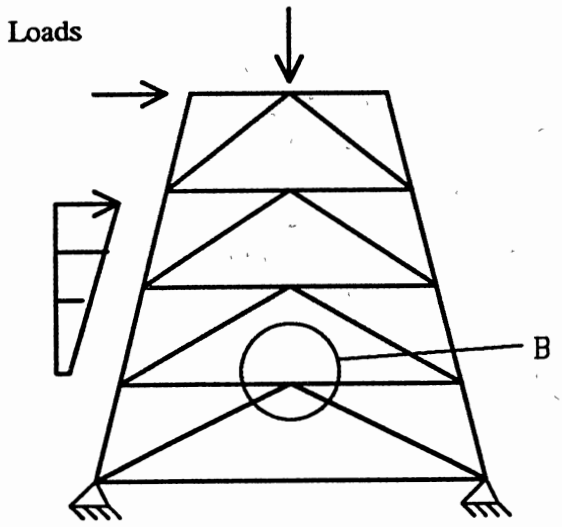

Figure 87. A Two-Dimensional Frame with K Joints

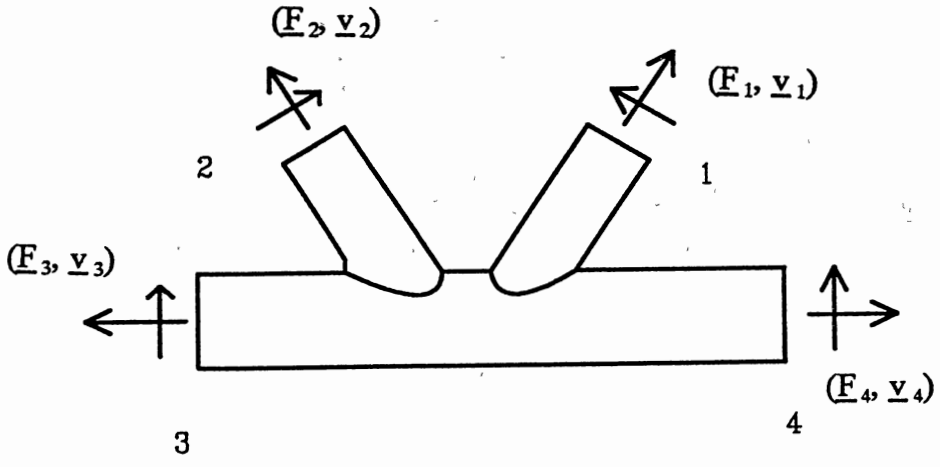

Figure 88. A K-Joint with Multiple Boundary Conditions

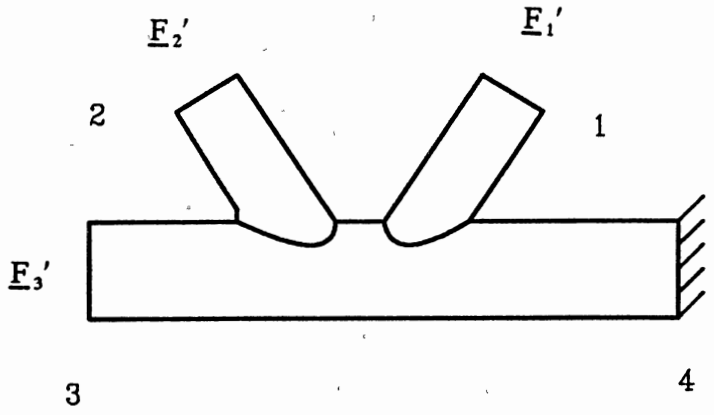

Figure 89. The Load Model of the K-Joint

In Figure 90, $\underline{v}_{4t}= [0\ 0\ 0\ \theta_x\ \theta_y\ \theta_z]^T$ is the rotational displacement vector at end 4 in Figure 88. The translational displacement components have no effect. The reactional loads at each end can be calculated as,

$$\begin{aligned} \underline{F}_1'' &= \underline{e}_{11}\theta_x + \underline{e}_{12}\theta_y + \underline{e}_{13}\theta_z \\ \underline{F}_2'' &= \underline{e}_{21}\theta_x + \underline{e}_{22}\theta_y + \underline{e}_{23}\theta_z \\ \underline{F}_3'' &= \underline{e}_{31}\theta_x + \underline{e}_{32}\theta_y + \underline{e}_{33}\theta_z \end{aligned} \qquad (30)$$

where $\underline{e}_{ij}$ is the reactional load influence coefficient vector at end i due to unit rotation θ_j (j = x, y, z) at all the joint ends.

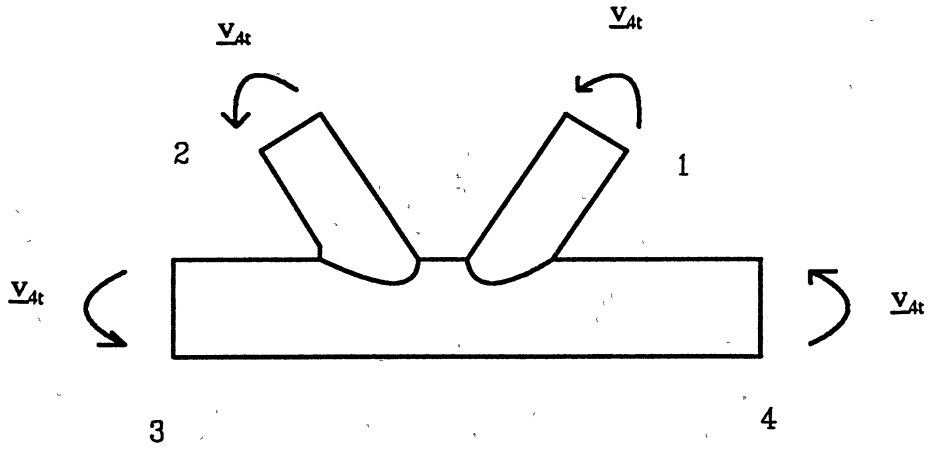

Figure 90. The Constraint Model of the K-Joint

The SIF at a crack front location can be written as,

$$\underline{K}'' = \underline{t}_x \theta_x + \underline{t}_y \theta_y + \underline{t}_z \theta_z \tag{31}$$

where $\underline{t}_j$ (j = x, y, z) is the SIF influence coefficient vector due to unit rotation θ_j at all the joint ends.

It has been shown by the author that for the model in Figure 89,

$$\begin{aligned} \underline{F}_1' &= \underline{F}_1 - \underline{F}_1'' \\ \underline{F}_2' &= \underline{F}_2 - \underline{F}_2'' \\ \underline{F}_3' &= \underline{F}_3 - \underline{F}_3'' \end{aligned} \tag{32}$$

where $\underline{F}_i$ (i = 1, 2, 3) are given in Figure 88, and $\underline{F}_i''$ (i = 1, 2, 3) are given by Equation 30.

The SIF at a crack front location of the problem in Figure 88 can be obtained by combining Equations 29 and 31, i.e.

$$\underline{\boldsymbol{K}} = \underline{\boldsymbol{K}}^{I} + \underline{\boldsymbol{K}}^{II} \tag{33}$$

This procedure is systematic and efficient. To take into account the boundary effect of a tubular joint, only the coefficients $\underline{e}_{ij}$ and $\underline{t}_i$ need to be calculated using FEM. The boundary rotation condition $\underline{v}_{4t}$ is arbitrary, but in small deformation.

The TUJAP system can be modified to apply the non-zero boundary conditions of rotational displacement. Alternatively, another general purpose FE program, like ABAQUS, can be used to perform the FE analysis of tubular joint.

BIBLIOGRAPHY

[1] Rhee, H.C. and Kanninen, M.F. Opportunities for Application of Fracture Mechanics for Offshore Structures, *Applied Mechanics Reviews*, Vol.41, pp.23-35, 1988.

[2] de Back, J. The Design Aspects and Fatigue Behavior of Tubular Joints, *Steel in Marine Structures*, Edited by C. Noordhoek and J. de Back, pp.205-223, Elsevier Science Publishers B.V., Amsterdam, 1987.

[3] *Design of Tubular Joints for Offshore Structures*, Vol.2, UEG Publication UR33, UEG 6 Story's Gate, Westminister, London SW1P 3AU. 1985.

[4] Kanninen, M.F. and Popelar, C.H. *Advanced Fracture Mechanics*, Oxford University Press, New York, 1985.

[5] Barsom, J.M. and Rolfe, S.T. *Fracture and Fatigue Control in Structures*, Second Edition, Prentice-Hall, Inc., Englewood Cliffs, New Jersey, 1987.

[6] Rhee, H.C. and Salama, M.M., Mixed Mode Stress Intensity Factor Solutions of a Warped Surface Flaw by Three-Dimensional Finite Element Analysis, *Engineering Fracture Mechanics*, Vol.28, pp.203-209. 1987.

[7] Mahajan, R.V. and Ravi-chandar, K. An Experimental Investigation of Mixed-Mode Fracture Mechanics, *International Journal of Fracture*, Vol.41, pp.235-252, 1989.

[8] Broek, D. *Elementary Engineering Fracture Mechanics*, 4th Edition, Martinus Nijhoff Publishers, 1987.

[9] Shields, E.B., Srivatsan, T.S. and Padovan, J. Analytical Methods for Evaluation of Stress Intensity Factors and Fatigue Crack Growth, *Engineering Fracture Mechanics*, Vol.42, pp.1-26, 1992.

[10] Rhee, H.C. Stress Intensity Factor Evaluation from Displacements along Arbitrary Crack Tip Radial Lines for Warped Surface Flaws, *Engineering Fracture Mechanics*, Vol.32, pp.723-730, 1989.

[11] SESAM, *PRETUBE, A Finite Element Preprocessor for Tubular Joints, User's Manual.* VSS Report No.91-7038, Veritec, Oslo, Norway. 1991.

[12] Han, S. and Rhee, H.C. *KAARL: Stress Intensity Factors Along Arbitrary Radial Line--A Postprocessor for Stress Intensity Factor Solution from Displacements in the Vicinity of a Crack Front*, Research Report 107-1005-1-91, Conoco, Inc. 1991.

[13] Liebowitz, H., Noor, A.K. and Moyer, Jr. T.E. New Computing Systems and Their Impact on Structural and Fracture Mechanics Calculations, *Engineering Fracture Mechanics*, Vol.40, pp.687-704, 1991.

[14] *TUSTRA, Tubular Joint Structural Analysis Module, User's Manual*, Veritec, Oslo, Norway, 1985

[15] American Welding Society, *Structural Welding Code*, ANSI/AWS D1.1-92, 1992.

[16] API RP2A, *Recommended Practice for Planning, Designing and Constructing Fixed Offshore Platforms*. American Petroleum Institute, 19th Edition, 1991.

[17] BS6235, *Code of Practice for Fixed Offshore Structures*, British Standard Institution, London, 1982.

[18] Offshore Installations, *Guidance on Design and Construction*, Department of Energy, London, 1984.

[19] Lloyds Register of Shipping, *Fatigue Analysis of Fixed Steel Platform Welded Tubular Joints*, July, 1980.

[20] Norwegian Petroleum Directorate, *Regulations for the Structural Design of Fixed Structures on the Norwegian Continental Shelf*, 1977.

[21] Det Norske Veritas, *Rules for the Design Construction and Inspection of Offshore Structures*, DnV, Oslo, Norway. 1977.

[22] Marshall, P. State of the Art in the U.S.A., *Steel in Marine Structures*, Edited by C. Noordhoek and J. de Back, pp.39-48, Elsevier Science Publishers B.V., Amsterdam, 1987.

[23] Dijkstra, D.D. and Hartog, J. Dutch Part of the Large Scale Tubular Joint Fatigue Test Programme, *Offshore Steel Research Seminar*, Cambridge, 1978.

[24] Marshall, P. Tubular Joint Design, *Planning and Design of Fixed Offshore Platforms* edited by B. McClelland and M.D. Reifel, pp.624-691. Van Nostrand Reinhold Company, New York, 1986

[25] Paris, P. and Erdogan , F. A Critical Analysis of Crack Propagation Laws, *Transactions of the ASME, Journal of Basic Engineering*, pp.528-534, 1963.

[26] Burns, D.J., Lambert, S.B. and Mohaupt, U.H. Crack Growth Behaviour and Fracture Mechanics Approach, *Steel in Marine Structures*, Edited by C. Noordhoek and J. de Back, pp.137-160, Elsevier Science Publishers B.V., Amsterdam, 1987.

[27] Rhee, H.C. Fatigue Crack Growth Analyses of Offshore Structural Tubular Joint, *Journal of Offshore Mechanics and Arctic Engineering*, Vol.111, pp.49-55, 1989.

[28] Kim. D.S., Tsai, C.L. and Wylde, J.G. Numerical Analysis of Crack Propagation Behavior in a Welded Joint, *Proceedings of the 8th International Conference on Offshore Mechanics and Arctic Engineering*, Vol.III, pp.153-158. The Hague, 1989.

[29] Sih, G.C. Strain Energy Density Factor Applied to Mixed Mode Crack Problems, *International Journal of Fracture*, Vol.10, pp.305-321, 1974.

[30] Sih, G.C. and Cha, B.C.K. A Fracture Criterion for Three-Dimensional Crack Problems, *Engineering Fracture Mechanics*, Vol.6, pp.699-723, 1974.

[31] Aaghaakouchak, Glinka, G. and Dharmavasan, S. A load shedding model for fracture mechanics analysis of fatigue cracks in tubular joints, *Proceedings of the 8th International Conference on Offshore Mechanics and Arctic Engineering*, Vol.III, pp.159-165. The Hague, 1989.

[32] Sih, G.C. *Handbook of Stress Intensity Factors*, Lehigh University, Bethlehem, Pa., 1973.

[33] Tada, H., Paris, P.C. and Irwin, G.R. *Stress Analysis of Cracks Handbook*, Del Research Corporation, Hellertown, Pa., 1973.

[34] Rooke, D.R. and Cartwright, D.J. *Compendium of Stress Intensity Factors*, Hillingdon, Uxbrodge, England. 1976.

[35] Newman, J.C., Jr. and Raju, I.S. An Empirical Stress Intensity Factor Equation for Surface Cracks, *Engineering Fracture Mechanics*, Vol.15, pp.185-192, 1981.

[36] Scott, P.M. and Thorpe, T.W. A critical review of crack tip stress intensity factors for semi-elliptical cracks, *Fatigue of Engineering Materials and Structures*, Vol.4, pp.291-309, 1981.

[37] C. Maosheng, W. Shan and L. Shaofu, Crack Growth and Fatigue Life Estimation in Weld T-Tubular Joints Based on Fracture Mechanics, *Proceedings of the 9th International Conference on Offshore Mechanics and Arctic Engineering*, Vol.III, Part A, pp.351-358. 1990.

[38] Hsu, T.M. Prediction of Fatigue Crack Growth in Tubular T-Joints, *Proceedings of the 9th International Conference on Offshore Mechanics and Arctic Engineering*, Vol.III, Part A, pp.379-386. 1990.

[39] Van Deft, D.R.V., Dijkstra, O.D. and Snijder, H.H. The Calculation of Fatigue Crack Growth in Welded Tubular Joints Using Fracture Mechanics, *Offshore Technology Conference*, OTC 5352. Houston, May 5-8, 1986.

[40] Stacey, A. Remaining Fatigue Life Predictions for a Tubular Joint in a Fixed Platform, *Proceedings of the 10th International Conference on Offshore Mechanics and Arctic Engineering*, Vol. III, Part B, pp.477-486. 1991.

[41] Rice, J.R. Some Remarks on Elastic Crack-Tip Stress Fields, *International Journal of Solids and Structures*, Vol.8, pp.751-758, 1972.

[42] Labbens, R.C., Heliot, J. and Pellissier-Tanon, A. Weight Functions for Three-Dimensional Symmetrical Crack Problems, *Cracks and Fracture, ASTM STP 601*, pp.448-470, 1976.

[43] Paris, P.C., McMeeking, R.M. and Tada, H. The Weight Function Method for Determining Stress Intensity Factors, *Cracks and Fracture, ASTM STP 601*, pp.471-489, 1976.

[44] Oore, M. and Burns, D.J. Estimation of Stress Intensity Factors for Embedded Irregular Cracks Subjected to Arbitrary Normal Stress Fields, *ASME, Journal of Pressure Vessel Technology*, Vol. 102, pp.202-211, 1980.

[45] Burdekin, F.M., Chu, W.H., Chan, W.T.W. and Manteghi, S. Fracture Mechanics Analysis of Fatigue Crack Propagation in Tubular Joints, *International Conference on Fatigue and Crack Growth in Offshore Structures*, C133/86, pp.31. London, April 7-8, 1986.

[46] Connolly, M.P. and Dover, W.D. On the Fatigue Fracture Mechanics Analysis of Tubular Joints, *Proceedings of the 6th International Conference on Offshore Mechanics and Arctic Engineering*, pp.287-293. 1987.

[47] Dover, W.D. and Connolly, M. Fatigue fracture mechanics assessment of tubular welded Y and K -joints, *International Conference on Fatigue and Crack Growth in Offshore Structures*, C141/86, pp.117. London, 7-8 April, 1986.

[48] Mattheck, C., Morawietz, P. and Munz, D. Stress Intensity Factors at the Surface and Deepest Point of a Semi-Elliptical Crack in Plates under Stress Gradients, *International Journal of Fracture*, Vol.23, pp.201-212, 1980.

[49] Irwin, G.R. The Crack Extension Force for a Part-Through Crack in a Plate, ASME Transactions, *Journal of Applied Mechanics*, Vol.29, pp.651-654, 1962.

[50] Dharmavasan, S. *Fatigue fracture mechanics analysis of tubular welded Y-joints*, Ph.D Thesis, university of London, 1983.

[51] Forbes, J.W., Desjardins, J.L., Glinka, G. and Burns, D.J. Stress Intensity Factors for Semi-Elliptical Surface Cracks in Weldments, *Proceedings of the 10th International Conference on Offshore Mechanics and Arctic Engineering*, Vol.III, Part B, pp.529-536. 1991.

[52] Rice, J.R. and Levy, N. The Part-Through Surface Crack in an Elastic Plate, *Journal of Applied Mechanics*, Vol.39, pp.185-194, 1972.

[53] ABAQUS, *User's Manual*, Hibbitt, Karlsson and Sorensen, Inc. 1989.

[54] Brown, D.K. On the Analysis of Cracked Tubular Joints, *International Conference on Fatigue and Crack Growth in Offshore Structures*, C143/86, pp.93. London, April 7-8, 1986.

[55] Raju, I.S. and Newman, J.C. Stress Intensity Factors for a Wide Range of Semi-Elliptical Surface Cracks in Finite Thickness Plates, *Engineering Fracture Mechanics*, Vol.11, pp.817-829, 1979.

[56] Kim, D.S. et al. *Determination of Stress Intensity Factor in Tubular Joints Using Finite Element Method*, Edison Welding Institute Annual Report, WDI No. 529284, 1987.

[57] Huang, X., Du, Z-Z and Hancook, J.W. A Finite Element Evaluation of the Stress Intensity Factors of Surface Cracks in a Tubular Joint, *Offshore Technical Conference*, OTC 5665. Houston, 1988.

[58] Raju, I.S. and Newman, J.C. Jr. Stress Intensity Factor for Internal and External Surface Crack in Cylindrical Vessels, *Journal of Pressure Vessel Technology*, Vol.102, pp.342-346, 1980.

[59] Pan, R.B. and Plummer, F.B. A Fracture Mechanics Approach to Nonoverlapping Tubular K - Joint Fatigue Life Prediction, *Offshore Technical Conference*, OTC 2645. Houston, 1976.

[60] Dover, W.D. and Dharmavasan, S. Fatigue Fracture Mechanics Analysis of T and Y Joints, *Offshore Technical Conference*, OTC 4404. Houston, 1982.

[61] Kam, J.C.P., Topp, D.A. and Dover, W.D. Fracture Mechanics Modelling and Structural Integrity of Welded Tubular Joints in Fatigue, *Proceedings of the 8th International Conference on Offshore Mechanics and Arctic Engineering*, Vol.III, pp.279-286. 1987.

[62] Grover, J.L. Thickness, Weld Profile, and Initial Flaw Considerations for Tubular Joints, *Proceedings of the 8th International Conference on Offshore Mechanics and Arctic Engineering*, Vol.III, pp.39-47. The Hague, 1989.

[63] Kam, J.C.P. and Vinas-Pich, J. A Review on the State of the Art on Tubular Joint Fatigue under Multiple Axes of Loading, *Proceedings of the 9th International Conference on Offshore Mechanics and Arctic Engineering*, Vol.III, Part B, pp.343-350. Houston, 1990.

[64] Recho, N. Simplified Crack Propagation in T-Welded Tubular Joints Submitted to Fatigue, *Proceedings of the 9th International Conference on Offshore Mechanics and Arctic Engineering*, Vol.III, Part B, pp.373-378. Houston, 1990.

[65] Ebecken, N.F.F. and Ferrante, A.J. Elastoplastic Analysis of Tubular Joints of Offshore Platforms, *Proceedings of Energy-Source Technology Conference and Exhibit*, New Orleans, Louisiana. 1986.

[66] Cheema, P.S., Swamidas, A.S.J. and Muggeridge, D.B. Fracture and Fatigue Life of Cruciform Welded Joints, *Proceedings of 6th International Offshore Mechanics and Arctic Engineering Symposium*, Vol.III, pp.403-408. Houston, 1987.

[67] O'Donoghue, P.E., Atluri, S.N. and Rhee, H.C. An Alternating Technique for Flaws in Welded Components, *Proceedings of the 1st OMAE Specialty Symposium on Offshore and Arctic Frontier*, pp.85-90. New Orleans, Louisiana. 1986.

[68] Nishioka, T., Atluri, S.N., and Rhee, H.C. Alternating Method for Elliptical Surface Cracks in Pressure Vessels and Pipes, *Proceedings of the 5th OMAE Symposium*, Vol.II, pp.153-160. Tokyo, 1986.

[69] Rhee, H.C. Application of Finite Element Alternating Method to Offshore Structural Fatigue Analysis, *Offshore Technical Conference*, OTC 5111, Houston, 1986.

[70] Rhee, H.C. Fatigue Crack Growth Analyses of Offshore Structural Tubular Joints, *Engineering Fracture Mechanics*, Vol.34, pp.1231-1239, 1989.

[71] Gallagher, R.H. Survey and Evaluation of the Finite Element Method in Linear Fracture Mechanics Analysis, *Proceedings of First International Conference on Structural Mechanics in Reactor Technology*, Vol.6, Part L, pp.637-653. Berlin, Germany, 20-24 September, 1971.

[72] Zienkiewicz, O.C. *The Finite Element Method*, 3rd Edition, McGraw-Hill Book Company (UK) Limited, Reprinted 1985.

[73] Hellan, K. *Introduction to Fracture Mechanics*, McGraw-Hill Book Company, New York, 1984.

[74] Ewalds, H.L. and Wanhill, R.J.H. *Fracture Mechanics*, Edward Arnold (Publishers) Ltd, 1984.

[75] Anderson, T.L. *Fracture Mechanics Fundamentals and Applications*, CRC Press Inc., Boston, 1991.

[76] Wilson, W.K. *On Combined Mode Fracture Mechanics*, University of Pittsburgh, Ph.D Dissertation, 1969.

[77] Hilton, P.D. and Sih, G.C. Applications of the Finite Element Method to the Calculation of Stress Intensity Factors, in *Mechanics of Fracture, Vol.1, Methods of Analysis and Solutions of Crack Problems*, Edited by G.C. Shi, pp.426-483, Noordhoff International Publishing, 1973.

[78] Rhee, H.C. and Atluri, S.N. Hybrid Stress Finite Element Analysis of Bending of a Plate with a Through Flaw, *International Journal for Numerical Methods in Engineering*, Vol.18, pp.259-271, 1982.

[79] Atluri, S.N. edited, *Proceedings of the International Symposium on Hybrid and Mixed Finite Element Methods*, Atlanta, GA. April 1981.

[80] Barsoum, R.S. On the Use of Isoparametric Finite Element in Linear Fracture Mechanics, *International Journal for Numerical Methods in Engineering*, Vol.10, pp.25-37, 1976.

[81] Barsoum, R.S. Triangular Quarter-Point Elements as Elastic and Perfectly-Plastic Crack Tip Elements, *International Journal for Numerical Methods in Engineering*, Vol.11, pp.85-98, 1977.

[82] Henshell, R.D. and Shaw, K.G. Crack Tip Finite Elements Are Unnecessary, *International Journal for Numerical Methods in Engineering*, Vol.9, pp.495-507, 1975.

[83] Ingraffea, A.R. and Manu, C. Stress-Intensity Factor Computation in Three Dimensions with Quarter-Point Elements, *International Journal for Numerical Methods in Engineering*, Vol.15, pp.1427-1445, 1980.

[84] Ritchie, D. and Voermans, C.W.M. Stress Intensity Factors in an Offshore Tubular Joint test Specimen, *Numerical Methods in Fracture Mechanics*, pp.715-726, Proceedings of the Fourth International Conference held in San Antonio, Texas, 23rd - 27th March, 1987.

[85] Sih, G.C. and Liebowitz, H. Mathematical Theories of Brittle Fracture, *Fracture*, Volume II, Edited by H. Liebowitz, Academic Press, New York, 1968.

[86] Irwin, G.R. Analysis of Stresses and Strains Near the End of a Crack Traversing a Plate, *ASME Transactions, Journal of Applied Mechanics*, Vol.24, pp.361-364, 1957.

[87] Williams, M.L. On the Stress Distribution at the Base of a Stationary Crack, *ASME Transactions, Journal of Applied Mechanics*, Vol.24, 109-114, 1957.

[88] *DISSPLAY, Display Integrated Software System and Plotting Language. User's Manual*, Verson 9.0, Integrated Software System Corporation, San Diego, California. 1981.

[89] SESAM, *POSTFEM, General Finite Element Graphics Postprocessor, User's Manual*, Report No. 89-7007, Veritec, Oslo, Norway, 1989.

[90] Hellier, A.K., Connolly, M.P. and Dover, W.P. Stress Concentration Factors for Tubular Y- and T-Joints, *International Journal of Fatigue*, Vol.12, pp. 13-23, 1990.

[91] Rhee, H.C., Han, S. and Gipson, G.S. Reliability of Solution Method and Empirical Formulas of Stress Intensity Factors for Weld Toe Cracks of Tubular Joints, *Proceedings of the 10th International Conference on Offshore Mechanics and Arctic Engineering*, Vol.III, Part B, pp.441-452. Stavanger, Norway, 1991.

[92] RS/DISCOVER, Version 2.0, *Statistical Appendices*, BBN Software Products Corporation, December 1988.

[93] RS/DISCOVER, Version 2.0, *Reference Manual*, BBN Software Products Corporation, September 1988.

[94] RS/EXPLORE, Version 2.0, *Mulreg Reference Manual*, BBN Software Products Corporation, January 1989.

[95] VAX UNIX *MACSYMA, Reference Manual*, Version 11, Symbolics, Inc. November 1985.

[96] Han, S. and Rhee, H.C. *Fracture Mechanics Behavior of Weld Toe Defects of Tubular Joints*, Research Report No. 107-1206-2-92, Conoco Inc., 1992.

VITA

Shizhong Han

Candidate for the Degree of

Doctor of Philosophy

Title: FRACTURE MECHANICS STUDY OF TUBULAR JOINT WELD TOE DEFECTS WITH THREE-DIMENSIONAL FINITE ELEMENTS

Major Field: Civil Engineering

Biographical:

Personal Data: Born in Shenyang, China, September 7, 1959, the son of Zhaofa Han and Sumei Lu. Married Xiaolu Shan on August 2, 1985.

Education: Received the Bachelor of Science Degree in Mechanical Engineering from the Northeast University of Technology at Shenyang, China in January, 1982; received the Master of Science Degree in Mechanical Engineering from the Northeast University of Technology at Shenyang in April, 1986; completed requirements for the Doctor of Philosophy Degree at Oklahoma State University in December, 1992.

Professional Experience: Faculty member for design and analysis of mining machinery, Department of Mechanical Engineering, Northeast University of Technology at Shenyang, China, from February, 1982 to December, 1985. Visiting Scholar and Research Associate for engineering solid mechanics and finite element method in analysis and design, Department of Mechanical & Aerospace Engineering, the University of Virginia at Charlottesville, Virginia from February, 1986 to December, 1988. Graduate Research Associate for a project of fracture mechanics techniques for Production and Research Department of Conoco Inc. at Ponca City, Oklahoma, from June, 1989 to July, 1990. Teaching Assistant, from January, 1989 to May, 1989; and Graduate Research Associate for a major Joint Industry Project on fracture mechanics from September, 1990 to December, 1992 for Oklahoma State University at Stillwater, Oklahoma.

Affiliations: ASME, Chi Epsilon